TURUN
YLIOPISTO
UNIVERSITY
OF TURKU

ADVANCING ANTIBODY ENGINEERING:

Development of a Novel Bxb1 Landing Pad-Based Mammalian Display Platform for the Selection of Biophysically Favorable Antibodies

Olli Huhtinen

TURUN YLIOPISTON JULKAISUJA – ANNALES UNIVERSITATIS TURKUENSIS
SARJA – SER. F OSA – TOM. 48 | TECHNICA – INFORMATICA | TURKU 2024

TURUN
YLIOPISTO
UNIVERSITY
OF TURKU

ADVANCING ANTIBODY ENGINEERING:

Development of a Novel Bxb1 Landing Pad-Based Mammalian Display Platform for the Selection of Biophysically Favorable Antibodies

Olli Huhtinen

TURUN YLIOPISTON JULKAISUJA – ANNALES UNIVERSITATIS TURKUENSIS
SARJA – SER. F OSA – TOM. 48 | TECHNICA – INFORMATICA | TURKU 2024

University of Turku

Faculty of Technology
Department of Life Technologies
Biotechnology
Drug Research Doctoral Program (DRDP)

Supervised by

Professor Urpo Lamminmäki, PhD
Department of Life Technologies
University of Turku
Turku, Finland

Rune Salbo, PhD
R&D, Orion Pharma
Turku, Finland

Stuart Prince, PhD
Institute of Biomedicine
University of Turku
Turku, Finland

Reviewed by

Professor Peter Kristensen, PhD
Department of Chemistry and Bioscience
Aalborg University
Aalborg, Denmark

Professor Johan Rockberg, PhD
Division of Protein Technology
KTH Royal Institute of Technology
Stockholm, Sweden

Opponent

Scientific Director, Achim Doerner, PhD
Antibody Discovery and Protein Engineering
Merck Healthcare KGaA
Darmstadt, Germany

ISBN 978-951-29-9949-1 (PRINT)
ISBN 978-951-29-9950-7 (PDF)
ISSN 2736-9390 (Print)
ISSN 2736-9684 (Online)
Painosalama, Turku, Finland 2024

To everyone supporting me during the journey.

UNIVERSITY OF TURKU
Faculty of Technology
Department of Life Technologies
Biotechnology
OLLI HUHTINEN: Advancing antibody engineering: Development of a novel Bxb1 landing pad-based mammalian display platform for the selection of biophysically favorable antibodies
Doctoral Dissertation, 202 pp.
Drug Research Doctoral Program (DRDP)
December 2024

ABSTRACT

Owing to their high clinical success rate, advancements in biotechnology, and increased understanding of disease mechanisms, therapeutic antibodies have become an important modality for the treatment of many diseases. Therapeutic antibodies are engineered and recombinantly produced immunoproteins that specifically recognize cell surface proteins to, for example, block proliferation signaling or activate and target immune cells toward tumor cells. In addition to having high specificity and affinity towards their intended target, therapeutic antibodies must exhibit low aggregation propensity, high thermal and colloidal stability, and high solubility to ensure efficient drug manufacturing, storage, and administration.

Recent reports have shown the correlation between antibody display level achieved on mammalian cell surface and the biophysical properties of the antibody. To facilitate the high-throughput selection of developable antibodies, a novel mammalian display platform utilizing a Bxb1 integrase-based landing pad in Chinese hamster ovary (CHO) cells was developed in this thesis. As the primary limitation of mammalian display is its limited library size, the genomic integration efficiency of the developed platform was substantially improved by enhancing the nuclear localization of Bxb1 integrase. To provide further evidence supporting the ability of mammalian display to distinguish between antibodies with differing biophysical properties**,** the correlation between these properties and the display level on mammalian cells was assessed using 37 clinical-stage antibodies. Additionally, the applicability of the platform was demonstrated by improving the biophysical properties of two antibodies using both rational and random mutagenesis strategies. Finally, to overcome the stable genomic integration bottleneck, a method for inducing random mutations near the complementary determining regions of the antibody *in situ* was developed. This was achieved by incorporating G-quadruplex structures in the antibody gene and coupling somatic hypermutation with mammalian display.

As demonstrated in this thesis, this novel mammalian display platform can be adopted by biopharmaceutical laboratories to discover and engineer antibodies with favorable biophysical properties.

KEYWORDS: antibody engineering, mammalian display, Bxb1 integrase

TURUN YLIOPISTO
Tekniikan tiedekunta
Bioteknologian laitos
Biotekniikka
OLLI HUHTINEN: Vasta-ainemuokkauksen edistäminen: Uuden Bxb1 integraasiin perustuvan nisäkässoluilmentämisalustan kehittäminen biofysikaalisesti suotuisten vasta-aineiden valintaa varten
Väitöskirja, 202 s.
Lääketutkimuksen tohtoriohjelma
Joulukuu 2024

TIIVISTELMÄ

Terapeuttisista vasta-aineista on tullut tärkeä hoitomuoto monien sairauksien hoidossa, johtuen niiden hyvästä kliinisestä menestyksestä, bioteknologian kehittymisestä ja sairauksien mekanismien lisääntyneestä ymmärryksestä. Terapeuttiset vasta-aineet ovat rekombinanttisesti tuotettuja immunoproteiineja, jotka tunnistavat spesifisesti solun pintaproteiineja esimerkiksi estääkseen syöpäsolujen lisääntymissignaaleja tai aktivoidakseen immuunisoluja tuhoamaan niitä. Hyvän spesifisyyden ja sitoutumisvoimakkuuden lisäksi terapeuttisten vasta-aineiden on osoitettava matalaa aggregoitumistaipumusta, korkeaa stabiiliutta sekä korkeaa liukoisuutta, jotta lääkkeen tehokas valmistus, säilytys ja annostelu voidaan varmistaa.

Viimeaikaiset tutkimukset ovat osoittaneet korrelaation nisäkässolupinnan vasta-aineiden ilmentymistasojen ja vasta-aineiden biofysikaalisten ominaisuuksien välillä. Tässä väitöskirjassa kehitettiin uusi nisäkässoluilmentämisalusta, joka hyödyntää Bxb1-integraasiin perustuvaa stabiilia integraatiota kiinalaisissa hamsterin munasarjasoluissa (CHO-solut), joka mahdollistaa biofysikaalisesti suotuisten vasta-aineiden tehokkaan valinnan. Kehitetyn alustan genomisen integraation tehokkuutta parannettiin merkittävästi lisäämällä Bxb1-integraasin tumalokaalisoitumista. Lisäksi väitöskirjassa annettiin lisää näyttöä nisäkässoluilmentämisalustan kyvystä erottaa vasta-aineet, joilla on erilaisia biofysikaalisia ominaisuuksia, tutkimalla näiden ominaisuuksien ja ilmentymistasojen välistä korrelaatiota käyttäen 37 kliinisessä vaiheessa olevaa vasta-ainetta. Alustan sovellettavuus osoitettiin parantamalla kahden vasta-aineen biofysikaalisia ominaisuuksia sekä rationaalisella että satunnaisella mutageneesistrategialla. Väitöskirjassa myös kehitettiin menetelmä satunnaisten mutaatioiden aikaansaamiseksi vasta-aineen hypervariaabelialueen läheisyyteen. Tämä saavutettiin sisällyttämällä G4 rakenteita vasta-ainegeeniin ja yhdistämällä somaattinen hypermutaatio nisäkässoluilmentämisalustaan.

Tässä väitöskirjassa osoitettiin monipuolisesti kehitetyn uuden nisäkässoluilmentämisalustan kyky valita biofysikaalisesti suotuisia vasta-aineita, jota voidaan hyödyntää lääkekehityksessä.

ASIASANAT: vasta-ainemuokkaus, nisäkässoluilmentämisalusta, Bxb1 integraasi

Table of Contents

Abbreviations

AC-SINS	Affinity-capture self-interaction nanoparticle spectroscopy
ADA	Anti-drug antibody
ADC	Antibody-drug conjugate
ADCC	Antibody-dependent cellular cytotoxicity
ADCP	Antibody-dependent cellular phagocytosis
AID	Activation-induced cytidine deaminase
APC	Antigen presenting cell
APC	Allophycocyanin
AttB	Bacterial attachment site
AttP	Phage attachment site
BBB	Blood brain barrier
BCR	B-cell receptor
BFP	Blue fluorescent protein
bGH	Bovine growth hormone
BiTE	Bispecific T-cell engager (specific antibody format with two scFvs)
BLI	Biolayer interferometry
bsAb	Bispecific antibody
BSD	Blasticidin S deaminase
bsTCE	Bispecific T-cell engager (broad term for bispecific antibodies designed to engage T-cells for therapeutic purposes)
C1	Complement factor 1
Cas9	CRISPR-associated protein 9
CDC	Complement-dependent cytotoxicity
CDR	Complementary determining region
CE-SDS	Capillary electrophoresis-SDS PAGE
CHO	Chinese hamster ovary
CIC	Cross-interaction chromatography
CMV	Cytomegalovirus
CRISPR	Clustered regularly interspaced palindromic repeats
CRS	Class switch recombination

CTLA-4	Cytotoxic T-lymphocyte antigen 4
DAR	Drug-to-antibody ratio
DBE	Diversifying base editor
DLS	Dynamic light scattering
DSC	Differential scanning calorimetry
DSF	Differential scanning fluorimetry
E. coli	Escherichia coli
EGFR	Epidermal growth factor receptor
ELISA	Enzyme-linked immunosorbent assay
epCAM	Epithelial cell-adhesion molecule
epPCR	Error-prone polymerase chain reaction
Fab	Antigen binding fragment
FACS	Fluorescence-activated cell sorting
Fc	Fragment crystallizable
FcRn	Neonatal Fc receptor
FCS	Furin cleavage site
FcγR	Fcγ receptor
FDA	United States Food and Drug Administration
FGFR1c	Fibroblast growth factor receptor 1c
FRT	FLP recombinase target site
G4	G-quadruplex
GFP	Green fluorescent protein
HC	Heavy chain
HDR	Homology directed repair
HEK	Human embryonic kidney
HER2	Human epidermal growth factor receptor 2
HIC	Hydrophobic interaction chromatography
HIV	Human immunodeficiency virus
HPLC	High pressure liquid chromatography
HRP	Horseradish peroxidase
ICI	Immune checkpoint inhibition
icIEF	Imaged capillary isoelectic focusing
Ig	Immunoglobulin
K_D	Diffusion interaction parameter
K_D	Dissociation coefficient
kDa	Kilodalton
KLB	β-Klotho, coreceptor of FGFR1c
KLH	Keyhole limpet hemocyanin
LAT1	L-type amino acid transporter 1
LC	Light chain

LDL	Low density lipoprotein
LP	Landing pad
LPS	Lipopolysaccharide
mAb	Monoclonal antibody
MAC	Membrane attack complex
MHC	Major histocompatibility complex
MS	Mass spectrometry
NGS	Next generation sequencing
NHEJ	Non-homologous end joining
NK	Natural killer
NLS	Nuclear localization signal
NPL	Nucleoplasmin
nSIE	Normalized stable integration efficiency
PBS	Phosphate-buffered saline
PCSK9	Proprotein convertase subtilisin/kexin type 9
PD-1	Programmed cell death 1
PDGF	Platelet-derived growth factor
PDGFRβ	Platelet-derived growth factor receptor β
PDI	Polydispersity index
PD-L1	Programmed cell death ligand 1
PD-L2	Programmed cell death ligand 2
PEG	Polyethylene glycol
pI	Isoelectric point
PTM	Post translational modifications
PuroR	Puromycin resistance gene
RanGAP	Ran GTPase-activating protein
RanGTP	GTP-binding nuclear protein Ran
RCC1	Regulator of chromosome condensation 1
RFP	Red fluorescent protein
RMCE	Recombinase mediated cassette exchange
RSV	Respiratory syncytial virus
RT	Room temperature
RT-PCR	Reverse transcription-polymerase chain reaction
SARS-CoV-2	Severe acute respiratory syndrome-Corona virus-2
scFv	Single-chain variable fragment
SDS-PAGE	Sodium dodecyl suplhate-polyacryl amide gel electrophoresis
SEC-MALS	Size exclusion chromatography-multi angle light scattering
SHM	Somatic hypermutation
SIE	Stable integration efficiency
SMAC	Standup monolayer chromatography

SPR	Surface plasmon resonance
SV40	Simian virus 40 large T antigen
TALEN	Transcription activator-like effector nuclease
TCR	T-cell receptor
TdT	Terminal deoxynucleotidyl transferase
TM	Transmembrane domain
V_H	Variable heavy domain
V_L	Variable light domain
YAC	Yeast artificial chromosome

List of Original Publications

This dissertation is based on the following original publications, which are referred to in the text by their Roman numerals, and on previously unpublished data presented in this thesis.

I Huhtinen, O., Salbo, R., Lamminmäki, U., and Prince, S. Selection of biophysically favorable antibody variants using a modified Flp-In CHO mammalian display platform. *Front. Bioeng. Biotechnol.* 2023; 11: 1170081.

II Huhtinen, O., Prince, S., Lamminmäki, U., Salbo, R., and Kulmala, A. Increased stable integration efficiency in CHO cells through enhanced nuclear localization of Bxb1 serine integrase. *BMC Biotechnol*. 2024; 24: 44.

III Kulmala, A., Salbo, R., Östman, S., Huhtinen, O., and Lamminmäki, U. Antibody discovery and development method (WO2024/062161A1).

1 Introduction

To survive in competitive environments, organisms must defend themselves against pathogens aiming to exploit their resources, while preserving their own cells from injury. The need for self-protection in the continuous battle for survival ultimately drove the development of complex immune systems more than 500 million years ago [1]. Biologists have discovered that even simple multicellular organisms, such as sponges, have many of the same elements used by vertebrates for immune recognition and defense against microbes. These ancient defense mechanisms, referred to as innate immunity, defend against infections through the relatively nonspecific recognition of pathogen patterns [1]. In humans, innate immunity is provided by the physical barrier formed by skin and mucous membranes, immune cells recognizing pathogen-specific patterns, and the various proteins involved in the complement system. The innate immunity is activated immediately after infection, to rapidly control the replication of the infecting pathogen [2].

When innate immunity is insufficient to eradicate the invader, adaptive immunity kicks in to generate a targeted immune response and immunological memory against the pathogen [3]. Innate immunity is found in almost all animals, providing a basic defense against pathogens. However, lymphocytes bearing somatically diversified antigen receptors are unique to vertebrates, where they play fundamental roles in adaptive immunity. Adaptive immunity relies heavily on two types of specialized immune cells: thymus-derived T-lymphocytes (T-cells) and bone marrow-derived B-lymphocytes (B-cells). T-cells and B-cells play distinct roles in the immune response, with T-cells primarily involved in cell-mediated immunity, while B-cells drive humoral immunity through the secretion of antibodies. These cells work together with phagocytic cells and other immune cell types to mediate effective adaptive immune response, which is driven by the recognition of antigens by the receptors of T-cells and B-cells. The remarkable diversity of the receptors, capable of recognizing virtually any antigen, arises from the recombination of a limited number of germline gene segments in an error-prone process during T-cell and B-cell maturation [4,5].

While the significance of the immune system in protecting the host from microbial pathogens is widely accepted, convincing data supporting the role of the

immune system in preventing tumorigenesis has only been shown just over two decades ago [6]. Along with the technological advancements in biotechnology, this finding has partly sparked interest in the development of recombinant antibodies for the treatment of infectious diseases, autoimmunity, and especially cancer. This thesis focuses on the development of human antibodies, their application in a therapeutic context, and key factors to consider in the engineering of effective therapeutic antibody candidates. More specifically, this thesis highlights the importance of the biophysical properties of therapeutic antibodies during their development towards clinical molecules.

2 Review of the Literature

2.1 What are antibodies?

Antibodies, also known as immunoglobulins (Ig), are proteins produced by the immune system in response to the presence of foreign substances called antigens. They are an essential part of the adaptive immune response, which helps the body recognize and neutralize harmful pathogens such as viruses, bacteria, or other foreign invaders. Antibodies are secreted to the plasma and extracellular fluids by B-cells, and they mediate so-called humoral immunity. Three main functions of humoral immunity are neutralization, opsonization, and complement activation [7] (**Figure 1**).

Neutralization is the process where antibodies directly bind to antigens on pathogens, preventing them from entering or infecting host cells (**Figure 1A**). Prevention of viral infection prevents the virus from replicating and thus causing harm to the body. Neutralization is also the form of immunity elicited by most vaccines [8].

Many bacteria, however, can proliferate in the extracellular space, which is why neutralization by antibodies is insufficient to stop their infection. These pathogens can also hide from the innate immune system with an outer coat, which is not recognized by the pattern recognition receptors of immune cells [7]. Fortunately, antibodies can bind to a vast array of antigens on the outer coats of the pathogens. Immune cells, called phagocytes, have receptors that bind to the constant region of the antigen-bound antibody, facilitating e.g., phagocytosis of the pathogen, or antibody-dependent cellular cytotoxicity (ADCC) against a host cell infected with the pathogen (**Figure 1B**). The coating of pathogens and foreign particles with antibodies is called opsonization.

The third function of antibodies is the activation of the complement cascade (**Figure 1C**). When antibodies bind to antigens on the pathogens, they can initiate the complement system by facilitating the binding of C1q to their constant region. This binding of C1q to the antibody molecules on the pathogen surface activates the protease activity of C1r, which in turn triggers the complement cascade. This cascade attracts immune cells to the site of infection, enhances phagocytosis and can lead to the formation of a membrane attack complex that directly lyses e.g., bacterial cells [7].

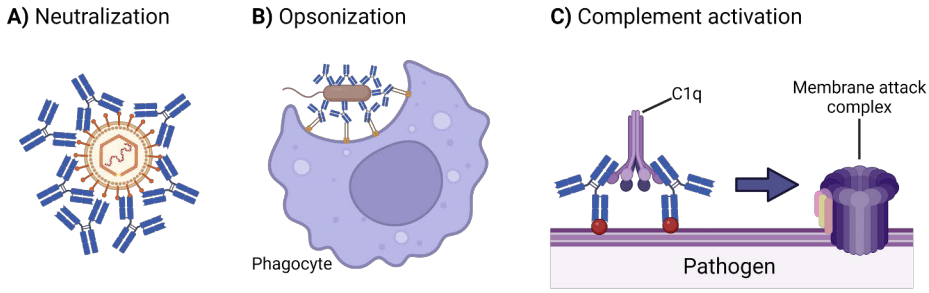

Figure 1. Antibodies have three main functions in the body: neutralization, opsonization and complement activation. **A)** Antibodies can neutralize pathogens e.g., viruses, by directly binding to their antigens, preventing them from infecting cells. **B)** Antibodies can recognize antigens on pathogens, marking them for immune cells, facilitating e.g., phagocytosis and antibody-dependent cellular cytotoxicity. **C)** Lastly, antibodies bound to the antigens of a pathogen can activate the complement system by binding of C1q, which attracts immune cells, enhances phagocytosis, and can directly kill e.g., bacterial cells by formation of a membrane attack complex. Created with BioRender.com

2.1.1 B-cell development

To fully grasp the structural and functional components of antibodies, it is essential to understand the natural process by which they are formed in the body. Antibodies are produced by mature B-cells, known as plasma cells. Before B-cells begin secreting antibodies, they undergo a complex maturation and selection process. This process ensures the selection of B-cells that possess receptors with high affinity for a particular antigen, thus enhancing the efficacy of the immune response against the targeted pathogen [7].

B-cell development begins in the bone marrow, where hematopoietic stem cells differentiate into pro-B-cells. These pro-B-cells initiate the rearrangements of their immunoglobulin genomic regions, eventually leading to the formation of a fully functional antibody gene, composed of a heavy chain and a light chain. The combination of the light chains and the transmembrane-anchored heavy chains forms the B-cell receptor (BCR) expressed on the surface of immature B-cells, which determines the antigen specificity of the resulting antibody. Before these immature B-cells leave the bone marrow, they undergo a critical negative selection process that eliminates B-cells with receptors that strongly recognize self-antigens, thereby preventing autoimmunity. B-cells that successfully pass the selection then migrate to peripheral lymphoid tissues, such as the spleen and lymph nodes, where they complete their maturation.

Before encountering an antigen, mature B-cells are considered naïve. At this stage, the antibody is surface-expressed as part of the BCR, waiting for activation. When a naïve B-cell recognizes an antigen via the BCR, it rapidly proliferates and

forms a germinal center, a site where the humoral immune response is fine-tuned through processes such as affinity maturation, clonal expansion, and class switching. Germinal center B-cells that fail to be activated by antigens presented by dendritic cells undergo apoptosis, ensuring only the most effective B-cells are selected.

The activated B-cells then differentiate into plasma cells and memory B-cells. Plasma cells are responsible for secreting large quantities of antibodies specific to the activating antigen, providing a humoral response. Meanwhile, memory B-cells circulate in the blood and reside in the spleen, lymph nodes, and bone marrow, offering long-lasting immunity by enabling a more rapid and robust generation of plasma cells upon subsequent encounters with the same antigen [7].

Overall, B-cell maturation is a highly regulated process involving genetic rearrangements, selection processes, and differentiation steps to produce mature B-cells capable of recognizing and responding to specific antigens, thus ensuring effective humoral response.

As discussed later in the thesis, antibody engineering can harness a similar principle of antibody presentation on the cell surface and the selection of antigen-specific antibodies *in vitro* through the use of a mammalian display platform, where recombinant antibodies are commonly expressed on the surface of engineered Chinese hamster ovary (CHO) cells or human embryonic kidney (HEK) cells.

2.1.2 Antibody structure and generation of diversity

Antibodies are multidomain, Y-shaped glycoproteins composed of two copies of a longer polypeptide, known as the heavy chain (~50 kDa in IgG), and two copies of a shorter polypeptide, known as the light chain (~25 kDa, **Figure 2**) [9]. These chains are further divided into two main regions: a highly polymorphic variable region, responsible for antigen recognition, and a conserved constant region, responsible for mediating the effector functions of humoral immunity [10]. The variable regions are referred to as the variable heavy domain (V_H) and the variable light domain (V_L).

Structurally, an antibody molecule can be divided into two primary fragments: the antigen binding fragment (Fab) and the fragment crystallizable (Fc). The Fab region includes the entire light chain, V_H domain, and the first domain of the heavy chain's constant region (C_H1). The Fc region encompasses the remaining heavy chain constant regions (C_H2 and C_H3 in IgG) [7].

The antigen-binding site of an antibody is primarily formed by three hypervariable loops within each variable domain, known as complementary determining regions (CDRs): CDR-H1, 2, and 3 in the heavy chain and CDR-L1, 2, and 3 in the light chain. As the name suggests, these CDRs contain the most variability in the antibody and they are responsible for antigen contact and specificity. Three key processes during B-cell development generate the diversity

needed to produce a wide array of antibodies capable of recognizing virtually any antigen. These processes are combinatorial diversity, junctional diversity, and somatic hypermutation [7], and are illustrated in **Figure 3**.

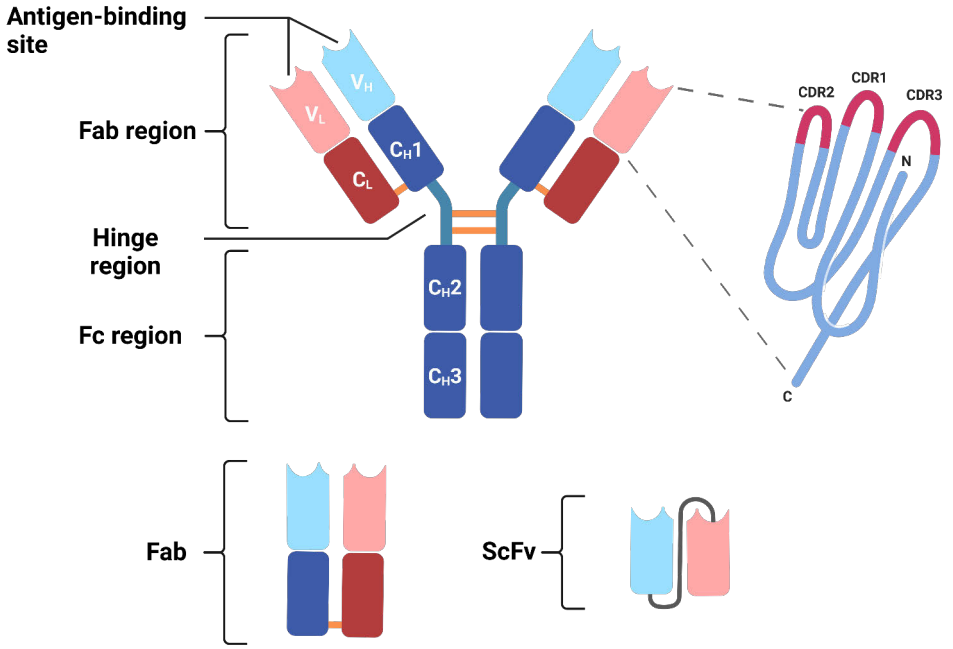

Figure 2. Structure of an IgG1 antibody. The IgG consists of two heavy chains (blue) and two light chains (red), which are covalently connected via interchain disulfide bonds (yellow). The heavy chain is formed by a variable domain (V_H) and three constant domains (C_H1-3). The light chain is formed by a variable domain (V_L) and a constant domain (C_L). Antigen binding occurs at the tip of the Fab region, where the variable regions form three loops of hypervariable regions, called complementary determining regions (CDR). Recombinantly produced antigen binding fragment (Fab) or single-chain variable fragment (scFv) are often used in applications where the constant region is not needed. Created with BioRender.com

2.1.2.1 Combinatorial diversity

Antibodies are encoded by genes that are composed of multiple gene segments, which are organized into three genetic loci: the κ (kappa) light chain locus, the λ (lambda) light chain locus, and the heavy chain locus, each located on different chromosomes. These loci contain the genes responsible for both the variable (V-domain) and constant (C-domain) regions of the antibody chains. The gene segments encoding the V-domain are further divided into three clusters: variable (V), diversity (D), and joining (J) segments. The process of combinatorial diversity arises from the rearrangement and combination of these gene segments in a process known as V(D)J

recombination. The light chain genes only contain V and J segments, whereas the heavy chain genes contain all three – V, D, and J.

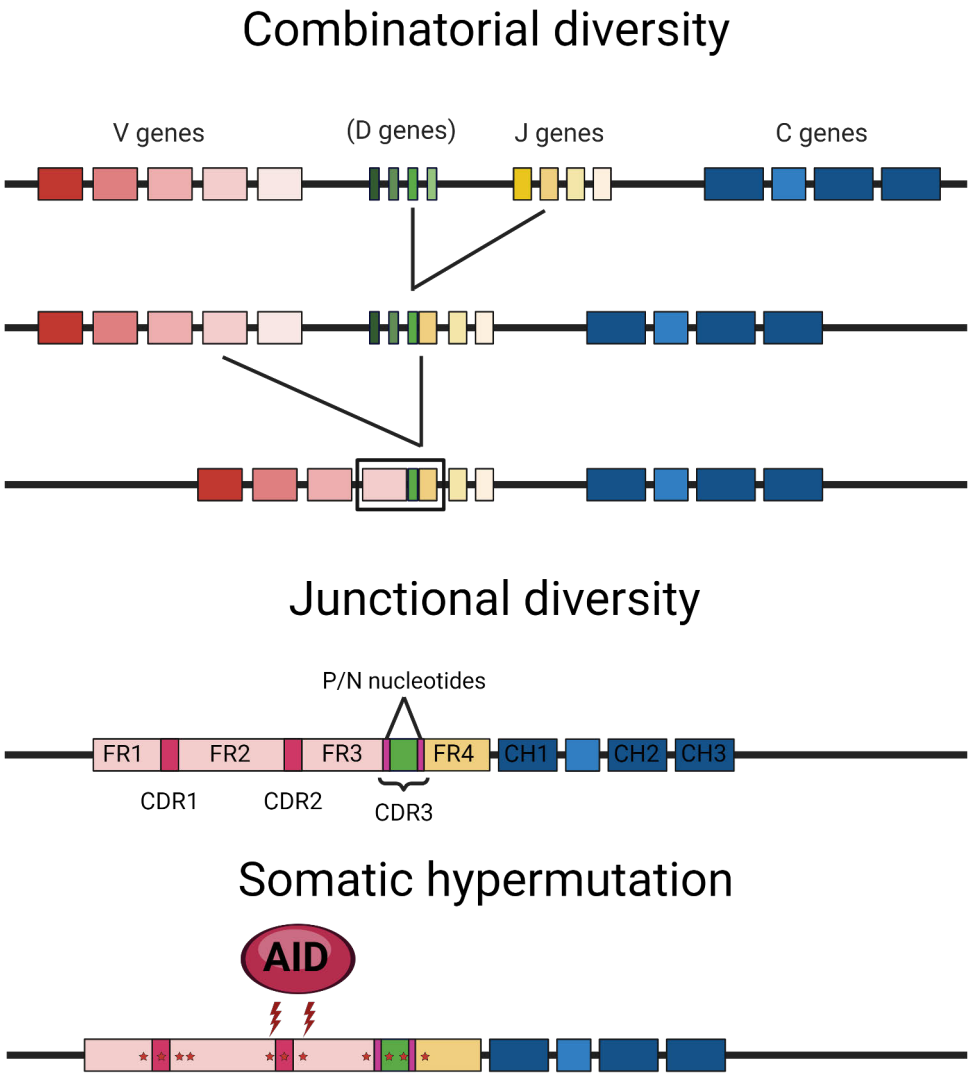

Figure 3. Generation of antibody diversity. In the heavy chain locus, variable (V), diversity (D) and joining (J) gene segments are combined to form a complete V region. The κ and λ light chain loci only contain V and J gene segments. This form of diversity is called combinatorial diversity. Random insertions and deletions (P and N nucleotides) occur during the recombination, causing junctional diversity. Lastly, random mutations along the V region are introduced by activation-induced cytidine deaminase (AID) during an immune response to mature the affinity of a given antibody to the antigen. Created with BioRender.com

There are multiple copies of the V, D, and J gene segments, each contributing to the assembly of the immunoglobulin V-region. For example, the human κ light chain locus contains approximately 40 functional V_κ gene segments and 5 J_κ gene segments, resulting in about 200 possible V_κ regions. Similarly, the λ light chain locus has approximately 30 V_λ gene segments and 4-5 J_λ gene segments, allowing at least 120 possible V_λ regions. combined, these provide at least 320 different possible light chains.

The human heavy chain locus is even more diverse, with approximately 40 functional V_H gene segments, 25 D gene segments, and 6 J_H gene segments, resulting in around 6000 different possible V_H regions. Since the heavy chain rearrangement occurs before light chain gene rearrangement, the same heavy chain can be paired with different light chains, resulting in approximately 1.9×10^6 different antibody specificities, based on the combination of 6000 heavy chains with 320 light chains [7].

This theoretical estimate of diversity is further increased by the fact that in some rare cases, multiple D gene segments can be incorporated, which is seen in approximately 1 in 800 circulating B-cells [11]. The observed antibody combinatorial diversity is slightly reduced because V-gene segments are grouped into 7–8 conserved families, with members within each family sharing at least 80% DNA sequence identity. This high sequence similarity among family members limits the variability introduced by V-gene selection, thus slightly reducing the overall diversity of antibodies produced. [12]. Despite these nuances, the combinatorial diversity before additional diversification mechanisms is still vast.

2.1.2.2 Junctional diversity

V(D)J recombination is an error-prone process initiated by recombinases RAG1 and RAG2. During this process, a D and J gene segment are first rearranged to form a continuous exon, after which a V gene segment recombines with the formed D-J complex. Junctional diversity is introduced during this rearrangement by insertions and deletions of random nucleotides. Insertions are caused by palindromic nucleotide sequences (P-nucleotides) added by RAG1/2 and other proteins, as well as random non-templated nucleotides (N-nucleotides), added by the enzyme terminal deoxynucleotidyl transferase (TdT) [13,14] (**Figure 3**).

In an assembled V-domain, most of the exon is encoded by the V gene segment, which includes two of the three CDRs. These two CDRs are different in different germline genes, providing germline-encoded diversity, which however is quite limited due to the conserved nature of the V genes. The third CDR, known as CDR3, is encoded by the V(D)J junctional region and contains the most variation due to the combinatorial and junctional diversity introduced during the rearrangement process. The addition of P- and N-nucleotides and deletions of nucleotides at the gene segment junctions leads to the length variation in the CDR3 region, particularly in CDR-H3 [15].

Since the junctional diversification process involves the addition or deletion of random numbers of nucleotides, only one-third of the V(D)J rearrangements preserve the reading frame, generating a functional heavy- or light chain exon. Nonproductive rearrangements are eliminated during B-cell maturation [7]. Despite this, the naïve antibody repertoire, originating from the combinatorial and junctional diversity mechanisms is estimated to be as high as 10^{18} members based on theoretical combinatorial calculations [16]. This diversity far exceeds the actual number of B-cells in the human body (~10^{11}) [17] and ensures that even weak binders to virtually any antigen can be identified, with the potential to mature into strong binders through subsequent somatic hypermutation.

2.1.2.3 Class switch recombination and somatic hypermutation

After V(D)J recombination, B-cells initially express IgM antibodies on their surface, forming the primary immunoglobulin repertoire. When these naïve B cells encounter an antigen, they become activated and can undergo isotype or class switching, a process in which they transition from expressing IgM to expressing other antibody classes. This switch modifies the effector function of the antibody, enhancing its ability to eliminate the pathogen that triggered the immune response [18].

Class switching is achieved through a process known as class switch recombination (CSR), which involves deletional recombination between two specific DNA sequences called switch regions. Each switch region is associated with a different heavy chain constant region gene, determining the antibody class. The process is initiated by the enzyme activation-induced cytidine deaminase (AID), which converts cytosines in these switch regions into uracils. The uracils are then removed by various DNA repair pathways, resulting in mutations, single-strand DNA breaks, and double-strand breaks. These double-strand breaks are crucial for CSR and are repaired by the non-homologous end joining (NHEJ) mechanism. This repair process deletes the intervening DNA between the two switch regions, bringing the variable region of the antibody gene in close proximity to a different constant region gene. As a result, the B-cell starts producing antibodies of different classes, like IgG, IgE or IgA, each with distinct effector functions suited to different types of immune responses [19].

In addition to class switching, the affinity of the antibodies is fine-tuned through a process called somatic hypermutation (SHM) to achieve a more effective response against the antigen. During SHM, random mutations are introduced into the V regions of both the heavy and light chains of the antibody gene [20]. This process is also initiated by AID and occurs in activated B-cells within germinal centers (**Figure 3**). B-cells that express antibodies with improved affinity for the antigen are preferentially selected and expanded through multiple rounds of SHM. This iterative

process can increase the affinity of antibodies for their specific antigen by 10- to 5000-fold over the course of an immune response [21].

From a structural perspective, the affinity improvements resulting from SHM can arise through various changes at the antibody-antigen interface. These changes can include increased complementarity between the antibody and antigen, increased burial of total hydrophobic surface area, enhanced electrostatic interactions, stronger hydrogen bonding, and conformational preorganization of the antibody's binding site (paratope) [21]. The CDR-H3 loop is particularly important in SHM, as it makes the most contact with the antigen and shows the highest structural variation [22].

Mutations in the CRD-H3 loop can significantly enhance antibody affinity, but mutations outside this region, such as in the framework regions, can also contribute to stabilizing the formation of the H3 loop close to its bound state. This rigidification of the paratope often leads to increased specificity for the antigen [21] and may also reduce the antibody's hydrophobicity and thermal stability [23].

In the conventional model of antibody affinity maturation, a flexible, low-affinity, and polyspecific unmutated precursor antibody undergoes SHM, incorporating mutations that improve both its affinity and specificity for the target antigen. These mutations optimize contact residues at the antibody-antigen interface and rigidify the paratope through changes in both proximal and distal amino acids. This process results in an antibody with higher specificity and affinity, better suited to effectively neutralizing the antigen [24].

2.2 Antibodies as therapeutics

Historically, the beginning of monoclonal antibody (mAb) development can be said to have started with the invention of the hybridoma technology by Köhler and Milstein in 1975 [25]. Hybridomas are created by fusing antibody-secreting B-cells from immunized animals with myeloma cells to create cell lines secreting monoclonal antibodies [26]. The potential of mAbs as a new class of therapeutic agent was soon realized, leading to the first clinical approval of a therapeutic mAb in 1986 [27]. The first approved therapeutic mAb, orthoclone OKT3 (Muromonab-CD3), was a murine mAb targeting CD3 on T-cells and was used as an immunosuppressor for the treatment of kidney transplant rejection [28].

In 2015, the United States Food and Drug Administration (FDA) approved its 50th therapeutic mAb, and just 6 years later the 100th [29]. As of November 2023, nearly 200 mAbs have been granted marketing approval or are currently in the regulatory review in at least one country and 138 more are undergoing late-stage clinical development [30]. The rapid growth of mAbs is partly explained by their rapid route to a clinical proof-of-concept for activating, inhibiting, or blocking of new targets.

As antibodies are generally well-tolerated and highly specific, the risk of unexpected safety issues in human clinical trials of mAbs is lower than with many other therapeutic agents [27], resulting in a more than 70% success rate in phase I clinical trials [31]. The likelihood of a monoclonal antibody to gain FDA approval after entering the clinical trials is roughly between 15 – 30%, depending on the estimation approach [31]. Nowadays, mAbs are dominating the pharmaceutical market, having global sales of $215 billion in 2022, which is expected to reach over $600 billion by 2032 with a compound annual growth rate of 11.8% [32].

2.2.1 Mechanisms of action

Traditionally, monoclonal antibodies have been used for the treatment of cancer, autoimmune diseases, and infectious diseases [33]. Antibodies are a viable treatment option when the molecular mechanisms of the disease are clearly elucidated, and the specific proteins or molecules involved in the pathogenesis are identified. Therapeutic antibodies can target the treatment to specific cells through cell surface targets. For example, in cancer treatment, therapeutic antibodies can act through several different mechanisms including tumor signaling disruption, Fc-domain mediated activation, and targeting of immune checkpoints [34].

2.2.1.1 Signal disruption

Therapeutic antibodies can disrupt the tumor cell signaling by targeting different membrane-bound receptors or neutralizing cytokines or growth factors that are critical to cellular growth and proliferation (**Figure 4**). Several receptors involved in growth signaling pathways have been identified as targets for cancer treatment. For example, a mutated, constitutively activated version of the epidermal growth factor receptor (EGFR) is overexpressed in many different cancers [35], leading to pro-oncogenic effects including proliferation and chemotherapeutic resistance [36,37]. Cetuximab is an anti-EGFR mAb, which induces cell cycle arrest and apoptosis in tumor cells by blocking ligand binding and receptor activation [38].

Another important cancer cell target is the human epidermal growth factor receptor 2 (HER2), which has no known ligands. HER2 is a receptor tyrosine kinase that constitutively adopts an open configuration, priming it for heterodimerization with other HER family members [39]. Overexpression of HER2, like in certain aggressive types of breast cancer, increases mitogenic signaling leading to promoted cell-cycle progression and inhibited apoptosis [40]. Trastuzumab and pertuzumab are anti-HER2 mAbs targeting different domains of HER2 [41], both inhibiting the receptor dimerization and are thus in combination with docetaxel the first-line therapy for HER2-positive metastatic breast cancer [42].

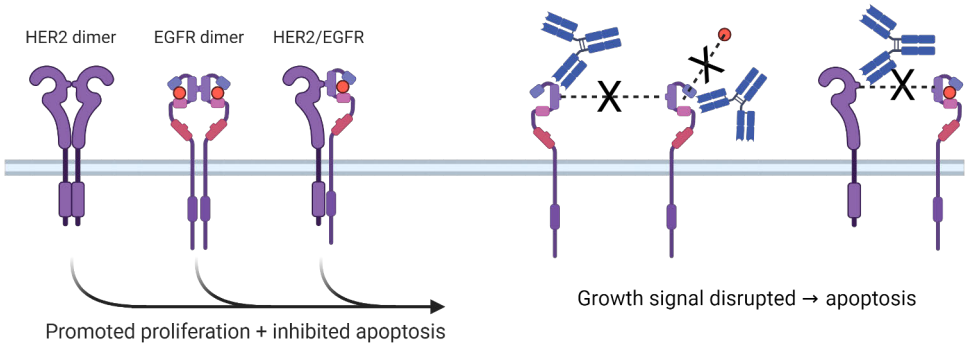

Figure 4. Tumor signaling disruption by therapeutic antibodies. Therapeutic antibodies can prevent tumor growth signaling e.g., by inhibiting ligand binding or receptor dimerization. Created with BioRender.com

2.2.1.2 Fc-mediated effector functions

The tumor signal disruption described above is mediated by the blocking of receptor-ligand interaction or dimerization of receptors, which is dependent only on the binding of the variable region of the antibody. The Fc region of the antibody plays an important role in recruiting immune effector cells and activating the complement pathway, both leading to the destruction of the tumor cells. The coating of tumor cells by IgGs can activate three different Fc-mediated mechanisms that lead to the destruction of cancer cells (**Figure 5**): antibody-dependent cellular cytotoxicity (ADCC), antibody-dependent cellular phagocytosis (ADCP), and complement-dependent cytotoxicity (CDC) [34].

ADCC occurs when the antibodies are bound to a tumor cell, which is then recognized by an immune effector cell. The activation of the immune effector cell occurs when the antibodies opsonize the tumor cell and the Fcγ receptors (FcγR) expressed on leukocytes, such as neutrophils, bind to the Fc regions of the antibodies. Upon activation, neutrophils can induce apoptosis or necrosis, killing the tumor cell [43]. Another type of leucocyte, natural killer (NK) cell, can destroy tumor cells upon activation via the release of lytic factors [44]. The activation of macrophages can trigger ADCP, eliminating tumor cells from the circulation [45].

Alternatively, the destruction of tumor cells can be mediated by the activation of the classical complement pathway in a process called CDC. The complement pathway is activated when the six globular heads of the C1q subunit of complement factor 1 (C1) bind to the Fc regions of IgGs bound to the tumor cell [46]. The activation eventually leads to the formation of the membrane attack complex (MAC), a pore that leads to cell lysis [47]. Fc-mediated effector functions often play a combinatorial role with other mechanisms of action. For instance, in addition to inhibiting cell

growth by signal disruption, trastuzumab activates ADCC and ADCP against HER2-positive cells [48].

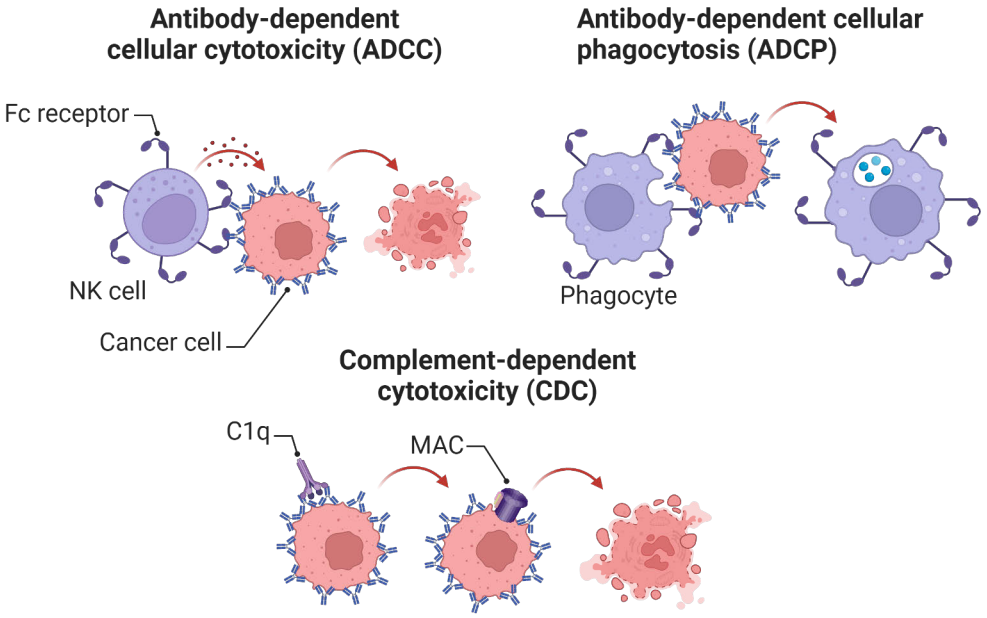

Figure 5. Fc-mediated effector functions of therapeutic antibodies. Antibodies recognize tumor-associated antigens on cancer cells, marking them for immune effector cells and the complement system. The activation of immune effector cells, including natural killer cells (NK cells) and phagocytes, is initiated by the binding of Fcγ receptors to the Fc region of antibodies, leading to the destruction of cancer cells. Created with BioRender.com

2.2.1.3 Immune checkpoint inhibition

Development of therapeutic antibodies against various immune checkpoint molecules has progressed with impressive results in recent years, revolutionizing cancer treatment [49]. To understand the mechanisms of immune checkpoint inhibition (ICI) therapy for cancer, it is essential to understand the processes governing T-cell activation and inhibition (**Figure 6**).

T-cell activation requires two signals to be activated. The first signal originates from the interaction between the T-cell receptor (TCR) and major histocompatibility complex (MHC)-presented antigens. The second signal is induced by the interaction between the T-cell's costimulatory surface receptor CD28 and its ligand CD80 or CD86, which are presented by antigen-presenting cells (APCs), such as dendritic cells [50]. After T-cell activation, T-cells start to express coinhibitory cell surface receptors, also called immune checkpoint molecules, such as programmed cell death

1 (PD-1) and cytotoxic T-lymphocyte antigen 4 (CTLA-4), to prevent continued activation [51].

In normal tissue, immune checkpoint pathways aim to downregulate T-cell activity to prevent autoimmunity [52]. The T-cell function is inhibited when PD-1 is bound by the PD-1 ligand 1 (PD-L1) or PD-1 ligand 2 (PD-L2), or when CTLA-4 binds to CD80 or CD86 on antigen-presenting cells, competing with the costimulatory surface receptor CD28. Tumor cells exploit these inhibitory molecules, for example by overexpressing PD-L1, to induce tumor tolerance and T-cell exhaustion [50].

In addition to T-cell inhibition, PD-1 has been linked to NK cell exhaustion, making PD-1 pathway inhibition an effective strategy for circumventing tumor escape from both T-cell- and NK cell-mediated immune surveillance [53]. Several clinically used monoclonal antibodies block the immune checkpoint molecules or the ligand binding to these molecules, consequently reinvigorating the immune system against the cancer. These antibodies include nivolumab, pembrolizumab, and cemiplimab against PD-1, atezolizumab, durvalumab and avelumab against PD-L1, and ipilimumab against CTLA-4 [49]. One major benefit of ICI treatment compared to other anticancer therapies, such as chemotherapy or targeted therapies, is the long-lasting response even after cessation of treatment in patients, which is caused by the induction of tumor-specific immunological memory by the differentiation of a subset of effector T cells into effector memory T cells [54].

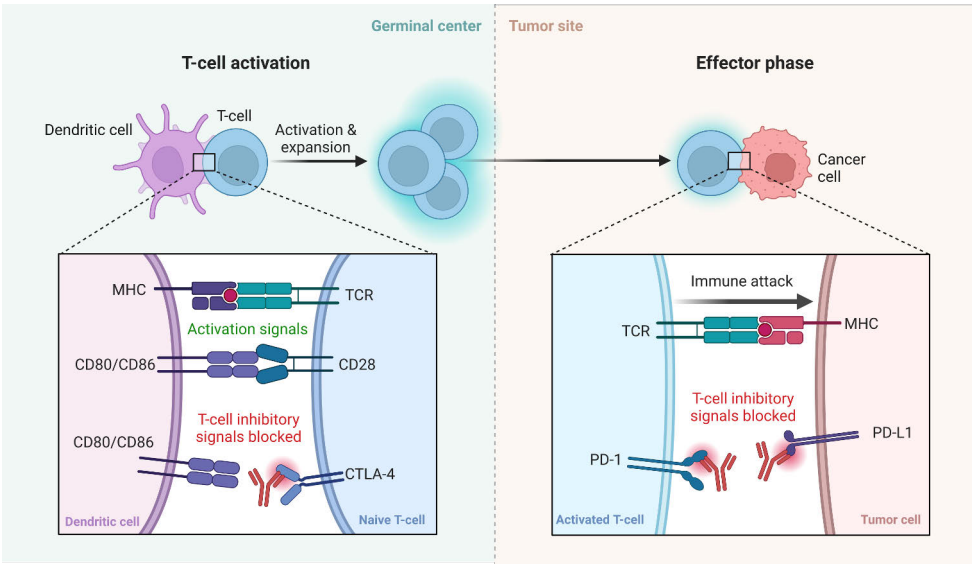

Figure 6. Immune checkpoint inhibition (ICI) therapy. Cancer cells can overexpress T-cell inhibitory molecules, such as PD-L1 to induce T-cell exhaustion. ICI therapy aims to block the inhibitory signals with therapeutic mAbs. Created with BioRender.com

2.2.2 Next-generation antibody drugs

The rapid clinical success of therapeutic monoclonal antibodies, developments in recombinant DNA technology, and a better understanding of disease biology have incited the design of next-generation antibody drugs. Next-generation antibody drugs aim to e.g., exploit novel modes of action, interact with two targets with bispecific antibodies (bsAb) or use a targeted toxic payload delivery with antibody drug conjugates (ADC). Next-generation antibody drugs are often developed against clinically well-validated targets where competing first-generation antibody drugs are already on the market [55].

2.2.2.1 Bispecific antibodies

Bispecific antibodies combine the binding specificities of two antibodies. They are an attractive modality that features potential for novel functionalities, termed obligate features, which are not achievable with a mixture of the parental antibodies. They have the possibility of physically linking two binding specificities, such as linking an effector cell to a target cell [56].

The concept of preparing an antibody with two binding specificities [57] was already demonstrated by Nisonoff et al. more than 60 years ago using rabbit antibodies [58]. The potential of dual-targeting antibodies for therapeutic use was demonstrated *in vitro* in the mid-1980s [59], but the translation of these concepts into treatment was only clinically validated in 2009 with the approval of the first clinical bsAb catumaxomab, targeting CD3 and epithelial cell-adhesion molecule (epCAM), for the intraperitoneal treatment of malignant ascites [60]. Catumaxomab was later withdrawn from the market due to commercial reasons, but it was soon followed by the approval of blinatumomab in 2014, a bispecific T-cell engager (BiTE) targeting CD3 and B lymphocyte antigen CD19, for the treatment of acute lymphoblastic leukemia (**Figure 7A**). Blinatumomab treatment was associated with a complete remission of 43% of patients in phase II trial in adults with relapsed or refractory disease [61]. The phenomenal success of blinatumomab partly fueled the development of a "zoo" of different bsAb species, nowadays comprising more than 100 different formats [62].

The most commonly pursued functionality in bsAbs is T-cell redirection and engagement [56]. Bispecific T-cell engagers (bsTCE) aim to redirect the cytotoxic activity of effector T-cells to specifically eliminate tumor cells. This involves the physical cross-linking of T-cells to tumor cells through bsAbs containing a T-cell-binding domain and a tumor-targeting domain, forming a cytolytic immune synapse leading to tumor cell destruction. Typically, the T cell-binding domain targets CD3 in the TCR complex, bypassing MHC restriction and inducing T-cell activation irrespective of the TCR specificity [56]. Several studies have shown that the affinity of

the CD3-binding arm has to be fine-tuned to allow efficient tumor distribution without rapid CD3-mediated plasma clearance or trapping of the antibody in T-cell-containing tissues, like spleen and lymph nodes [63–65]. While high affinity is usually preferred in therapeutic antibodies, in the case of CD3 targeting bsAbs, lower CD3 affinity has resulted in better biodistribution and tumor targeting.

In addition to targeting CD3 in T cells for tumor destruction, many other interesting forms of cell-bridging bsAbs are under investigation, such as bsAbs against regulators of other T cell activation pathways or immune checkpoints [56], redirection of NK cells through CD16 binding [66], virus-specific bsTCE to redirect T cells to kill virus-infected cells expressing viral surface antigens [67], and targeted homing of endogenous circulating stem cells to restore tissue damage by cross-linking the stem cells with activated platelets through CD41 and CD34 binding [68].

All the above-mentioned bsAbs bind to two distinct targets in two different cells, thus they are working *in-trans*. The functionality of *in-trans* bsAbs is dependent on the physical linkage of the cells and cannot be obtained by combining separate antibodies with the same specificities [56]. Another type of function exhibited by bsAbs is *in-cis* binding, whereby the bsAbs engage with two targets on the same cell. While targeting two targets on the same cell is a combinatorial concept, some molecules display obligate features [56]. For example, treatment with a bsAb targeting HER2 and HER3 has resulted in increased local concentration of HER3 Fab on HER2 positive cells, inhibiting HER3 signaling more effectively than a combination treatment of anti-HER2 and anti-HER3 mAbs [69].

BsAbs can also be designed to be biparatopic: targeting two non-overlapping epitopes on the same target to increase the binding strength through antigen crosslinking and aggregation, or to drive more rapid internalization. Weisser at al. showed that a biparatopic bsAb against HER2 elicited complement-dependent cytotoxicity and superior *in vivo* antitumor activity compared to trastuzumab and a combination of trastuzumab and pertuzumab [70].

Unlike inhibitory antibodies that block pathogenic signaling, certain therapeutic approaches necessitate receptor signaling activation using agonistic antibodies. Roche has ongoing clinical development of an agonistic bsAb targeting fibroblast growth factor receptor 1c (FGFR1c) and the coreceptor β-Klotho (KLB) for treating obesity and diabetes [71]. FGFR1c is normally activated by fibroblast growth factor 21 (FGF21) when bound to its obligate coreceptor KLB, but systemic dosing of recombinant FGF21 has led to stunted growth, bone loss, female infertility, and an increase in serum glucocorticoid in rodents, preventing its clinical use. The developed bsAb is designed to activate a metabolic pathway by bridging the FGFR1c and KLB, leading to weight loss (**Figure 7B**). In addition to the obligate functionality brought by the bispecific nature of the molecule, the bispecific format also reduces off-target activation, since co-targeting of these receptors restricts the signaling

activation only to tissues that co-express both targets. A similar co-targeting strategy has also been used for the development of a bsAb targeting factor IXa and factor X to mimic the factor VIII cofactor function to treat hemophilia A [72].

An intriguing potential application of bsAbs involves targeted delivery of therapeutic antibodies across the blood brain barrier (BBB) by hijacking a transcytosis pathway. This approach, demonstrated to overcome the typically inefficient protein transfer across the BBB, utilizes bsAbs with one arm targeting a transferrin receptor with low affinity and the other targeting a central nervous system target with high affinity [73]. While transferrin receptor has been the most studied target for brain drug delivery [74], a recent study demonstrated a more efficient shuttle to the mouse brain with prolonged retention of the bsAb in the brain, by targeting the heavy chain of the L-type amino acid transporter 1 (LAT1) [75].

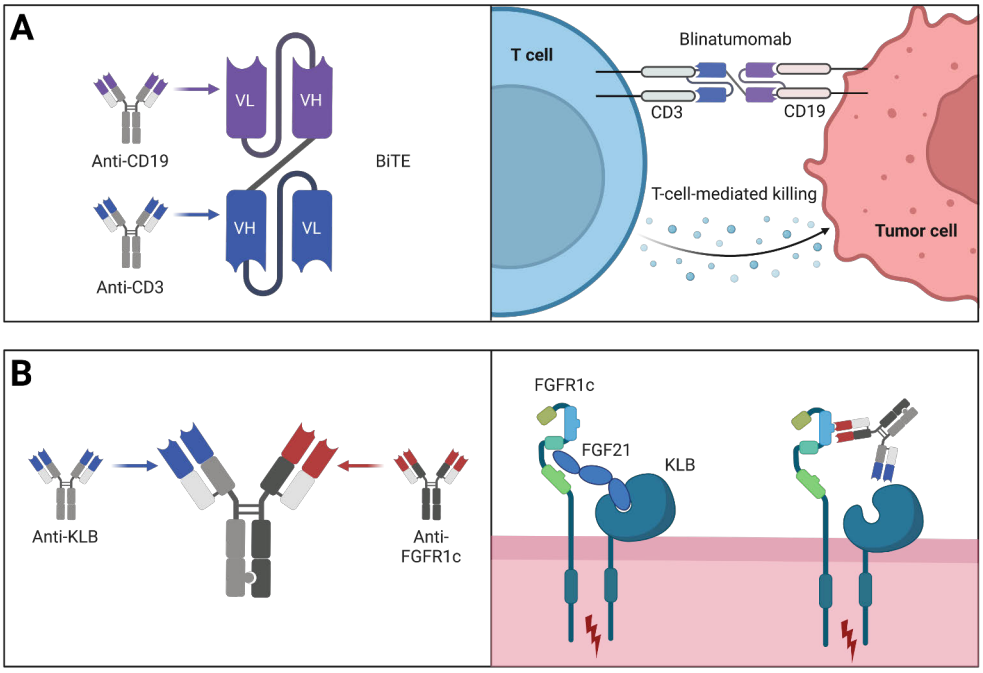

Figure 7. Functions of bispesific antibodies. **A**) *In-trans* bsAbs physically cross-link two cells, usually to elicit tumor cell destruction by effector cells. Blinatumomab BiTe is formed by fusing lymphoma-targeting anti-CD19 scFv with a T-cell-targeting anti-CD3 scFv. Blinatumomab physically cross-links lymphoma cells with T-cells, eliciting T-cell-mediated tumor killing. **B**) *In-cis* bsAbs target two antigens expressed on the same cell. Fibroblast growth factor 21 (FGF21) binds to FGF receptor 1c (FGFR1c) and its coreceptor β-Klotho (KLB), activating a metabolic pathway. A bispecific anti-KLBxFGFR1c antibody mimics FGF21 by bringing KLB and FGFR1c in close proximity, activating the metabolic pathway without the adverse effects associated with the administration of recombinant FGF21 protein. Created with BioRender.com

2.2.2.2 Antibody drug conjugates

Antibody drug conjugates (ADC) are mAbs that are covalently conjugated to cytotoxic chemicals (known as payload) via synthetic linkers. ADCs combine the antitumor potency of highly toxic small molecule drugs with the selective targeting and pharmacokinetic properties of mAbs. ADCs aim to increase the therapeutic window – reducing off-target toxicity and increasing the maximum tolerated dose of the toxic small molecule drugs by targeting it to the tumor cell via an antibody. In addition to the targeted drug delivery, ADCs can also elicit other mAb-typical mechanisms of action like signal disruption and Fc-mediated effector functions (**Figure 8**). The first FDA-approved ADC, gemtuzumab ozogamicin, gained market access in 2000, but was withdrawn due to no improved survival and higher rate of fatal toxicity than chemotherapy alone [76]. Although the two second generation ADCs were approved in the early 2010s, subsequent advancements in the development of next-generation ADCs have made significant progress across all five components of the ADC: the target antigen, the mAb, the linker, the conjugation strategy, and the payload [77]. Nowadays ADCs are one of the fastest-growing classes of oncology therapeutics, with already eleven ADCs approved by the FDA [78] and more than 100 in the clinical development [79].

The selection of the target antigen for ADC treatment requires several considerations. First, as the ADC is highly toxic, the target antigen should ideally be highly expressed in tumors and have little or no expression in normal tissue, to reduce off-target toxicity [80]. Second, as with all mAbs, the target antigen should be expressed on the cell surface to be accessible to the circulating mAbs. Third, the target antigen should be an internalizing antigen to allow transportation of the ADC inside the cell, where the payload is released to exert its effect. Additionally, the antibody's affinity against the target must be carefully assessed. Inadequate affinity may hinder effective internalization, while excessively strong affinity can lead to suboptimal tumor tissue penetration and distribution, constraining efficacy [81]. Notably, antibodies against the same target may exhibit varying internalization based on the epitope. Achieving increased crosslinking, as seen with biparatopic antibodies, can enhance internalization [70,82]. Many ADCs are developed against targets that are already well-validated with naked mAbs, but they are also being developed against novel indications for which there are no effective treatment options available [83].

Most of the payloads used in the clinical ADCs are microtubule binding or DNA damage-inducing agents with high potency [79]. Having a high drug-to-antibody ratio (DAR) increases the efficacy of the ADC, but may compromise on the stability, as many of the payloads are hydrophobic, increasing the tendency of the immunoconjugate to aggregate [84]. The selection of the payload also determines if the ADC has a bystander effect or not. Bystander effect means the diffusion of the

cytotoxic drug to the neighboring cells, killing them. As solid tumors often express the target antigen in a heterogeneous manner, having bystander effect is often desired for completely eradicating such tumors [85]. The potency of the bystander effect is determined by the charge of the linker-payload derivative released from the ADC, as charged molecules cannot passively cross the cell membrane [86].

The function of the linker is to ensure that the payload remains bound to the antibody during circulation but is released at the tumor site. The premature release of the drug can cause systemic toxicity and a lower therapeutic index. Effective linker design needs to balance between good stability in the circulation for several days, and rapid cleavage upon delivery into the target cell [77]. The linker can either be cleavable or non-cleavable. Cleavable linkers release the payload on reduction, proteolysis, or hydrolysis inside the tumor cell (due to e.g., proteases or pH), but non-cleavable linkers require complete lysosomal degradation for the payload release [79]. The non-cleavable linker provides more stability, leading to a better safety profile, compared to cleavable linkers, but can reduce the potential for bystander effect.

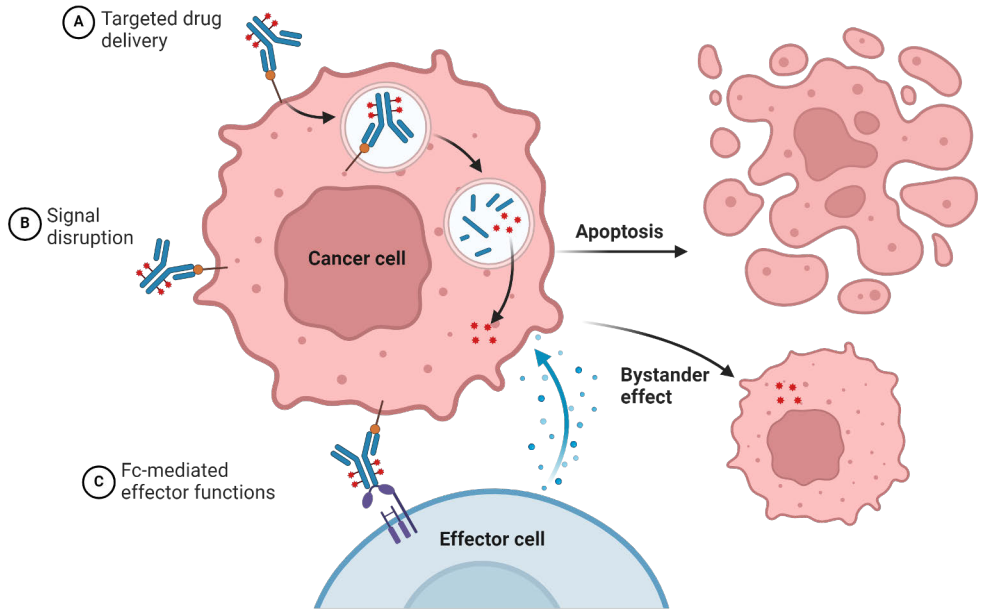

Figure 8. Mechanisms of action for antibody drug conjugates (ADC). ADCs usually target tumor-associated antigens that internalize upon antibody binding. The internalization facilitates the release of the payload inside the cell, inducing apoptosis. Depending on the charge of the linker-payload, it can elicit a bystander effect, killing neighboring cells. The bystander effect is often desired as tumors may have heterogenous antigen expression. In addition to targeted drug delivery, ADCs can block tumor signaling and elicit Fc-mediated effector functions. Created with BioRender.com

Traditionally, conjugation of linker-payload to an antibody takes place at solvent-accessible reactive amino acids such as lysines or cysteines derived from the reduction of inter-chain disulfide bonds in the antibody [87]. This results in heterogeneity of an ADC mixture by two levels; the ADCs differ in drug load and conjugation site, which both can influence the *in vivo* pharmacokinetic properties of the molecules. To address this challenge, site-specific conjugation strategies have been developed utilizing e.g., engineered cysteines [88], unnatural amino acids [89], enzyme-assisted ligation to a site-specifically tagged protein [90] and glycan remodeling and glycoconjugation [91].

2.2.2.3 Fc engineering

Advancements in antibody effector function engineering, such as the introduction of point mutations to the Fc region [92,93] or modification of glycosylation [94,95] have improved the efficacy and safety of therapeutic antibodies. The purpose of these mutations is to influence the affinity of different Fc interactions [96] (**Figure 9**). Effector functions are more effective with highly expressed target antigens with low rate of internalization.

In cases where tumor cells exhibit insufficient target antigen expression and cannot trigger effector functions through a regular antibody Fc, these functions have been enhanced by introducing mutations in the Fc region. These mutations improve the affinity towards activating FcγRs, leading to increased ADCC and ADCP [97]. Furthermore, mutations in the Fc region improving affinity towards C1q have been introduced to enhance CDC, leading to increased cytotoxic potency [98]. Moreover, antibody afucosylation has demonstrated increased Fc affinity for FcγRIII receptors, leading to enhanced NK cell-mediated killing and ADCP [99]. This concept was promptly implemented in clinical settings [100].

In certain therapeutic contexts, effector functions, as observed in bsTCEs, may be considered undesirable [56]. The anti-tumor activity of bsTCEs relies on the direct killing of tumor cells by T-cells, making effector functions non-essential. The inclusion of effector functions in bsTCEs may lead to unintended side effects, such as cytokine release syndrome, neurotoxicity, and immunogenicity [101]. Frequently, IgG2 and IgG4 subclasses are utilized due to their minimal binding to most FcγRs [102], but complete effector silencing can be achieved only through Fc engineering.

The removal of the Fc N297 glycan by mutating the glycosylation site attenuates but does not entirely abolish ADCC and ADCP [103]. However, glycan removal may lead to antibody aggregation [104], resulting in anti-drug antibody formation, as evidenced by the clinical antibody Atezolizumab [105]. Alternatively, mutations in the lower hinge, such as L234A/L235A (known as LALA mutation), disrupt the FcγR binding site [106], leading to significantly reduced cytokine release [107].

The addition of P331S mutation in the C_H2 results in an almost complete loss of binding to several effector molecules [108]. Furthermore, the introduction of L248E mutation can fully remove the binding to FcγRs and C1q without affecting the binding the neonatal FcR (FcRn) [109].

The long half-life of antibodies is attributed to the recycling of endocytosed antibodies back to the plasma membrane via the FcRn. The FcRn binds to the antibodies at high affinity only at an endosomal pH of 6.0 and not at physiological pH of 7.4. Following endocytosis, the IgG in acidic endosomes binds FcRn and is recycled back to the plasma membrane, where it is released at the physiological pH of the extracellular space, protecting the IgG from lysosomal degradation [110]. Mutations to the Fc have been introduced, which promote the FcRn binding at endosomal pH but have no detectable affinity at physiological pH, significantly improving the half-life of the IgG [111]. These Fc mutations are utilized in sweeping antibodies by Chugai Pharmaceuticals, which are designed to eliminate soluble antigens from the circulation by having pH-dependent binding of both the antigen and the Fc [112].

Fc engineering is also employed for generating novel bispecific antibody formats. A widely employed bispecific format, known as knobs-into-holes, incorporates a single point mutation in the C_H3 domains of the heavy chains, aiming to enhance heterodimerization efficiency. The “knob” variant features a T366Y mutation, while the “hole” variant includes a Y407T mutation. These mutations significantly improve heterodimerization, achieving up to 92%, in contrast to 57% heterodimerization observed with the wild-type C_H3 [113]. Another bispecific format, called DuoBody, utilizes post-production separation and exchange of Fab-arms to form bispecificity [114]. The DuoBody works by expressing two separate IgG1 antibodies with two matching point mutations, K409R and F405L, one in either IgG1, at the C_H3:C_H3 interface. The IgG1s are subsequently mixed and the disulfide bonds are reduced, allowing the recombination of the heteromeric heavy chain-light chain pairs, driven by the introduced mutations, followed by reoxidation of the interchain disulfide bonds [115].

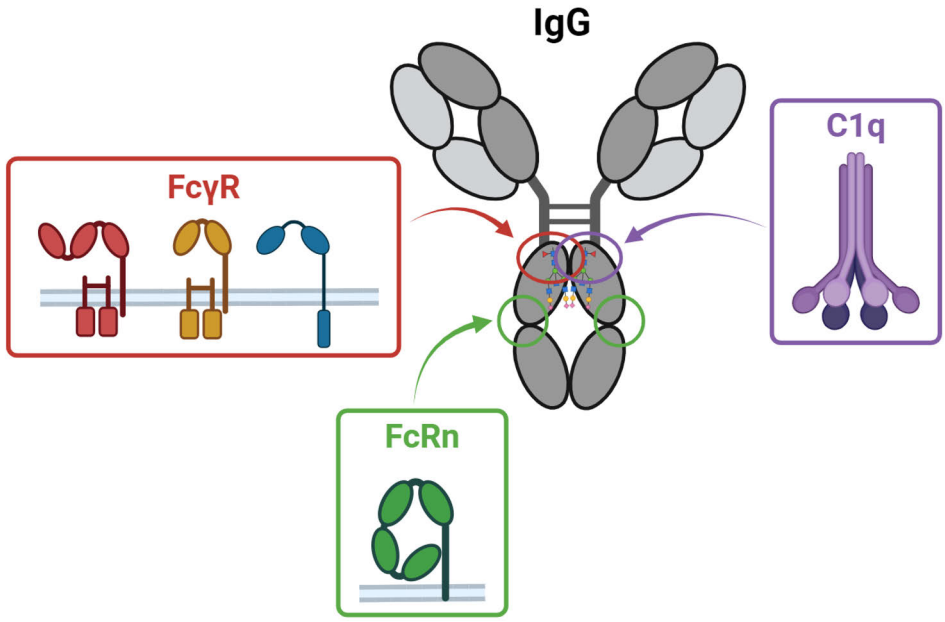

Figure 9. IgG Fc interactions can be modified by Fc engineering. Introduction of point mutations in the lower hinge region can modulate the affinity of Fcγ receptors (FcγR) and C1q, affecting the effector functions. The neonatal Fc receptor (FcRn) binds to the two histidines at the C_H2:C_H3 interface, making the interaction pH-dependent [96]. Created with BioRender.com

2.2.3 Developability of therapeutic antibodies

Traditionally, most drug candidates are initially screened and selected solely based on affinity and functionality. The binding of the therapeutic antibody to its defined target antigen attains the desired biological modification in a cell, which is usually considered to be the most important property of a therapeutic antibody. Often less attention is paid to other biophysical properties of the antibody, such as high-level expression, high solubility, covalent integrity, conformational and colloidal stability, low poly-specificity, and low immunogenicity [116]. In a study by Jain et al., 137 clinical-stage antibodies, including 48 approved therapeutic antibodies, were assessed for their biophysical properties [116]. The number of antibodies with biophysical liabilities was significantly lower in the later stages, suggesting that many clinical candidates face an expensive late-stage failure due to their biophysical properties. Aggregation propensity and polyspecificity in particular were identified as the most correlated with a product failure [117]. Thus, the concept of developability used to define the suitability of a candidate mAb to be developed as a successful

drug, and the ability to screen for optimal biophysical properties at the early stages of therapeutic antibody discovery are crucial [118].

The generation and selection of developable antibodies require methodologies such as *in silico* analysis and high-throughput screening throughout the early stages of antibody discovery and engineering. *In silico* analysis includes the identification of sequence liabilities, which have the potential to lead to unwanted post-translational modifications (PTM) or degradation [119]. These include asparagine deamidation, aspartate isomerization, methionine oxidation, tryptophan oxidation, unpaired cystines, and glycosylation motifs in the variable domains, which can lead to decreased affinity, increased heterogeneity, and increased immunogenicity.

In addition to sequence-based *in silico* analysis, structure-based methods for the identification of aggregation-prone regions have been developed [120–123]. They utilize the crystal structure of the antibody or model the 3D structure based on a closely related antibody, to construct an aggregation propensity function using the distribution of hydrophobic and electrostatic patches on the protein surface. The spatial aggregation propensity can also be used to guide the rational design of point mutations to reduce the aggregation [124] or to guide the design of an antibody library [125–127].

Evaluating the developability properties of numerous antibody candidates is a laborious yet crucial task for informed candidate selection. The developability properties assessed experimentally during the antibody discovery and engineering phase are listed in **Table 1**. Typically, the screening and elimination of antibodies with suboptimal developability are carried out sequentially, giving priority to higher-throughput methods, which reduces the number of antibodies analyzed in the subsequent lower-throughput methods.

Antibody colloidal stability, which refers to the stability of the protein in its native structure in solution to remain monomeric and avoid aggregation, precipitation, or phase separation, is one of the key biophysical properties to consider when developing high-concentration mAb formulations [128]. Measuring antibody solution behavior in different formulations using methods such as polyethylene glycol (PEG) induced precipitation assay, viscosity, and opalescence measurements can be laborious [129]. Therefore, high-throughput methods for assessing the propensity for low colloidal stability have been developed [130].

Affinity-capture self-interaction nanoparticle spectroscopy (AC-SINS) simulates high-concentration antibody solutions by capturing monoclonal antibodies on the surface of gold nanoparticles. The high local concentration of antibodies on the nanoparticles induces self-interaction of aggregation-prone antibodies, which can be detected by a plasmon wavelength shift of the gold nanoparticles. This shift can be easily measured using a standard plate reader with a monochromator [131]. It has been shown that self-interaction measured by AC-SINS correlates with solubility

and other biophysical properties[132], as well as fast plasma clearance [133], indicating that weak self-interactions detected with AC-SINS can manifest themselves in different ways and lead to complex biophysical behaviors.

Another method for assessing the solubility and colloidal stability of antibodies is cross-interaction chromatography (CIC), which measures the interaction between the therapeutic antibody candidate and a chromatography resin with immobilized monoclonal or polyclonal antibody [134,135]. The retention time in CIC has shown a significant correlation with the aggregation propensity and solubility of the antibody.

The measurement of the diffusion interaction parameter (k_D) has been shown to correlate well with solution behaviors, such as opalescence and viscosity at high concentrations, making it ideal for identifying antibodies suitable for high-concentration formulation [129]. Although the measurements can be done using dynamic light scattering (DLS), the low throughput and the amount of purified antibody required however make the assay unsuitable for early screening.

Therapeutic mAbs must withstand storage for several years. Throughout manufacturing and storage, these antibodies are exposed to various stresses, ranging from rapid changes in temperature and pH to high concentration and mechanical strain, all of which can lead to denaturation or aggregation[136]. These physical instabilities can result in loss of activity and more importantly, an increased potential for immunogenicity [137]. The product storage stability can be assessed by measuring the conformational stability of the mAb. Conformational, or thermal stability is defined as a change in Gibbs free energy between the native and denatured state [138], and can be evaluated using methods such as differential scanning fluorimetry (DSF) or differential scanning calorimetry (DSC).

The binding specificity of mAbs can be categorized into polyspecificity and polyreactivity [139]. Polyspecificity refers to antibodies exhibiting significant off-target reactivity with structurally and/or functionally different targets. This characteristic has been associated with faster plasma clearance and unpredictable toxicity [140,141]. The assessment of polyspecificity is required by the FDA prior to human clinical trials and is usually performed by protein or cell microarrays [142].

In the context of natural antibody repertoire, polyreactivity is often defined as the ability of a mAb to bind various unrelated self and foreign antigens. The property is often attributed to a conformationally flexible antigen binding pocket, which gets more rigid and consequently less polyreactive during affinity maturation [143]. In the therapeutic context, polyreactive mAbs can exhibit undesirable low-affinity interactions with extracellular matrix components or cell membranes through nonspecific interactions. These interactions, often resulting from excess positive charge or hydrophobicity in the variable regions of the antibody, can significantly impact the pharmacokinetics and bioavailability of antibody therapeutics [133].

Table 1. Developability properties screened for during antibody discovery and engineering.

Developability property	Method	Rationale
Affinity	SPR, BLI, ELISA, flow cytometry	Measurement of the binding strength to cells or recombinant human and toxicology species target protein
Functional activity	*In vitro* functional assays with engineered cell lines or primary cells	Measurement of the drug's potency in the target cells
Binding specificity	Polyreactivity ELISA, protein microarrays, SPR, BLI	Measurement of non-target binding and binding to homologous proteins that present sequence or structural similarities with the target of interest. Off-target binding could lead to fast plasma clearance or off-target effects
Sequence and epitope diversity	*In silico* sequence clustering, epitope binning with SPR, BLI, or ELISA	Broad epitope coverage is needed in the discovery phase to discover candidates with desired functionality
Colloidal stability/self-interaction	AC-SINS, DLS, viscosity screening	AC-SINS and DLS can be predictive of a higher risk of aggregation or increased viscosity at high concentration
Hydrophobicity	HIC, SMAC	High retention time is indicative of surface hydrophobicity which might correlate with an increased risk of aggregation or nonspecific binding
Solubility	0-40% PEG	PEG-induced protein precipitation can extrapolate apparent protein solubility. High solubility is needed especially for drugs administered through subcutaneous injection
Thermostability/ conformational stability	Tm/Tagg: DSF, DSC	Low Tm could be indicative of poor storage stability
PTM/Chemical stability	Assessment of sequence liabilities in CDR regions by *in silico* analysis and peptide mapping (MS)	Oxidation, deamidation, isomerization, and glycosylation in CDR regions can impact binding and function. Free cysteines can cause aggregation
Aggregation and fragmentation of stressed samples	SEC-MALS, CE-SDS, intact mass, sub-visible particles	Stressed (e.g., elevated temperature, high and low pH, freeze/thaw) sample analysis can be predictive of long-term stability, fragmentation can impact potency and increase aggregation rate.
Isoelectric point assessment and charge heterogeneity	Calculated pI, icIEF	pI outside the 7-9 range may result in losses during purification and challenges with viral inactivation and formulation.
Expression titer	BLI, Protein A HPLC methods	Low expression titer increases the cost of manufacturing

In vitro antibody discovery methods have been criticized for generating antibodies with significantly more developability issues in comparison to animal-

derived antibodies [144]. This arises from the fact that in most *in vitro* display methods, the selection pressure is directed towards affinity, with limited weight for other developability properties. Addressing this challenge, a recently developed mammalian cell-based display technology has showcased the capability to selectively enrich antibodies with superior biophysical properties during the library selection for functionality [125,126,145]. This pre-selection through mammalian cell display reduces the number of antibodies requiring experimental assessment for developability, thereby reducing the overall development timeline.

2.3 Therapeutic antibody discovery and engineering

The predominant approach in generating therapeutic antibodies has traditionally relied on utilizing the immunological processes inherent in nature, commonly referred to as *in vivo* antibody discovery [144]. This method, which involves immunizing animals, has been employed for over 120 years [146]. Additionally, the production of monoclonal antibodies through hybridoma technology has been established for nearly half a century [25], indicating the well-established nature of associated workflows. While antibodies generated *in vivo* benefit from undergoing the intricate process of *in vivo* antibody maturation, this approach relies on the immune system of the animal, thereby restricting researchers' control over the antibody generation process.

In vitro antibody discovery refers to the process of identifying antibodies using recombinant antibody repertoires and *in vitro* display technologies, eliminating the need for sacrificing animals for antibody discovery [147]. The basic principle in *in vitro* display platforms is to display large immunological diversity contained in the variable regions of the antibody, linking the phenotype (antibody binding) to the genotype (gene encoding the antibody). The use of *in vitro* methods for antibody discovery has been recommended by the EU due to ethical reasons concerning unnecessary animal consumption [148].

A third option for antibody discovery is *ex vivo* antibody discovery using single B-cell technology [149]. In single B-cell technology, the antibody encoding genes are isolated from antigen-specific B-cells of animal or human donors, retaining the V_H and V_L chain pairing.

Each of the strategies for antibody discovery has its strengths and weaknesses, which are elucidated below. The selection of the optimal discovery strategy is related to the type of antigen, costs, know-how, and access to the technologies. The discovery forms the basis for the therapeutic antibody development workflow, which is followed by engineering, characterization, and production, eventually leading to clinical candidate selection and clinical trials (**Figure 10**).

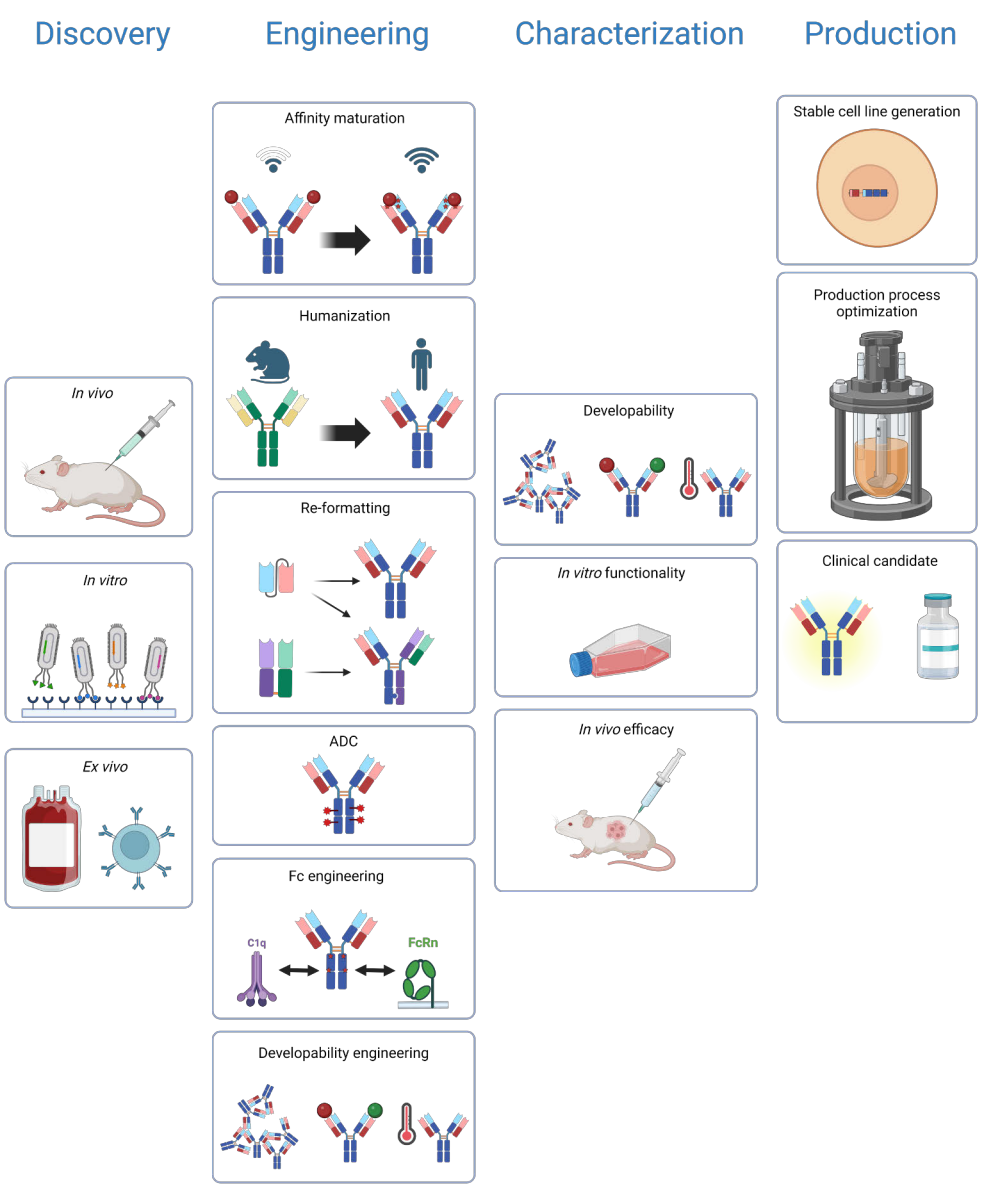

Figure 10. Therapeutic antibody development workflow. The selection of the optimal antibody discovery strategy depends on the therapeutic target, know-how, and technology availability. The identified hit antibodies usually require further reiterative engineering and characterization to match the target product profile. Once a candidate molecule has been identified that ranks well in biophysical characterization, shows adequate *in vitro* functionality in cell models, and *in vivo* efficacy and safety in pre-clinical mouse models, a stable cell line development is initiated, eventually leading to the production of a clinical therapeutic antibody. Created with BioRender.com

2.3.1 *In vivo* antibody discovery

In vivo monoclonal antibody discovery typically starts with the immunization of animals, such as mice or rabbits, with a selected antigen. This process involves a series of injections over a period of several weeks to stimulate B-cell differentiation into plasma B-cells and memory B-cells [150]. To generate antibodies against the antigen, the antigen must be immunogenic, or it must be modified to increase the immunogenicity, which has the possibility of leading to structural changes in the antigen. The lack of control over the antibody response can bias towards immunodominant antigenic regions, limiting sequence and epitope diversity [144]. One benefit of *in vivo* antibody discovery is that it can also be done without access to purified antigens when using DNA immunization [151], which is especially useful when raising antibodies against antigens that are difficult to express and purify recombinantly in their correct native form e.g., transmembrane proteins.

Following the immunization, the animal is sacrificed and the activated B-cells are isolated from the spleen using density gradient centrifugation [150]. The presence of antigen-specific antibodies is usually confirmed at this stage using methods like enzyme-linked immunosorbent assay (ELISA). The isolated B-cells are next fused with myeloma cells to immortalize them, leading to hybridoma cells producing antibodies [25]. As the hybridoma fusion rate is only about 1 to 2%, the fused cells are selected from unfused cells with selection media, taking about 10-14 days [150]. Next, the hybridoma cells are cloned using e.g., limiting dilution. The hybridoma cells secrete the antibodies to the supernatant, which can then be screened for antigen binding using ELISA.

Animal-derived antibodies may be immunogenic because of their non-human origin, leading to their fast elimination by the patient's immune system. This can lead to allergic reactions and hinder the ability of the patient's immune system to initiate effector functions in response to the animal Fc region [152]. One of the techniques that has advanced the development of therapeutic antibodies is the generation of humanized antibodies by the CDR grafting technique [153]. In CDR grafting, non-human antibody CDR sequences are transplanted into a human framework to maintain target specificity. Humanization of antibodies mitigates the immunogenicity of the therapeutic agents, allowing the treatment of diseases that require long-term treatment, such as cancer, chronic pain, and especially autoimmune diseases [154].

The first humanized mAbs entered clinical development in 1988 [155] and the first humanized mAb, daclizumab, was approved by the FDA in 1997 [156]. Daclizumab was created by using a combination of CDR grafting and a human framework that is maximally homologous to the murine framework to minimize the loss of antigen specificity [157]. It is known that often amino acids in the framework are crucial to maintain antibody binding activity. These residues may be involved in stabilizing

the CDR loops to form the antibody paratope, or directly interact with the antigens [158]. Framework mutations in animal-derived monoclonal antibodies introduced during affinity maturation by SHM may present an extra challenge in the humanization and de-immunization process, resolvable by testing a variety of clones with "back mutations" that are closer to naturally occurring human germline sequences.

The main benefit of *in vivo* antibody discovery is that the isolated antibodies have gone through the complex *in vivo* antibody maturation process and negative selection to eliminate autoreactive binders. This process ensures that a large proportion of the obtained antibodies have a high affinity against the used antigen. The drawbacks of the hybridoma technology are the time-consuming sequential antigen injections and the low number of successfully generated hybridoma cells, limiting the obtained antibody diversity.

The emergence of high-throughput DNA sequencing (next-generation sequencing, NGS) has enabled the exploitation of immune repertoire sequencing in antibody discovery [159]. Immune repertoire sequencing aims to bioinformatically identify enriched V_H and V_L regions from immunized donors without prior wet-lab screening. The enriched V_H and V_L regions can be subsequently combined based on their relative frequency to identify novel binders. This eliminates the need for hybridoma generation, massively increasing the analyzed diversity.

2.3.1.1 Transgenic mice

Transgenic mice present a technology for obtaining fully human mAbs by immunization. The technology was introduced in 1994 by the publication of two transgenic mouse lines, the HuMAb mouse [160], and XenoMouse [161]. Both of the lines were genetically modified such that human Ig genes were introduced into the genome, replacing the endogenous mouse Ig genes, thus making the animals capable of producing fully human antibodies upon immunization [162]. The HuMAb had an 80 Kb DNA segment encoding human IgH locus genes integrated into the mouse genome, which consists of only 6% of the total human IgH locus genes. A similar proportion of the human Igκ locus was integrated into the genome. Since most of the antibody diversity comes from the recombination of the germline V(D)J genes, the antibody diversity obtained from the HuMab was low.

A competing strategy used yeast artificial chromosome (YAC) vectors to integrate 800-Kb of Igκ locus genes and 970-Kb of IgH locus genes into mouse embryonic stem cells and crossing the human Ig mouse with murine IgH and IgL knockout mice to generate the XenoMouse [163,164]. The XenoMouse contained approximately 80% of the human V_H and V_κ gene repertoire, thus succeeding better in generating more diversity than the HuMab mouse [165]. While the development of

the XenoMouse lines had expanded the inclusion of human Ig genes in mice, the efficiency of human antibody generation, Ig class-switching, and somatic hypermutation remained low due to the random integration site of the Ig genes in the mouse genome and the lack of modulatory signaling between the human Fc and mouse BCR coreceptors [166]. The second generation of humanized mice thus retained the mouse Ig constant regions and only replaced the mouse variable genes with human variable genes, achieving a humoral immune response indistinguishable from that of wild-type mice. The constant region of the resulting chimeric antibody can easily be replaced with the use of recombinant DNA technology to create a fully human antibody [158].

The generation of antibodies against self-antigens has remained a challenge with transgenic mice. To circumvent this, researchers have made mouse strains where non-essential genes encoding targets of interest have been knocked-out to enable the generation of antibodies against them [167]. A similar strategy can be utilized to generate antibodies against human proteins with high sequence homology to the analogous mouse protein, increasing the chances of obtaining cross-reactive antibodies that recognize the target both in humans and in preclinical mouse disease models.

The first human antibody generated in a transgenic mouse was an anti-epidermal growth factor receptor (EGFR) antibody, panitumumab, which was approved by the FDA in 2006 [168,169]. It was developed using the XenoMouse technology [168]. The number of approved therapeutic fully human antibodies developed using transgenic animals has increased rapidly, with the number of approved drugs in 2018 at 19 [158].

2.3.2 *Ex vivo* antibody discovery: single B-cell technology

The antibody responses in the human immune system are robust, neutralizing, highly specific, and self-tolerant. Isolation of antigen-specific mAbs from matured human B-cells of pathogen-exposed individuals is an attractive approach for therapeutic antibody development [149].

MAbs can technically be isolated and generated from any type of naïve or antigen-exposed B-cell type, as they all contain V(D)J rearranged Ig genes [170]. In humans, the most commonly used B-cell subsets are memory B-cells and plasma cells as they can be readily extracted from the blood of healthy donors or patients [171]. Depending on the cell type, the antibody discovery can essentially be divided into two approaches: analysis of the membrane-bound BCR and analysis of the B-cell secreted antibody [172].

The isolation of B-cells expressing antigen-specific BCR can be done by staining the cells with a fluorescently labeled antigen and using fluorescence-activated cell sorting (FACS)[173] or by using antigen-coated magnetic beads [174] in a process called

antigen baiting. After the B-cell isolation, the amplification of each Ig heavy chain and corresponding light chain can be performed by reverse transcription-polymerase chain reaction (RT-PCR). By using the mRNA of a single B-cell as the template for each RT-PCR reaction, the DNA encoding the antibody can be cloned into a mammalian expression vector for recombinant expression, maintaining the chain pairing [173]. Maintaining the correct heavy chain and light chain pairing is important, as "shuffling" the chain pairing from a diverse pool of binders can generate many clones with reduced affinity or specificity, which must be eliminated through screening.

The analysis of antibody-expressing plasma cells requires specialized equipment and technology. Several different technologies have been developed for this purpose, including micro-engraved microwells [175], microdroplets [176], microfluidic chambers [177] and microcapillary devices [178]. They all work by isolating single cells in tiny compartments and subsequently analyzing the antigen specificity of the secreted antibody using various immunoassays. The cells of interest can then be isolated for clonal expansion or antibody gene retrieval using RT-PCR.

The single B-cell technologies are especially useful for the development of therapeutic antibodies against viruses, as neutralizing antibody sequences can be obtained directly from the B-cells of vaccinated human donors [179] or convalescent individuals [180]. There are currently several single B-cell technology-derived virus-targeting mAbs approved and in clinical trials, including mAbs against the Ebola virus [181], HIV [182], different influenza viruses [183–186], respiratory syncytial virus (RSV) [187,188] and SARS-CoV-2 [189–191].

2.3.3 *In vitro* antibody discovery

In vitro antibody discovery utilizes the selection of desired antibodies from large recombinant antibody repertoires using *in vitro* display technologies. The isolation of the desired antibody relies on the linkage of the antibody of interest (i.e., the phenotype) to its genetic information (i.e., the genotype). The phenotype-genotype coupling allows for "barcoding" of up to several billion different antibody variants from where specific binders can be selected through high-throughput isolation in an iterative process. Several different display technologies are available today, including phage display, yeast surface display, ribosome display, and mammalian display, each having its own strengths and weaknesses and use cases [192].

The discovery of antibodies with *in vitro* methods requires the construction of antibody libraries. In principle, the libraries can be divided into immune libraries and universal libraries. Immune libraries can be constructed by isolating the antibody sequences from the blood or tissues of immunized animals [193,194]. When using animal-derived immune libraries, the antibodies need to be later humanized, if intended for therapeutic use. Another option is to use transgenic animals for

immunization to build fully human immune libraries [195]. Moreover, immune libraries can be generated by isolating antibody genes from B-cells of humans who have either been vaccinated [196] or who have suffered from a disease [197]. These types of libraries contain antibodies that have gone through the complex *in vivo* antibody maturation process, thus having a high affinity towards the antigen of interest. However, immune libraries are usually only applicable to the antigen(s) used during immunization and thus must be constructed separately for new antigens.

On the contrary, universal libraries are designed for the isolation of antigen-specific antibodies against virtually any target. Universal libraries can be further divided into naïve, synthetic, and semi-synthetic libraries [198].

Naïve libraries utilize rearranged Ig V genes from the IgM mRNA of B-cells of unimmunized human donors [199]. This natural primary antibody repertoire contains a large array of antibodies that recognize a variety of antigens. As the gene sequences are derived from B-cells of human donors, the naïve libraries are relatively close to the human antibody germ line and thus have a low risk of immunogenicity [158]. Phage display was first used to discover sub-nanomolar fully human antibodies from a naïve antibody library constructed by using the V-gene segments from human donors already in the mid-1990s [200].

Synthetic libraries are designed to contain a limited number of frameworks, focusing on a predetermined level of randomization of CDR regions within the selected frameworks [201]. Synthetic libraries can be designed to maximize the functionality of the libraries e.g., by optimizing the library for better developability [202], using precise control of CDR loop length and amino acid composition.

Semi-synthetic libraries use a limited number of naïve variable regions, incorporating randomized synthetic CDRs, often focusing on randomizing only the CDR3 of heavy chains. The randomized CDR is thus combined with the naïve repertoire of other CDRs [203]. Currently, almost all commercially available phage display libraries are based on highly diverse non-immunized gene repertoires, which enables the selection of antibodies against virtually any antigen [204].

One of the key advantages of *in vitro* methods over *in vivo* methods for antibody discovery is the possibility of generating antibodies against self-antigens. Many therapeutic targets are self-antigens and since autoreactive antibodies (or BCRs) are eliminated during B-cell maturation, isolation of antibodies against self-antigens from a naïve library requires the random combination of the rearranged heavy and light chains during the library construction [192]. During an antigen encounter in the human body, the antibodies isolated from the naïve repertoire have a weak affinity against the target and require affinity maturation through SHM. Similarly, binders isolated from naïve libraries through *in vitro* methods often require further engineering to increase the affinity. There are several ways of performing *in vitro* affinity maturation, which are discussed in section 2.3.4.

2.3.3.1 Display technologies

2.3.3.1.1 Phage display

Phage display is the first and still the most widely used technology for *in vitro* antibody selection [158]. The technology was developed based on the work of George P. Smith in 1985 [205], who used recombinant DNA technology to fuse foreign peptides to the coat protein pIII of filamentous M13 bacteriophage to display the peptides on the bacteriophage surface. It was later discovered that the platform could be used to display fragments of antibodies to find antibodies with binding activity toward an antigen [206]. This revolutionary method was acknowledged by the scientific community by awarding George Smith and Sir Gregory Winter the Nobel Prize in Chemistry in 2018 [207]. Adalimumab (Humira) was the first fully human therapeutic antibody developed using phage display that was approved by the FDA in 2002 for the treatment of rheumatoid arthritis [208]. As of 2020, 70 phage display discovered monoclonal antibodies have entered the clinical trials and 14 have been approved [209].

In phage display, the antibody fragments, usually either single-chain fragment variable (scFv) or Fab, are genetically fused to the coat protein pIII of M13 bacteriophage (**Figure 11**). The phage can infect *Escherichia coli* (*E. coli*) bacteria, where it replicates and assembles into antibody-displaying phage particles. The purified phage particles are incubated with an immobilized antigen of interest in a process called biopanning, where unbound phage particles are washed away and clones with high affinity against the antigen are eluted and recovered. To achieve adequate enrichment, the biopanning is usually repeated 1-3 times with increasingly stringent conditions. The selected phage from each round is allowed to infect the bacteria to start the next biopanning round. The identified clones are eventually expressed, characterized by ELISA, and sequenced to assess the antigen-binding properties of the selected clones [210]. Due to the small size and high solubility of phage particles, repertoires of up to 10^{11} unique clones can be efficiently produced and displayed in a single library [211].

One advantage of phage display is the ability to perform the biopanning using whole cells instead of using only recombinant proteins [212]. This allows the discovery of antibodies against difficult-to-express membrane proteins as well as to select antibodies that may be internalized by mammalian cells [213,214], which is usually desired in e.g., ADC discovery [215]. As the phage display biopanning is an *in vitro* method, it allows precise control over the antibody selection process, thus enabling e.g., identification of antibodies against a certain epitope and species cross-reactive antibodies. Additionally, phage display has been used to identify antibodies with pH-dependent binding properties [216] and antibodies with increased thermal stability [217]. It also enables the identification of antibodies against both highly toxic and non-

immunogenic targets, which would not be possible to obtain using animal immunization [209]. The speed of phage display antibody discovery is also advantageous when identifying antibodies against novel or mutated pathogens e.g., in an outbreak of emergent infectious diseases, such as SARS-CoV-2 [218]. Currently, since most of the patents protecting phage display technology have expired [219], the technology is in widespread use in both academic and commercial laboratories developing antibodies for diagnostic and therapeutic purposes.

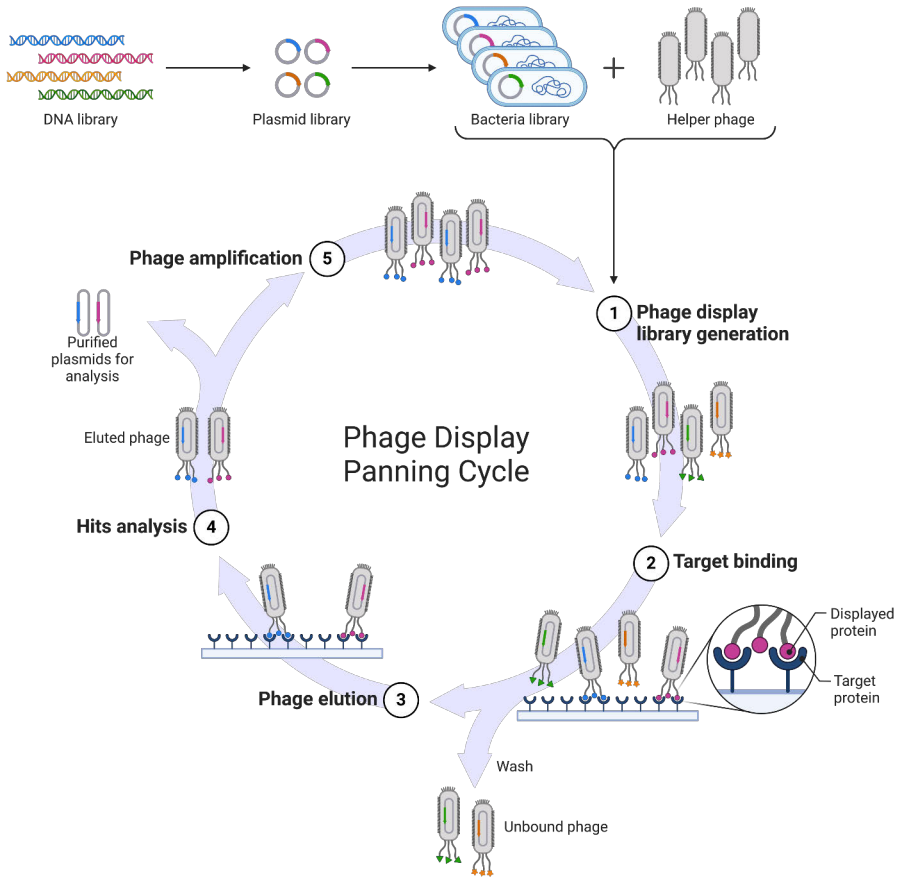

Figure 11. Phage display selection workflow. The antibody repertoire diversity is cloned into a phagemid plasmid, which is transformed into bacteria. Upon infection with a helper phage, the bacteria produce antibody-displaying phage particles. Through successive rounds of biopanning, phage particles displaying antibodies with affinity to the target protein are selected and used to infect bacteria for subsequent biopanning rounds. Eventually, the genes encoding the enriched antibodies are isolated, sequenced, and expressed for further characterization. Created with BioRender.com

2.3.3.1.2 Ribosome display

An alternative, completely cell-free *in vitro* display method, ribosome display allows the generation and screening of diversities in the range of 10^{12}-10^{13} variants [220]. Ribosome display is not limited by the transformation efficiency, as the antibody genes are transcribed and translated *in vitro*. The concept of ribosome display is simple: the displayed antibody gene is fused with a C-terminal spacer sequence without a stop codon, making the ribosome run to the very end of the mRNA molecule and not releasing from it [221]. The ribosomal tunnel is filled with the spacer sequence, allowing the antibody to fold properly while having adequate flexibility. This results in the formation of mRNA-ribosome-polypeptide complexes. The displayed antibodies can thus be biopanned similarly as with phage display and the genes encoding them can be retrieved by sequencing.

A limiting factor of ribosome display is the accessibility of functional ribosomes, usually derived from *E. coli* cell extract, limiting the library size [222]. Additionally, as the ribosome is attached to the translated mRNA, the displayed proteins are limited to a single polypeptide, limiting the display to single-chain antibody fragments e.g., scFv. Ribosome display also faces challenges in expressing and correctly folding complex eukaryotic proteins, compounded by the inherent instability of the mRNA-ribosome-protein complex, which can further impact the efficiency and reliability of the display system.

Ribosome display has been successfully used e.g., for isolating picomolar binders from a mouse immune library [223]. In this example, the antibody was hypothesized to incorporate a mutation during the ribosome display selection process due to the error-prone nature of the platform. This spontaneous mutation improved the affinity of the antibody 65-fold, exemplifying the applicability of ribosome display for antibody affinity maturation.

2.3.3.1.3 Yeast surface display

Another commonly used display platform, yeast surface display, utilizes the eukaryotic expression system by displaying antibodies on the surface of *Saccharomyces cerevisiae* [224]. The main advantage of using eukaryotic cells for antibody display is the more sophisticated quality control machinery for proper protein folding, enabling the engineering of more complex proteins compared to prokaryotic systems, and the ability to perform quantitative library analysis and screening by flow cytometry [225].

Yeast surface display works by fusing the antibody to the α-agglutinin complex subunit Aga2p. This subunit forms two disulfide bonds with Aga1p, which is expressed on the cell wall of the yeast cell, effectively tethering the expressed antibody on the yeast surface [226]. The main bottleneck of yeast surface display for

antibody discovery is its confined library size, which is in the range of 10^9 [227]. Consequently, yeast surface display has widespread applications in antibody engineering, including affinity maturation [228], isolation of high-affinity antibodies after animal immunization [194], and antibody humanization [229]. Moreover, yeast surface display has been used for engineering pH-dependent antibodies [230]. In certain instances, yeast surface display is utilized to select phage display "enriched" clones, combining the extensive naïve repertoire of phage display with yeast surface display's high-throughput FACS screening capability [231].

2.3.3.1.4 Mammalian cell display

Finally, displaying antibodies on the surface of mammalian cells has recently gained attraction, as it not only allows the selection of therapeutic antibodies in the production organism with eukaryotic post-translational modifications and human-like glycosylation [232,233], but is also able to select antibodies with good developability properties [125]. This is due to the mammalian cell's complex protein quality-control machinery that prevents the accumulation of misfolded, aggregation-prone, non-specifically sticky, or toxic polypeptides [234,235]. This inherent property of mammalian cells can be exploited in antibody engineering to select developable antibodies that are displayed at a high density on the mammalian cells, reducing the risk of expensive late-stage failure in drug development [126]. Another benefit of mammalian display over other *in vitro* display methods is the possibility to induce SHM via recombinant expression of AID in the cells displaying the antibody. This enables the affinity maturation of an antibody without the need for rational design of the library, as the clones undergo self-evolution [236].

Mammalian cell display of antibodies is typically enabled by genetically fusing the C-terminus of the antibody heavy chain constant region to a transmembrane domain of e.g., the murine H-2K^k protein [237], platelet-derived growth factor (PDGF) receptor [145] or CD8 transmembrane domain [126]. While transient transfection of the antibody genes has been historically used for the generation of mammalian cell libraries [238,239], stable integration to the host cell's genome is preferred as it allows multiple rounds of selection without the loss of genotype-phenotype coupling. Random integration of antibody genes to the genome via viral transduction [240,241], transposon technology [242] or episomal vectors [232,236], has the potential to display very large libraries, even in the order of 10^9 [237], thanks to the high integration efficiency. However, the above methods suffer from the possibility of integrating multiple antibody genes into a single cell negatively impacting the genotype-phenotype coupling. This can lead to erroneous combinations of heavy and light chains, which can result in the isolation of passenger antibody genes, thereby reducing the rate of enrichment of specific clones [145].

Random integration of antibody genes also has the downside of potential variation in transcription levels due to differences in the transcriptional activity of the integration sites. Conversely, site-specific integration of antibody genes has the advantage of transcriptional normalization, enabling the selection based solely on the properties of the displayed antibody. Several site-specific integration strategies have been used to create stable mammalian cell lines including the Flp/FRT system [243–246], nuclease-directed integration [125,145,247,248], and Bxb1 serine integrase mediated integration [249–253].

The Flp/FRT system relies on a pre-inserted genomic FLP recombinase target (FRT) site, where the gene is integrated via a strand exchange reaction catalyzed by FLP recombinase. The downside of the Flp/FRT system is that the reaction is reversible and able to introduce more than one transgene consecutively [145,251], negatively affecting its performance for library purposes.

Nuclease-directed integration of antibody genes commonly uses either transcription activator-like effector nucleases (TALEN) or clustered regularly interspaced palindromic repeats (CRISPR)/CRISPR-associated protein 9 (Cas9) -system to create a targeted double-stranded break in the genomic DNA. By flanking the antibody genes with DNA sequence homologous to the broken locus, the antibody genes are integrated into the cell's genome in a process called homology-directed repair (HDR) [145,254]. The nuclease-directed HDR approach does not require prior genomic modifications to the cell line, but is limited by the low transgene integration rate of usually <5% [145,248], which is a bottleneck for library construction.

Bxb1 integrase is a member of the large serine recombinase family and has been identified as the most accurate and efficient integrase for the integration of DNA into the human genome [255]. It is a 500 amino acid protein (56.2 kDa) isolated from mycobacteriophage Bxb1, which catalyzes the unidirectional and site-specific strand exchange between the bacterial attachment site (AttB) and phage attachment site (AttP), causing integration of the phage DNA into the genome of the bacteria [256,257]. Bxb1 integrase consists of a catalytic domain and DNA binding domain [258]. In its functional mechanism, it initially binds to a pair of attachment sites as a dimer, subsequently forming a tetramer that brings the DNA sites together in a synaptic complex [259]. Activation of all four subunits occurs simultaneously to cleave the DNA. Subsequent subunit rotation facilitates the exchange of the two DNA half-sites, rearranging them into a recombinant format. Ligation of the DNA backbone then produces the recombinant molecules.

Genomic integration of antibody genes into mammalian cells using Bxb1 integrase requires the generation of a cell line harboring a landing pad with Bxb1 integrase-specific attachment sites in an actively transcribed locus. The Bxb1 landing pad can be integrated into the cell genome in a defined locus using zinc finger nuclease [249], CRISRP/Cas9 system [250,251,253,260] or using a cell line with a pre-existing

FRT site [126]. Alternatively, it can be integrated pseudo-randomly using lentiviral vectors [252,261], as long as the copy number is subsequently verified to be one.

The landing pad for Bxb1 integrase usually contains two distinct AttB or AttP sites, which enable the recombinase-mediated cassette exchange (RMCE) [262]. Mutating the nonpalindromic central dinucleotide GT of the AttB and AttP sites prevents its ability to recombine with the wild-type AttP and AttB sites, respectively [263]. The directionality of the RMCE reaction with two distinct attachment sites can be controlled by making a compensatory GT to GA mutation to one of the two AttP and AttB sites [250].

To stably transfect the antibody library into mammalian cells with a Bxb1 landing pad, the antibody library is first incorporated into a targeting vector containing AttP or AttB sites flanking the antibody expression cassette (**Figure 12**). Co-transfection of the antibody library and a Bxb1 integrase expression vector induces the Bxb1 integrase to catalyze the RMCE reaction. This results in the integration of one copy of the antibody genes per cell into the landing pad in the genome. A selectable marker in the targeting vector facilitates the selection of cells with the correct integration [126].

FACS is used to select antibodies with favorable developability profiles, by selecting cells with the highest antibody display level and antigen binding level. Subsequent rounds of FACS typically involve lowering the antigen concentration to drive the selection towards higher affinity. Incubation with a non-labeled competing antigen helps eliminate clones with a rapid dissociation rate. After the selection, genomic PCR is used to extract the antibody genes, which are then cloned into a mammalian expression vector for subsequent expression, purification, and characterization.

A limitation of mammalian cell display is its constrained library size, typically around 10^8, restricting its utility primarily to antibody engineering, or enriched sub-library screening, rather than discovery from naïve libraries. Mammalian cell display's FACS selection works well with soluble protein antigens or virus-like particles but faces challenges with detergent-solubilized transmembrane proteins or whole-cell antigens, as the selection must be done in solution.

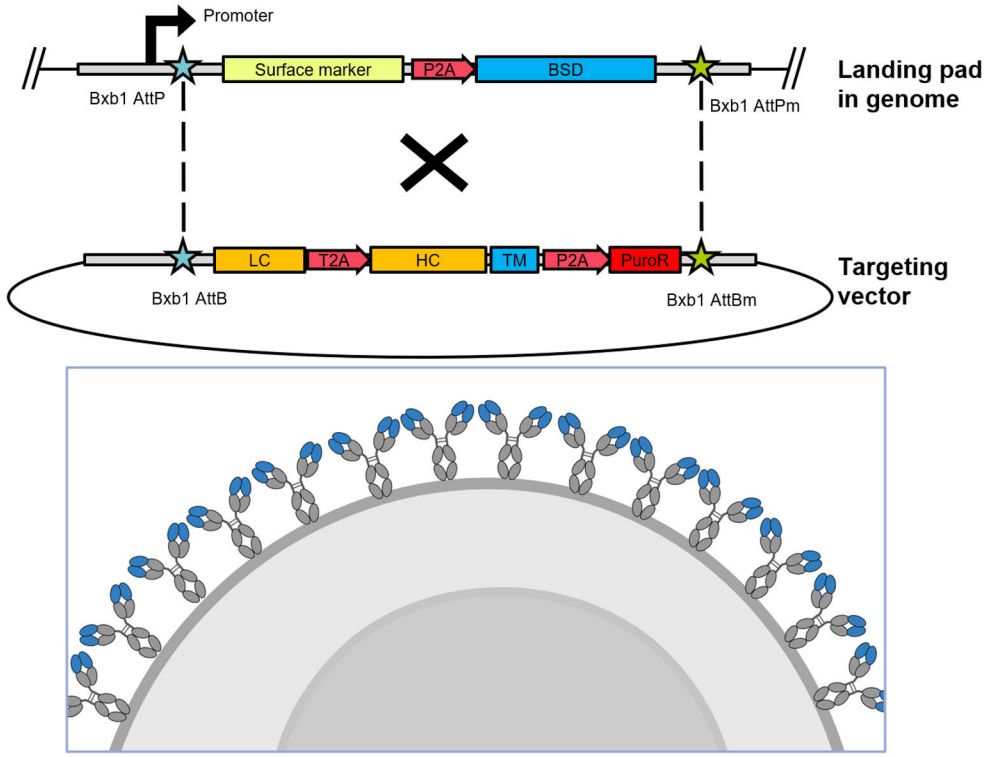

Figure 12. Antibody gene integration and expression using mammalian display with Bxb1 landing pad. The cell line contains a landing pad with a detectable surface marker and an antibiotic resistance gene e.g., blasticidin S deaminase (BSD), in the genome, flanked by two AttP sites, one of which has the central dinucleotide GT to GA mutation (AttPm). The targeting vector contains the light chain (LC) and heavy chain (HC) genes separated by e.g., a self-cleaving T2A peptide and a transmembrane domain (TM) anchoring the heavy chain to the cell membrane, followed by a different antibiotic resistance marker e.g., puromycin resistance gene (PuroR). The targeting vector expression cassette is flanked by Bxb1 AttB and AttBm sites to facilitate unidirectional recombinase-mediated cassette exchange (RMCE) between the cognate AttP and AttB sites upon co-transfection of the targeting vector and a Bxb1 integrase expression vector. After antibiotic selection, only cells with correct integration survive. Selection pressure for antigen binding and developability can be applied by selecting cells with the highest antigen binding and display level using FACS. Created with BioRender.com

2.3.4 *In vitro* antibody engineering

Monoclonal antibodies isolated from immunized animals generally often have high affinity towards the antigen used for the immunization, as the antibody has gone through the complex *in vivo* maturation and iterative SHM process during the immune response caused by the antigen encounter [144]. To turn the animal-derived antibody into a therapeutic agent suitable for humans, it has to be humanized using e.g., CDR grafting [153]. However, the humanization process may lead to a decrease in

affinity, often requiring additional affinity maturation [264]. On the other hand, antibodies derived from universal *in vitro* libraries, lacking the iterative SHM process, typically necessitate additional affinity maturation to achieve the desired affinity for the intended therapeutic functionality. During *in vitro* affinity maturation, a commonly used approach is to introduce mutations to the CDR regions and use progressively lower concentrations of the antigen in each successive round of panning to increase the selection pressure.

In addition to affinity, also other developability properties of therapeutic antibodies may need optimization after the discovery step. It has been reported that phage display in particular is prone to select antibodies with higher percentages of aliphatic residues in their paratopes, resulting in developability issues such as a high propensity for self-interaction and polyreactivity, which can lead to expensive late-stage clinical failure if not corrected in early development phases [265]. There are three main ways to do *in vitro* antibody engineering; random, semi-rational, and rational mutagenesis, which are discussed in the next sections.

2.3.4.1 *In vitro* antibody engineering by random mutagenesis

Random mutagenesis aims to mimic *in vivo* affinity maturation. There are several widely used methods for random mutagenesis, including error-prone PCR (epPCR) and DNA shuffling. DNA shuffling aims to combine different heavy and light chains, or different CDR regions, to mimic combinatorial diversity. EpPCR aims to introduce random mutations along the antibody sequence to mimic SHM. Performing affinity maturation using random mutagenesis has the benefits of being straightforward, inexpensive and it does not require structural information to guide the maturation library design.

EpPCR utilizes the natural error rate of a low-fidelity polymerase to introduce random mutations along the antibody variable regions, followed by the selection of improved variants using *in vitro* display technologies [266]. In a recent study, epPCR was used to improve the affinity of three antibodies directed against clinically relevant immuno-oncology targets. This was achieved by introducing mutations across the entire variable domain of the yeast-displayed scFv [267]. Notably, a comparable efficiency in affinity improvement was observed when comparing the epPCR random mutagenesis strategy, distributing the mutations across the entire V-region, to a semi-rational mutagenesis strategy. In the latter, mutations were targeted only to the CDR regions with a similar mutation rate. The random mutagenesis strategy with epPCR generated mutations also outside the CDR regions, which have the potential to rigidify the conformation of the CDR loops, improving the affinity [23]. However, while the introduction of random mutations across the variable domains of the antibody can lead to the identification of variants with improved affinity,

inevitably regions unrelated to the binding will also be mutated, which can lead to unstable antibodies with poor developability, requiring selection pressure or high-throughput screening to isolate antibodies with good developability [268].

Chain shuffling aims to improve the affinity of an antibody by combining one chain of the selected antibody randomly with a library of the other chains. In a study by Marks et al., the affinity of a hapten-binding antibody was improved 20-fold by combining the heavy chain with a repertoire of light chains obtained from unimmunized donors [269]. The affinity was further improved 15-fold by shuffling the CDR-H1 and CDR-H2, resulting in an affinity comparable to that of an antibody isolated from immunized mice.

In a more recent study, Teixeira et al. discovered an antibody from a naïve phage display library and subsequently affinity matured it using CDR shuffling [270]. The CDR shuffling involved shuffling of all CDR regions of the antibody, except CDR-H3, with natural CDR sequences from the same library, carefully purged from any sequence liabilities. The group was able to isolate 24 antibodies with picomolar affinity, all having the same epitope specificity and minimal polyreactivity.

2.3.4.2 *In vitro* antibody engineering by semi-rational mutagenesis

Semi-rational mutagenesis focuses the mutations on a defined region. The usual target regions for semi-rational mutagenesis are the three CDR regions in each variable domain, with CDR3 being the main target [271]. The targeted regions can be randomized through techniques such as site-saturation mutagenesis, employing degenerate primers to substitute the targeted amino acid with all possible 19 amino acids. Selection pressure is then applied to the library using *in vitro* display methods to select binders with the highest affinity. The size of the maturation library grows exponentially as the number of mutated residues is increased, which necessitates the use of sub-libraries, usually made separately for each CDR [272].

The strategies of sequential and parallel saturation mutagenesis of CDRs were examined by Yang et al. to assess the optimal way of combining sub-libraries [273]. In the study, the group either mutagenized the CDRs 1 and 3 sequentially, building the next CDR optimization library within the context of the selected highest affinity variant, termed CDR walking, or by combining the mutations of independently optimized CDRs. The affinity of the antibody was consistently improved during the sequential CDR walking strategy, resulting in an overall 96-fold improvement in affinity. On the other hand, the additive effects of the independently optimized CDRs were more unpredictable with only one out of six tested variants demonstrating additivity. However, the affinity of the combinatorial variant was improved 420-fold, demonstrating the effectiveness of CDR shuffling in combination with semi-rational mutagenesis.

The evolution and affordability of DNA synthesis technologies have facilitated the construction of more precisely controlled semi-rational mutagenesis libraries. Rather than randomizing a residue or a region of residues with all possible 19 amino acids, high-throughput DNA synthesis now allows the skewing of diversity towards specific types of residues at certain positions. This approach provides more meaningful amino acid diversity with fewer misfolded or dysfunctional clones, resulting in increased convenience and success rate. Moreover, it enables the design of "pairwise" mutagenesis libraries, where all combinations of two amino acid mutations are included for a defined region, such as CDR-H3, to maximize mutational coverage while maintaining manageable diversity [145].

2.3.4.3 *In silico* modeling-assisted rational mutagenesis

Recent advancements in computer-assisted *in silico* antibody modeling technology have given us new tools for a more thorough analysis of the antibody properties and interactions between antibodies and antigens, enabling more precise targeting of rational mutagenesis using protein structure-based 3D-models [274]. Different modeling strategies that can assist in antibody engineering have been developed, including homology modeling [275], molecular dynamics simulation [276], prediction of aggregation-prone regions [123], antibody-antigen docking [277] and the analysis of the electrostatic complementarity at the antibody-antigen interface [278].

At present, the low reliability of the pure *in silico* mutation predictions for antibody maturation can render it less effective than wet-lab optimization options [279]. In a recent study by Cannon et al., the epitope of an anti-murine CCL20 antibody was first determined experimentally using alanine scanning, followed by *in silico* mutagenesis to predict point mutations that would increase the affinity [280]. Using three different *in silico* tools in parallel, 87 different affinity-improving point mutations to the CDRs were suggested, out of which 20 were experimentally tested. Out of the 20 tested variants, only two showed a modest 4-fold improvement in binding affinity.

Although computational tools are not reliable enough to replace wet-lab optimization options at present, antibody-antigen complex crystal structures and *in silico* modeling can be used to identify regions to target the mutagenesis, enabling the construction of focused *in vitro* maturation libraries with a more conveniently manageable size and diversity and selection of improved variants using *in vitro* display technologies [281]. In a study by Barderas et al. *in silico* antibody-antigen docking was utilized for antibody maturation of an anti-gastrin17 scFv [282]. The CDR-H3 and CDR-L3 were first optimized sequentially using CDR walking, followed by molecular dynamics-based docking of the two selected scFvs to gastrin17, utilizing experimental epitope information. A mutagenesis library was built by identifying

residues from the complex structure with apparent packing defects. In the end, an scFv with a 454-fold improvement in affinity compared to the parental scFv was identified using phage display.

The introduction of AlphaFold has made accurate protein structure prediction accessible to all [283]. The spread of deep learning methods for structure prediction has also advanced antibody modeling. Despite typically exhibiting predictable canonical folds based on sequence similarity in five of the six CDR loops [284], the modeling of the CDR-H3 has proven challenging due to its high diversity both in sequence and length [285]. This challenge has sparked many antibody-specific deep-learning tools for antibody modeling such as DeepAb [286], ABlooper [287] and IgFold [288]. The advent of new and better open-source deep learning tools for antibody modeling lowers the bar for modeling-assisted rational mutagenesis of antibodies, ultimately moving the antibody engineering field rapidly forward.

2.3.4.4 Induced somatic hypermutation in mammalian display

Activation-induced cytidine deaminase (AID) is a 198 amino acid (24 kDa) enzyme responsible for *in vivo* SHM and CSR in B-cells [20]. It initiates the SHM by creating cytidine to uracil mismatches on single-stranded DNA, which are then repaired by a low-fidelity DNA polymerase, generating additional mutations [289]. The mutations created by AID are pseudo-random, meaning that they can be introduced randomly genome-wide [290], but occur more often in highly transcribed genes with G-quadruplex (G4) structures [291] or mutational hot spots, like in the Ig variable genes [292].

The ectopic expression of AID in murine fibroblast cells was shown to induce hypermutation of an artificial green fluorescent protein (GFP) substrate, suggesting its use for the directed evolution of proteins [293]. An interesting concept in antibody engineering is to mimic *in vivo* SHM for antibody affinity maturation by expressing recombinant AID in mammalian cells stably displaying an antibody [236,237,245,294–298]. This clever method introduces diversity through pseudo-random mutations along the antibody gene and employs simultaneous selection pressure for affinity and developability using mammalian display. The maturation process occurs during cell proliferation without the need for rational design or preparation of a random mutagenesis library. The cells bearing antibody mutants with improved affinity are selected through consecutive FACS selection rounds, usually yielding significant improvement in affinity in as low as three rounds of FACS selection [298].

Because the mutations introduced by AID are spread pseudo-randomly throughout the highly transcribed antibody gene, many of the mutations lead to non-functional antibody variants, especially when the mutations occur in the constant regions of the antibody. This lowers the efficiency of the mutational strategy, as the

proportion of potentially beneficial mutations is expected to be low. To address this problem, several research groups have fused AID with a catalytically deficient nuclease to target the AID-induced mutations to a specific region programmed by guide RNA [299–303].

Using AID fused to catalytically deficient CRISPR/Cas9 to target specific point mutations in the cell's genome has the benefit of not requiring double-stranded DNA breaks, which often leads to random insertions and deletions during cellular DNA repair. Different variants of the AID-nuclease fusions, termed diversifying base editors (DBEs), have been demonstrated to perform *ex vivo* affinity maturation by mimicking SHM [304,305]. Together these technologies expand the antibody engineering toolbox for developing even better therapeutic antibodies more efficiently.

3 Aims of the Study

Therapeutic antibodies in different formats may provide innovative and effective treatment options for indications with previously poor treatment options. In addition to generating a molecule with a desired way of modulating the correct target protein involved in the disease, the success of the therapeutic antibody is affected by the biophysical properties of the molecule. A correlation between the poor biophysical properties of clinical-stage therapeutic antibodies and the late-stage clinical failure was previously shown, indicating the importance of screening, and selecting for good biophysical properties in the early stages of the antibody development. Furthermore, it was shown that the display level of antibodies expressed on the surface of mammalian cells can be used as a proxy for the developability of the therapeutic antibody.

To this end, this doctoral thesis aimed to construct a novel mammalian cell display platform that enables the efficient display and selection of biophysically favorable antibodies from large libraries of full-length antibodies displayed on the surface of Chinese hamster ovary (CHO) cells.

More specifically, the aims of this thesis were:

1. To develop a novel mammalian display platform for the display of full-length antibodies on the surface of CHO cells.
2. To validate that the platform can be used to select developable antibodies by selecting cells displaying antigen-specific antibodies at high density.
3. To improve the stable transfection efficiency of the platform by improving the nuclear localization of Bxb1 integrase to enable the display of larger antibody libraries.
4. To explore the possibility of inducing targeted somatic hypermutation of displayed antibodies using activation-induced cytidine deaminase (AID) and by modifying the antibody codon usage to include G-quadruplex-rich areas.

4 Results and Discussion

This chapter summarizes the most relevant results and discussion in the thesis, presented in more detail in the relevant original publications. The related original publication is indicated in parenthesis, when applicable.

4.1 Generation of a landing pad cell line for mammalian display (I)

To achieve efficient single-copy integration of antibody genes into the genome of a host cell, a Bxb1 integrase-based landing pad (LP) platform was designed. The Bxb1 integrase LP approach was selected due to the superior integration efficiency and specificity of site-specific recombinases compared to nuclease-driven homologous recombination [306]. Furthermore, among the commonly used serine recombinases, Bxb1 integrase has demonstrated the highest accuracy and efficiency [255].

Given that most therapeutic antibodies are manufactured in Chinese hamster ovary (CHO) cells [307], CHO cell line was chosen as the host cell for the platform to enable the selection of the therapeutic molecules as close to the final format as possible. To simplify the cell line development, a commercial Flp-In CHO cell line, which contained a single copy of a Flp recombinase target (FRT) site in a transcriptionally active locus, was utilized. The Bxb1 LP was stably integrated into the cell line to make the Flp-In CHO cell line suitable for the display of antibody libraries.

The Bxb1 LP contained a cytomegalovirus (CMV) promoter-driven bicistronic expression cassette, flanked by two phage attachment sites (AttP) (**Figure 13**). One of these sites had a central GA dinucleotide mutation (AttPm), to facilitate unidirectional recombinase-mediated cassette exchange (RMCE). The expression cassette contained mouse IgG2a Fc, fused to the transmembrane domain of platelet-derived growth factor receptor beta (PDGFRβ), which served as a surface marker. Blasticidin S deaminase (BSD) gene was positioned as the final gene in the bicistronic expression cassette to ensure the continuous activity of the promoter through constant selective pressure. Given that this construct generates a single transcript encoding multiple genes, self-cleaving 2A peptides [308] and furin cleavage

sites [309,310] between successive gene products were employed. This design enabled the expression of several polypeptides from the same mRNA molecule.

To facilitate the stable integration of genes of interest into the LP, a promoterless targeting vector (pBxb1-TV) with AttB/AttBm sites was designed. The expression cassette contained the gene(s) of interest, followed by the puromycin-N-acetyltransferase (puroR) gene to enable the selection of cells with stable integration. The gene(s) of interest were separated by 2A peptides and furin cleavage sites to facilitate the expression of multiple polypeptides. The expression cassette between the AttB/AttBm sites in the pBxb1-TV integrates into the LP through an RMCE reaction catalyzed by Bxb1 integrase, which was expressed by the Bxb1 integrase expression vector (pBxb1-EV).

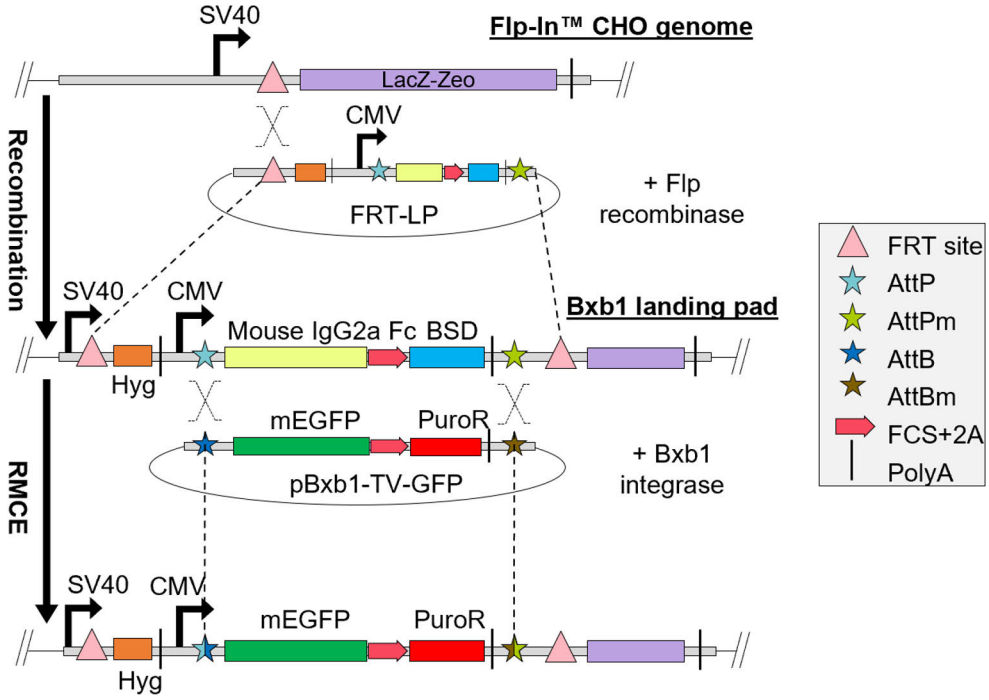

Figure 13. Design of the Bxb1 integrase-driven mammalian display platform. The Bxb1 LP contained CMV-promoter-driven expression of mouse IgG2a Fc and blasticidin S-deaminase (BSD), separated by furin cleavage site (FCS) and 2A peptide. The expression cassette was flanked by AttP and AttPm sites. To generate CHO-LP clones, the Bxb1 LP was integrated into Flp-In CHO cells by co-transfection of the LP in pcDNA5/FRT vector and Flp recombinase expression vector (pOG44). The pBxb1-TV contained the gene of interest and the puromycin-N-acetyltransferase (puroR) gene, flanked by AttB and AttBm sites. The recombinase-mediated cassette exchange (RMCE) between the LP and the pBxb1-TV is catalyzed by the Bxb1 integrase, facilitating efficient stable integration of the gene of interest into the genome of the CHO-LP cell line. Figure edited from [126].

To generate the CHO-LP cell line, the Bxb1 LP was stably integrated into the Flp-In CHO cell line by co-transfecting the LP in the pcDNA5/FRT vector and the plasmid encoding Flp recombinase. Cells with stable integration of the LP were selected using hygromycin, followed by single-cell cloning by fluorescence-activated cell sorting (FACS). To verify that a single copy of the LP was integrated into the Flp-In CHO cell line and that the RMCE reaction excises the surface marker from the LP, pBxb1-TV with a membrane-anchored enhanced green fluorescent protein (mEGFP) was stably integrated into the generated CHO-LP clones, by co-transfecting the pBxb1-TV-GFP and pBxb1-EV, followed by puromycin selection.

The staining of the cells for mouse IgG2a Fc detection, coupled with the monitoring of mEGFP, facilitated the identification of clones exhibiting solely mEGFP expression (**Figure 14A**). This exclusive expression signified the integration of only a single copy of the Bxb1 LP. Conversely, clones showing co-expression of both mouse IgG2a Fc and mEGFP indicated the presence of two or more integrated copies of the Bxb1 LP. Consequently, such clones were deemed

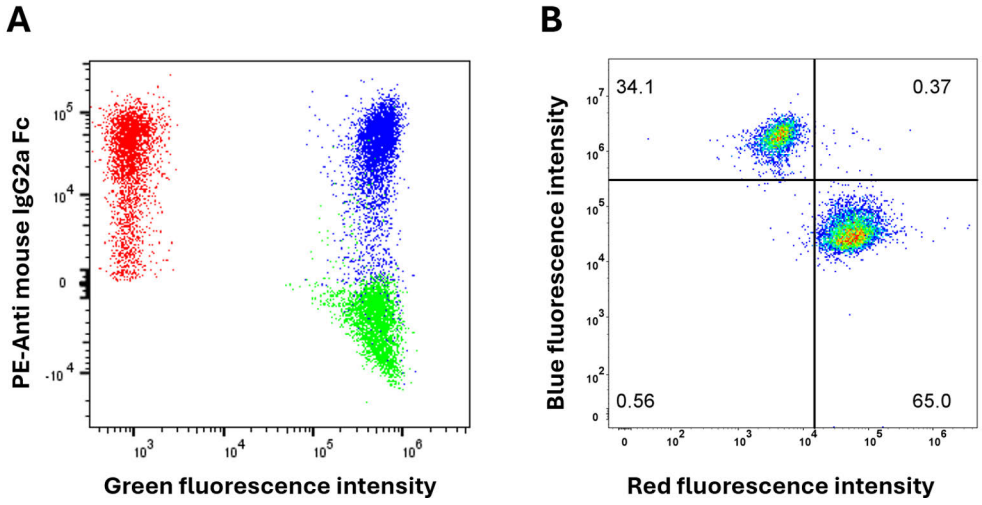

Figure 14. Confirmation of single copy Bxb1 LP in the CHO-LP cell line. **A)** Following the co-transfection with pBxb1-TV-GFP and pBxb1-EV and puromycin selection, the CHO-LP clones were analyzed for expression of mEGFP and mouse IgG2a Fc. Cells expressing both mEGFP and mouse IgG2a Fc (blue) contained two or more copies of the Bxb1-LP and were thus deemed unsuitable for mammalian display. The clone selected for mammalian display expressed mEGFP and had lost the expression of mouse IgG2a Fc, demonstrating the success of the RMCE reaction (green). Non-transfected CHO-LP cells were used as a control (red). **B)** The specificity of the Bxb1 LP platform was demonstrated by co-transfecting a mixture of blue and red fluorescent proteins along with the pBxb1-EV. Following puromycin selection, the assessment of the fluorescent protein expression revealed that more than 99% of the cells were only expressing one of the fluorescent proteins. Figure edited from [126].

unsuitable for mammalian display. To further confirm the presence of a single copy of the Bxb1 LP and to illustrate the specificity of the Bxb1 LP system, a mixture of pBxb1-TV with blue fluorescent protein (BFP) and red fluorescent protein (RFP) was co-transfected with pBxb1-EV. Following puromycin selection, the cells were measured for expression of both blue and red fluorescent proteins. More than 99% of the cells were expressing either BFP or RFP, affirming the high fidelity of the Bxb1 LP system (**Figure 14B**).

The selected CHO-LP clone was subsequently adapted to serum-free suspension culture by detaching the adherent cells and transferring them to a shaker flask. This adaptation enabled higher cell densities, thereby facilitating the display of larger diversity libraries within smaller volumes.

4.2 Increased stable integration efficiency through enhanced nuclear localization of Bxb1 integrase (II)

The diversity of the library displayed on mammalian cells is limited by the large culture volume of mammalian cells and the low stable integration efficiency. The culture volume is largely dependent on the size of the mammalian cells, which cannot be controlled, leaving the engineering of genomic integration the only option to increase the possible size of the displayed library.

The genomic integration of the TV into the LP takes place within the nucleus, requiring the translocation of the Bxb1 integrase into the nucleus. Given its large size (56.2 kDa) [258], Bxb1 integrase cannot efficiently enter the nucleus passively; instead, it necessitates a nuclear localization signal (NLS) for efficient nuclear entry [311,312]. NLSs serve as signal sequences directing proteins into the nucleus via an active translocation pathway. Proteins bearing NLSs are actively translocated into the nucleus by a complex mechanism involving importin α and importin β. Once inside the nucleus, the complex dissociates upon binding of Ran-GTP to importin β, which also initiates the recycling of the importins back to the cytoplasm. Exportin CAS-Ran-GTP then translocates importin α back into the nucleus, where it is released from the complex by Ran GTPase-activating protein (RanGAP), leading to the conversion of Ran-GTP to Ran-GDP. Ran-GDP is converted back to its active form, Ran-GTP, by the Regulator of chromosome condensation 1 (RCC1) protein within the nucleus [313–315] (**Figure 15**).

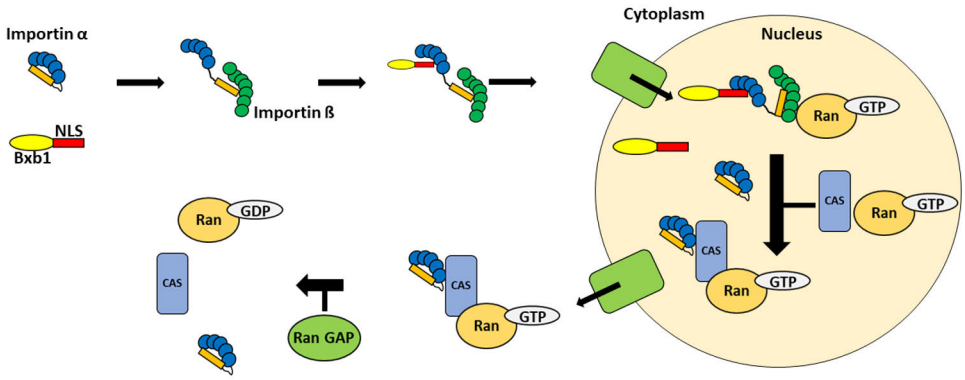

Figure 15. Illustration of the nuclear translocation process. Importin α interacts with importin ß, enabling the binding of the NLS sequence to it. The ternary complex is then translocated into the nucleus where binding of RanGTP to importin ß causes dissociation of the ternary complex. Subsequently, importin α binds to the exportin complex composed of CAS and RanGTP, and the complex is transported to the cytoplasm. The exportin complex is dissociated in the cytoplasm by RanGAP, converting Ran-GTP to RanGDP. Ran-GDP undergoes conversion back to its active form, Ran-GTP, within the nucleus, facilitated by the regulator of chromosome condensation 1 (RCC1) protein (not shown in the figure). Figure from [316]. Reproduced with permission from Springer Nature.

The role of nuclear translocation of Bxb1 integrase to the stable integration efficiency was studied by fusing the Bxb1 integrase with different NLS sequences as well as overexpressing the proteins involved in the nuclear translocation pathway. The impact of the NLS sequences and the nuclear translocation-associated protein overexpression was quantified by co-transfecting the Bxb1 NLS variants with pBxb1-TV-GFP and measuring the percentage of mEGFP expressing cells without selective pressure using flow cytometry. To enable comparison across experiments, all the measured stable integration efficiencies (SIE) were normalized to Bxb1 integrase without NLS, which was included in every experiment.

4.2.1 Nucleoplasmin NLS fusion in Bxb1 integrase significantly enhances stable integration efficiency (II)

The effect of different NLS fusions was first studied by fusing Bxb1 integrase with various NLS sequences either to the C- or N-terminus. The tested NLS sequences included Myc proto-oncogene (c-Myc) NLS, simian virus 40 large T antigen (SV40) NLS, transcription factor EGL-13 (EGL-13) NLS, and nucleoplasmin (NPL) NLS from *Xenopus laevis*.

Among the tested Bxb1-NLS fusions, NPL NLS improved the normalized stable integration efficiency (nSIE) significantly both N- and C-terminally, SV40 NLS only N-terminally and EGL-13 NLS only C-terminally. The C-terminal NPL NLS exhibited a more than sixfold increase in nSIE compared to Bxb1 integrase without NLS (**Figure 16**).

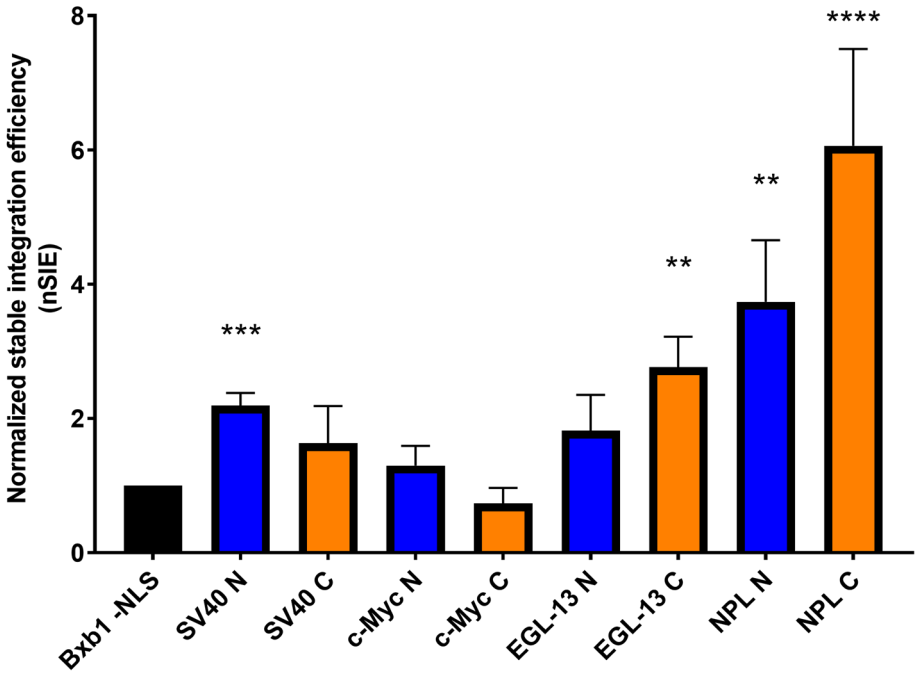

Figure 16. Normalized stable integration efficiencies (nSIE) of the tested Bxb1-NLS variants, either as N-terminal fusions (blue) or C-terminal fusions (orange). The error bars represent the standard deviation of three independent experiments (except NPL C, n = 6). Asterisks denote statistically significant differences to Bxb1 without NLS (black, Bxb1 -NLS). (**) $p < 0.01$; (***) $p < 0.001$; (****) $p < 0.0001$, T-test, equal variances assumed. Figure from [316]. Reproduced with permission from Springer Nature.

To the best of my knowledge, N-terminal SV40 NLS fusion is used in all the published studies describing the use of Bxb1 integrase for genomic integration in mammalian cells [126,249–252,317,318]. Noteworthy, it was shown in this study that the stable integration efficiency with the C-terminal nucleoplasmin NLS fusion to Bxb1 integrase was substantially better than that of the SV40 NLS fusions.

4.2.2 Stable integration efficiency was further enhanced by the fusion of two copies of nucleoplasmin NLS (II)

Some proteins inherently possess two distinct nuclear localization signals, each contributing to the nuclear transport [319]. After identifying the C-terminal nucleoplasmin NLS as having the highest improvement in stable integration efficiency, the effect of additional NLS fusions was assessed. To this end, the

different NLS sequences were fused to the N-terminus of the Bxb1 integrase with C-terminal NPL NLS fusion. Additionally, variants with two and three copies of the NPL NLS were tested as C-terminal fusions.

When compared to Bxb1-NPLC, the double NLS variant Bxb1-NPLCx2 significantly increased the nSIE of Bxb1 integrase, further improving the nSIE by more than twofold (**Figure 17**). Interestingly, the addition of three NPL NLS sequences did not result in a further increase in stable integration efficiency, instead it decreased it. This could be caused by the saturation of the nuclear translocation process, which has been observed in earlier studies [320]. The inclusion of three copies of the positively charged peptide in the C-terminus localizes a high positive charge in the protein, which could also cause instability or loss of catalytic activity [321].

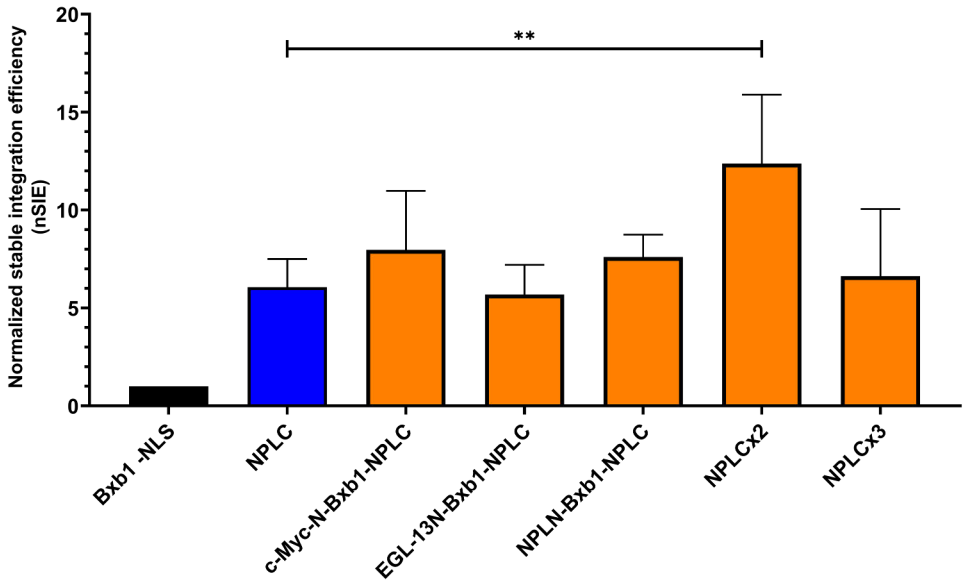

Figure 17. Comparison of the best single NLS variant, Bxb1-NPLC (blue), to Bxb1 variants containing one or two additional NLS sequences. The bars represent the average normalized stable integration efficiencies (nSIE) with error bars representing the standard deviation of three independent experiments (except NPLC, n = 6; NPLCx2, n = 9). (**) $p < 0.01$. Figure from [316]. Reproduced with permission from Springer Nature.

4.2.3 Co-expression of Ran GTPase-activating protein 1 (RanGAP) with Bxb1-NPLCx2 further enhanced stable integration (II)

It was hypothesized that the amount and availability of certain nuclear translocation-associated proteins could be the bottleneck limiting the nuclear transport and thus the integration efficiency. To test the hypothesis, proteins involved in the

translocation process were overexpressed along with the Bxb1-NPLCx2 variant to evaluate their effect on the integration efficiency. Specifically, the genes encoding mouse importin α, importin ß, GTP-binding nuclear protein Ran (RanGTP), regulator of chromosome condensation 1 (RCC1) and Ran GTPase-activating protein 1 (RanGAP) were cloned separately into the 3' end of the Bxb1-NPLCx2 variant, separated by a GS linker, furin cleavage site and T2A self-cleaving peptide, enabling the co-expression of the two proteins.

Of the tested constructs, co-expression of RanGAP was the only transport protein showing a statistically significant positive effect on the stable integration efficiency (**Figure 18A**), further improving it by 45 % compared to Bxb1-NPLCx2 expression alone. In contrast, co-expression of importin β and RCC1 lowered the integration efficiency by 58 % and 36%, respectively, and the rest of the proteins had insignificant effects. Overexpression of RanGAP has been previously reported to increase the NLS-mediated nuclear transport of DNA cargo [322], aligning with the result of this study.

Another aim of the study was to validate whether the findings obtained with the small, easily expressed GFP protein could be extended to complex multimeric protein constructs, such as antibodies. To this end, a comparative analysis was conducted using Bxb1 without NLS, Bxb1-NPLC, Bxb1-NPLCx2, and Bxb1-NPLCx2 co-expressed with RanGAP, with a DNA construct designed for the surface display of the clinical antibody abrilumab.

The nSIE of abrilumab increased over 10-fold with Bxb1-NPLC, 11-fold with Bxb1-NPLCx2, and 14-fold with Bxb1-NPLCx2 co-expressed with RanGAP, compared to Bxb1 without NLS (**Figure 18B**). Inclusion of two copies of NPL NLS in the C-terminus improved nSIE by 7% over one copy. Co-expressing RanGAP further improved nSIE by 27% compared to Bxb1-NPLCx2. While the improvements between NLS variants were more modest for abrilumab compared to GFP, the overall enhancement over Bxb1 lacking NLS was similar regardless of the construct size. These findings suggest that the enhanced stable integration efficiency achieved with the Bxb1-NLS fusion and co-expression of RanGAP applies to larger constructs, including antibody genes and libraries.

In the described experiments, the average percentage of cells expressing abrilumab using Bxb1 without the NLS fusion was 0.23%. This value was increased to 3.19% with the inclusion of NPLCx2 fusion and co-expression of RanGAP. This translates to an antibody library size of approximately $3x10^5$ variants per T75 flask (assuming $1x10^7$ cells per T75 flask at the time of transfection). Although these experiments were done with the adherent CHO-LP cell line for convenience, the CHO-LP cell line has been adapted to suspension culture, enabling the cultivation and transfection of larger cell numbers, thus theoretically allowing the screening of antibody libraries of up to 10^7 variants. Additionally, the stable integration efficiency

of the Bxb1-SV40N variant was enhanced earlier by optimizing the pBxb1-EV to pBxb1-TV plasmid ratio, total DNA amount, and employing electroporation for more efficient transfection [126]. It is anticipated that similar optimizations using the Bxb1-NPLCx2-RanGAP variant could further improve the stable integration efficiency, accommodating the transfection of even larger antibody libraries.

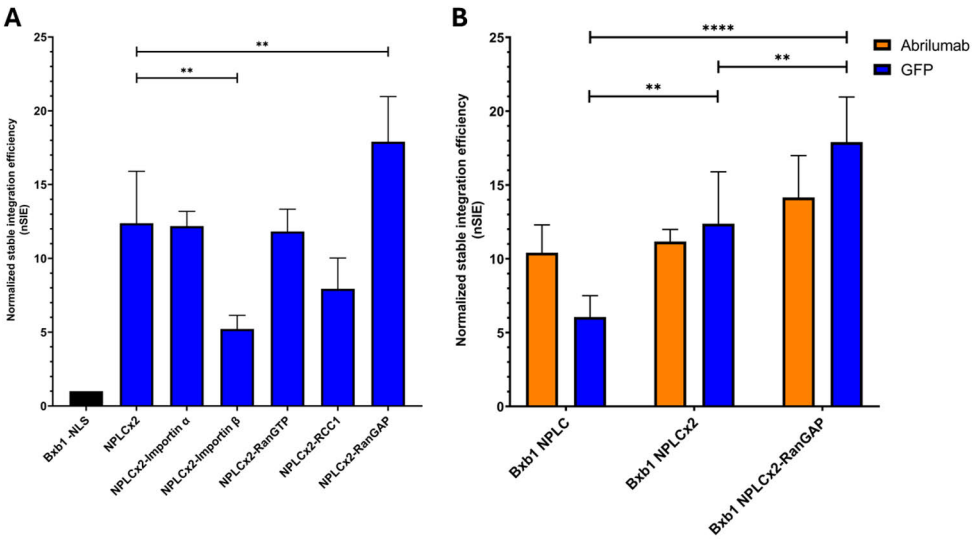

Figure 18. Normalized stable integration efficiencies (nSIE) of Bxb1-NPLCx2 variant with co-expression of nuclear translocation-associated proteins using **A)** GFP and **B)** GFP and membrane-anchored abrilumab. The bars represent the average normalized stable integration efficiencies (nSIE) of each Bxb1-NPLCx2 transport protein construct. The error bars represent the standard deviation of three replicate transfections (except NPLCx2, n = 9, NPLCx2-RanGAP, n = 6). (**) $p < 0.01$; (****) $p < 0.0001$. Figure from [316]. Reproduced with permission from Springer Nature.

4.3 Display level achieved upon mammalian cells correlates with the biophysical properties of the displayed antibody

It was recently demonstrated that antibodies with differing biophysical properties could be distinguished based on solely the display level achieved on mammalian cell surface, which could not be reproduced on yeast surface display [125]. The study also showed that mammalian display could be used to select biophysically superior variants from a mutant library. Although showing a broad correlation between the display level and the biophysical properties of the displayed antibody, the study was limited to one mutational library and three antibodies with biophysical liabilities and mutated versions of them with improved biophysical properties.

In this study, to support the claim that mammalian display can distinguish between biophysically different antibodies, 37 clinical antibodies with differing biophysical characteristics were selected based on the work of Jain et al. [116]. The variable regions of the selected antibodies were constructed into human IgG1 isotype (allele *01) with standard constant regions for kappa and lambda (alleles IGKC*01 and IGLC2*01, respectively), to allow the comparison strictly based on the variable domain differences. The selected antibody genes were synthesized, cloned into pBxb1-TV, and stably integrated into the genome of CHO-LP cells. The display levels of the antibodies were measured, and their correlation to biophysical properties was determined using the published biophysical characterization results.

As depicted in **Figure 19**, there was a statistically significant correlation between the display level and many of the published biophysical characterization results. The colloidal stability of the antibody, measured by affinity-capture self-interaction nanoparticle spectroscopy (AC-SINS) and cross-interaction chromatography (CIC), had the highest correlation with the display level with a Spearman rank correlation coefficient (ρ) of -0.48 and -0.47, respectively (*p*-values of 0.0028 and 0.0035, respectively). This was closely followed by thermal stability and polyspecificity, measured by Fab melting temperature ($\rho = 0.45$, *p*-value 0.005) and polyspecificity reagent (PSR) assay ($\rho = -0.43$, *p*-value 0.008), respectively. Hydrophobicity, measured by hydrophobic interaction chromatography (HIC), also had a significant correlation to the display level ($\rho = -0.35$, *p*-value 0.03), whereas the antibody titer, measured by transient HEK titer, surprisingly did not.

Although the listed assays measure different biophysical properties, many of these properties are interrelated. For example, hydrophobicity, colloidal instability, and polyspecificity have been correlated with faster plasma clearance, low solubility, and aggregation propensity [132–135,140,141,323]. These issues are often caused by excess positive charge or hydrophobicity in the antibody's variable region. When such charged or hydrophobic patches lead to misfolding or aggregation of the displayed antibodies in the mammalian cell's secretory pathway or plasma membrane, its quality control machinery degrades them [234,235], resulting in lower antibody display levels. This process could explain the observed correlation between the display level and various biophysical properties.

Although the Spearman correlation coefficients were modest, it was encouraging to observe statistically significant correlations with such a diverse set of antibodies. This data set gives more evidence to mammalian display's unremarkable ability to "filter out" antibodies with developability risks. It also gives evidence that mammalian display could be used to select biophysically favorable antibodies from a diverse naïve library, instead of only maturing a single antibody, as was demonstrated earlier [125,145] and in the following sections.

			**	*	**	**	**
Antibody	Display level (MFI)	HEK titer (mg/L)	Fab Tm (°C)	HIC RT (min)	AC-SINS (Δλmax)	CIC RT (min)	PSR
Polatuzumab*	1368776	225.1	74.0	8.8	-1.0	8.3	0.0
Pertuzumab*	1237140	31.4	78.5	10.1	-0.2	8.6	0.0
Denosumab*	1171595	134.2	69.5	8.5	5.9	8.8	0.0
Abrilumab	1166958	100.2	71.0	9.4	-0.9	8.4	0.0
Panitumumab*	1141686	179.6	78.5	9.5	-1.1	8.4	0.0
Elotuzumab*	1134867	213.2	83.5	10.3	-0.2	8.5	0.0
Mepolizumab*	1132867	221.5	78.5	9.2	-1.0	8.4	0.0
Brentuximab*	1055867	268.1	72.0	10.5	-0.5	8.6	0.2
Bevacizumab*	1015322	50.0	63.5	11.8	0.8	9.8	0.0
Tocilizumab*	955686	139.6	91.5	9.1	1.3	8.9	0.0
Efalizumab*	942413	167.0	72.5	8.7	0.7	8.5	0.0
Motavizumab	900413	133.6	86.0	9.7	2.5	8.7	0.0
Tremelimumab*	899140	229.6	75.0	11.6	29.6	11.2	0.1
Sirukumab	884958	109.8	68.0	11.3	29.6	10.8	0.4
Bococizumab	876515	95.8	67.0	10.2	29.6	10.6	0.8
Eldelumab	866867	89.3	59.5	12.4	1.2	10.2	0.0
Dacetuzumab	866776	128.5	68.0	8.5	0.0	8.5	0.0
Romosozumab*	820595	227.7	76.0	9.2	-1.0	8.4	0.0
Evolocumab*	815140	260.7	65.0	10.4	2.2	9.3	0.2
Tovetumab	804179	277.2	63.5	8.7	2.2	8.8	0.0
Veltuzumab	799140	225.0	70.0	11.1	4.8	8.8	0.0
Parsatuzumab	795685	40.0	64.5	9.1	7.4	8.7	0.1
Olaratumab*	750776	141.9	62.5	10.6	0.3	9.4	0.5
Matuzumab	750595	224.3	72.0	9.8	-0.9	8.6	0.0
Glembatumumab	736049	152.7	70.5	13.7	28.9	13.5	0.2
Atezolizumab*	718709	164.1	73.5	13.4	15.0	10.8	0.1
Cetuximab*	681231	109.2	68.5	10.1	1.3	8.9	0.0
Urelumab	652192	143.9	66.0	11.2	29.6	9.4	0.0
Belimumab*	649231	10.5	60.0	10.5	0.8	8.6	0.0
Basiliximab*	640437	107.5	60.5	9.6	28.8	9.4	0.4
Nimotuzumab*	578595	15.1	65.5	25.0	-0.6	8.5	0.0
Infliximab*	515651	6.6	64.5	10.4	29.6	9.0	0.0
Ponezumab	485767	17.0	61.0	10.5	-0.2	8.7	0.1
Inotuzumab*	370183	169.8	83.0	9.7	4.0	9.3	0.3
Lirilumab	318590	270.5	70.0	25.0	21.0	10.6	0.2
Bavituximab	71920	45.1	59.5	11.5	29.9	11.4	0.6
Lenzilumab	62095	184.7	74.0	8.7	29.6	10.1	0.7

Figure 19. Display levels and biophysical properties of the selected 37 clinical antibodies. Antibodies with an asterisk are approved for clinical use. The biophysical properties are from the publication by Jain et al. [116]. Asterisks denote the statistical significance of Spearman rank correlation between the biophysical property and the measured display level (two-tailed): (*) $p < 0.05$; (**) $p < 0.01$. HIC RT, hydrophobic interaction chromatography retention time; AC-SINS, affinity-capture self-interaction nanoparticle spectroscopy; CIC RT, cross-interaction chromatography retention time; PSR, polyspecificity reagent.

4.4 Selection of biophysically favorable antibodies using mammalian display (I)

To provide practical evidence that the mammalian display platform can be used to select biophysically favorable antibodies from antibody libraries, the biophysical

properties of two antibodies were improved using two distinct engineering strategies. First, a failed clinical antibody, bococizumab, was matured using *in silico* modelling-assisted rational mutagenesis strategy. Next, a phage display-derived anti-gelsolin antibody exhibiting high self-interaction, was matured using a random mutagenesis strategy. The main findings from these case examples are highlighted in the next sections.

4.4.1 Improvement of bococizumab through rational mutagenesis (I)

Bococizumab, developed by Pfizer, is an anti-proprotein convertase subtilisin/kexin type 9 (PCSK9) antibody intended to reduce low-density lipoprotein (LDL) cholesterol [324]. In Phase III clinical trials, nearly 50% of patients administered with bococizumab developed anti-drug antibodies (ADA) within a year [325], which ultimately led to the termination of the clinical program [326]. According to Jain et al., bococizumab exhibited several concerning biophysical properties, notably high polyreactivity and self-interaction tendencies [116]. Large non-denatured aggregates have been shown to elicit a potent antibody response *in vivo* [327]. Therefore, the poor biophysical properties of bococizumab likely contributed to the generation of ADAs in patients, leading to the failure of the clinical program.

Using the published crystal structure of bococizumab's antigen-binding fragment (Fab) bound to PCSK9 [324], Schrödinger BioLuminate platform was employed to identify residues that would be responsible for the poor biophysical properties of bococizumab. Two non-paratopic hydrophobic patches were identified with high AggScore (**Figure 20A**). AggScore predicts aggregation-prone regions based on the distribution, orientation, and intensity of hydrophobic and electrostatic patches on the protein surface [123]. The first patch was located within the CDR-L3, including leucine 94 (AggScore 15.0) and tryptophan 95 (AggScore 14.3). The second patch was found within the CDR-H2, involving proline 53 (AggScore 7.9) and phenylalanine 54 (AggScore 7.1). Importantly, based on the crystal structure, neither of these patches was directly involved in antigen binding, suggesting that mutating these residues should theoretically pose a low risk of severely compromising the antibody's affinity towards PCSK9. These two patches were targeted with site-saturation mutagenesis using degenerate NNK codons, generating a library with a theoretical diversity of 160,000 antibody variants. This library was subsequently stably transfected into the suspension-adapted CHO-LP cells.

The cells displaying the bococizumab library were stained with fluorescently labeled PCSK9 and anti-human light chain (LC) antibody to monitor the target binding and display level during fluorescence-activated cell sorting (FACS), using the parental bococizumab as a gating control (**Figure 20B)**. Cells exhibiting higher

display levels and target binding than the parental bococizumab were enriched through four rounds of FACS (**Figure 20C**). The enrichment of the variants was monitored with next-generation sequencing (NGS) to identify those with the highest enrichment. The enrichment was calculated by comparing the frequency of the variants in the pre-selection population to the FACS-sorted populations. The enrichment of individual residues in each targeted position was analyzed similarly.

After the four FACS rounds, the highest individual residue enrichment was observed for F54E mutation in V_H and W95Q mutation in V_L, with enrichment factors of 23 and 15, respectively. Interestingly, the parental F54 residue was de-enriched 30-fold during the selection, with a strong preference to replace it with a negatively charged residue. The replacement of certain variable domain residues with negatively charged residues has been shown previously to increase aggregation resistance [328].

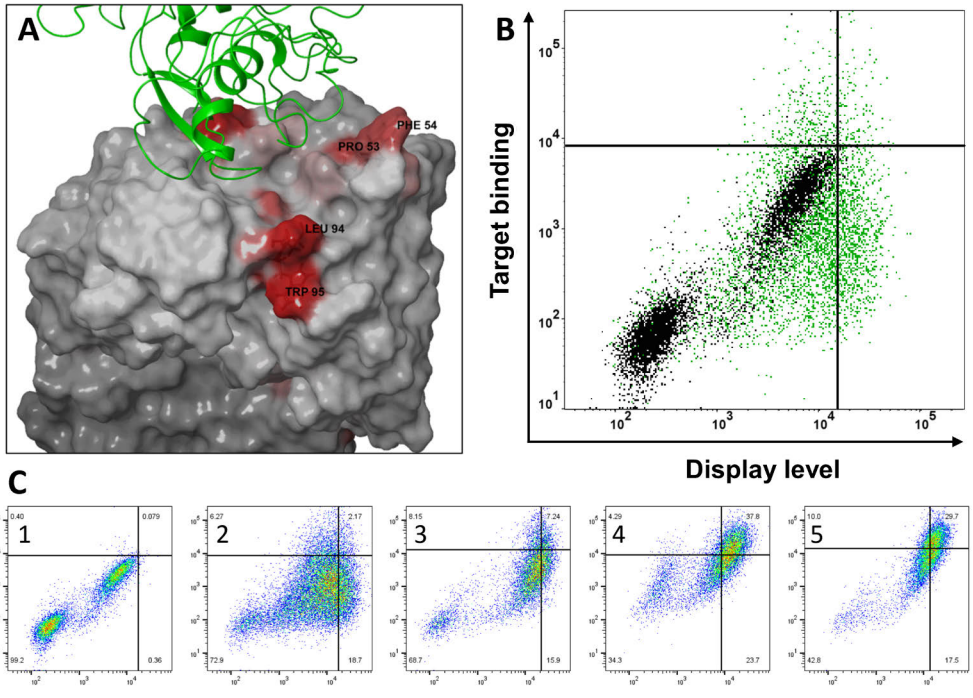

Figure 20. Bococizumab library design and selection. **A)** Using the Schrödinger BioLuminate platform for *in silico* modeling, two non-paratopic hydrophobic patches were identified based on the published crystal structure of bococizumab's Fab (grey) bound to PCSK9 (green), with AggScore intensities shown in red. The four amino acids were targeted with degenerate NNK codons to generate a library with 160,000 antibody variants. **B)** The library exhibited a heterogenous level of target binding and display level (green). The library was enriched for cells exhibiting higher target binding and display levels compared to bococizumab (black). **C)** The FACS was repeated four times (2-5), using the parental bococizumab as a gating control (1) in each round. Figure modified from [126]

Four of the most enriched antibody variants were selected for soluble expression and thorough characterization to validate the mammalian display platform's

capability to select antibodies with better developability. Additionally, variants with either a mutated V_H or V_L region only and the F54E point mutation variant were included to assess the effect of the individual residues and hydrophobic patches. The summary of the results is shown in **Table 2**.

All the enriched antibodies had significantly lower self-interaction and polyreactivity propensity, judged by lower AC-SINS and PR-ELISA scores while maintaining high affinity to PCSK9. The lowered aggregation propensity was also seen by a decrease in polydispersity index (PDI). Also, hydrophobicity was decreased, and thermal stability increased with these mutations. As seen by comparing the V_L only, V_H only, and F54E variant results, the F54E mutation had the highest impact on the biophysical properties and mutating only V_L had only a minor effect on its own. However, the combinatorial effects of the mutations significantly improved all the measured biophysical properties to levels close to that of trastuzumab, which was used as a reference due to its good biophysical properties.

Although significant improvements in the problematic biophysical properties were achieved for bococizumab using careful library design and *in silico* modeling with a published crystal structure, such structural information is not available in most cases where antibody engineering is performed. This complicates the rational design of a maturation library. To further test the platform and represent a realistic early-stage antibody engineering challenge, a maturation library was generated without structural information using random mutagenesis, and biophysically favorable antibodies were selected, as described in the next section.

Table 2. Summary of the biophysical characterization results of the selected bococizumab variants.

Variant	Mutated Residues	CDRH2 Sequence	CDRL3 Sequence	AC-SINS (nm)	PR-ELISA	PDI	HIC RT (min)	T_m (°c)	K_D (pM)
Bococizumab	PFLW	EISPFGGRTNYNEKFKS	QQRYSLWRT	22.6	1.56	0.30	4.6	65.9	250
1	SEGQ	...SE.....	.....GQ..	1.1	0.77	0.04	3.9	67	350
2	AEGQ	...AE.....	.....GQ..	0.7	0.44	0.05	3.7	67.7	190
3	AEPA	...AE.....	.....PA..	0.8	0.43	0.05	3.7	67.4	210
4	PEGQ	....E.....	.....GQ..	1.4	0.53	0.19	3.7	68.5	200
V_L only	PFGQ	.....	.....GQ..	19.2	1.54	0.59	4.3	67.6	250
V_H only	SELW	...SE.....	.....	2.5	0.87	0.05	4.1	65.8	270
F54E	PELW	....E.....	.....	1.4	0.72	0.46	3.9	66.6	190
Trastuzumab	-	-	-	0.5	0.15	0.03	4.4	70.6	-

4.4.2 Improvement of anti-gelsolin mAb through random mutagenesis

Gelsolin amyloidosis is a hereditary systemic protein misfolding disease caused by mutations in the gelsolin gene. These mutations predispose the secreted plasma gelsolin to abnormal proteolytic cleavages. The first identified and best-known mutation is the D187N variant, also known as the Finnish variant. This mutation compromises the stability of the protein, leading to the formation of amyloidogenic fragments. The primary product of this process is an 8 kDa fragment composed of 70 amino acids. Patients with gelsolin amyloidosis carrying the Finnish mutation experience a triad of ophthalmological, neurological, and dermal symptoms due to the accumulation of gelsolin fragments in the basement membrane of the skin, blood vessel walls, eyes, and peripheral nervous system. These accumulations lead to a significant disease burden starting from young adulthood. Currently, treatment options are limited to symptom alleviation and supportive care, highlighting a substantial unmet medical need for disease-modifying therapies [329].

In search for a disease-modifying therapy, Holm identified single-chain variable fragment (scFv) antibodies against the 8 kDa gelsolin fragment using phage display [330]. To enhance the affinity of these binders and to convert them to a more stable Fab format, Haavisto used phage display to isolate novel binders by first extracting the variable domains from Holm's phage display output, converting the binders to Fab format, and performing chain shuffling [331]. Furthermore, Leimu et al. demonstrated the functional performance of these matured Fabs by showing complete inhibition of the gelsolin fragment aggregation *in vitro* with the identified Fabs [332].

The conversion of the most functional Fab to IgG revealed its extremely high affinity towards the 8 kDa gelsolin fragment of 0.37 nM, but also showed its high self-interaction tendency, as indicated by high AC-SINS score (**Table 3**). A high AC-SINS score has been associated with high viscosity and opalescence in high concentrations, making formulation and dosing in high concentrations (>100 mg/ml) challenging [333,334]. As the therapy was proposed to be dosed through intravitreal injection, the antibody would have to be formulated at a high concentration, necessitating the engineering of the antibody to improve its colloidal stability.

To this end, the variable domains of the anti-gelsolin Fab were mutagenized using error-prone PCR (epPCR) and cloned into IgG1 format in the pBxb1-TV vector. The V_H and V_L libraries were stably transfected into the CHO-LP cells and subjected to one round of FACS sorting, followed by NGS analysis to monitor the enrichment. The most enriched V_H and V_L variants were subsequently selected and combined for soluble expression and subjected to thorough biophysical characterization to validate the results of the maturation campaign.

4.4.2.1 Library generation and selection of cells with high display level

The epPCR reaction was performed using the minimum recommended amount of template DNA to achieve an estimated error rate of ca. 15 DNA mutations per kilobase, resulting in an average of 1-2 amino acid mutations per variable domain. The V_H and V_L libraries were stably integrated into the CHO-LP cells, and the library sizes were estimated to be 3 x 10^5 and 4 x 10^5 functional variants for V_H and V_L libraries, respectively, as determined by flow cytometry. Next, the cells transfected with the library were pre-enriched by staining with an anti-human light chain antibody and collecting the cells with sufficient antibody display using magnetic beads, followed by a single round of FACS. The cells were sorted using the parental antibody as a control, selecting cells exhibiting higher display levels and binding to the 8 kDa gelsolin fragment than the parental antibody, as depicted in **Figure 21**. After sorting, the antibody genes were extracted using genomic PCR and sequenced using NGS to determine the enrichment of the antibody variants during the selection process.

As the epPCR reaction accumulates random mutations during subsequent amplification cycles, a large proportion of the amplified DNA does not contain any mutations. Indeed, before sorting, 19% and 22% of the sequencing reads in the V_H and V_L libraries, respectively, had the same amino acid composition as the parental antibody. This was also evident in the FACS plots of the libraries in **Figure 21**, which showed that a large number of cells exhibited similar display and target binding levels as the parental antibody. Notably, since the mutations generated by epPCR are random, the functional diversity of the library is also affected by stop codons in the transfected library, which were found in approximately 5% of the reads in both the V_H and V_L libraries.

As seen in **Figure 21**, the V_H library sorting revealed that a substantial number of cells showed improved display levels compared to the parental antibody, yet many exhibited a loss in target binding. This finding indicated that the V_H domain played a crucial role in both the antibody's target binding capability and its developability. The higher proportion of cells showing an increased display level and loss of binding compared to those with retained binding suggested that mutations improving the developability without compromising affinity could be relatively rare.

On the other hand, the V_L library FACS plot more closely resembled the parental mAb FACS plot, indicating that the V_L might be less involved in target binding than the V_H, which was later confirmed by characterization of the selected antibody variants (**Table 3**). Additionally, the V_L domain appears to be more tolerant to random mutations than the V_H. Interestingly, both libraries were absent of cells with significantly enhanced target binding signals, which aligned with the expectations given the already high affinity of the parental antibody.

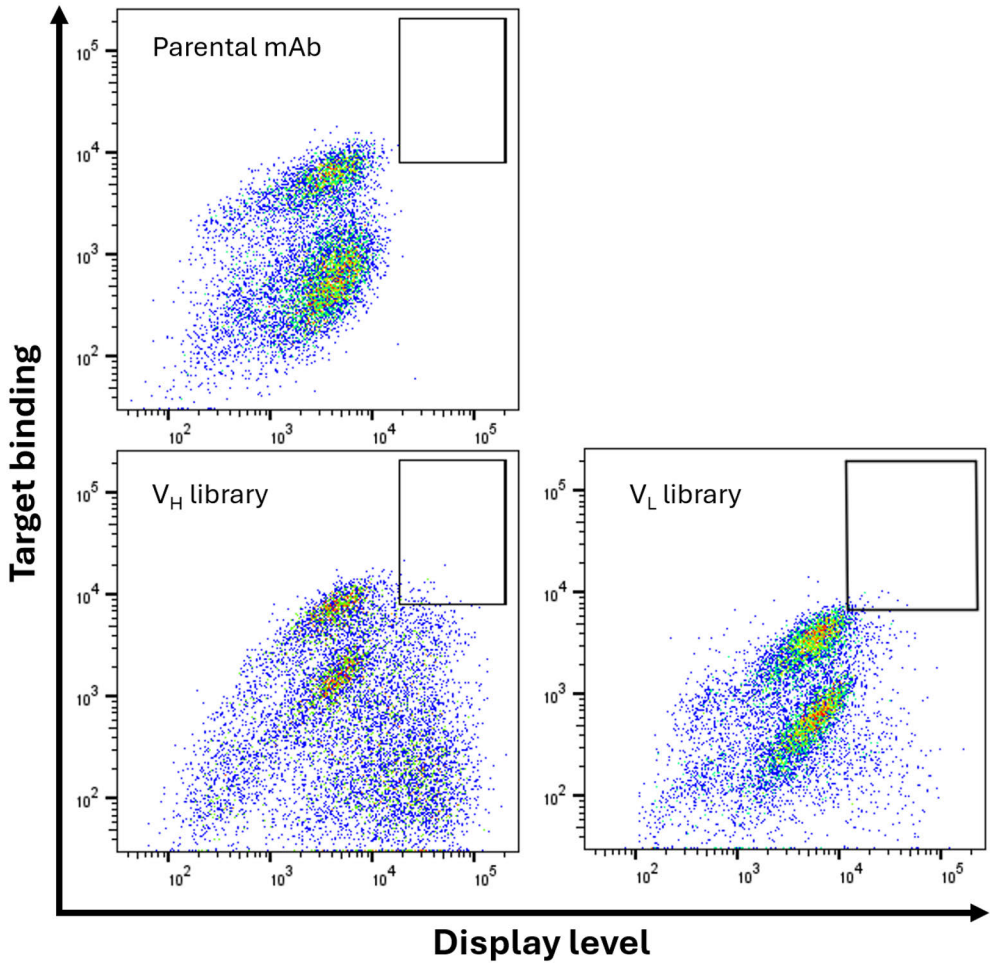

Figure 21. Fluorescence-activated cell sorting (FACS) of the anti-gelsolin antibody random mutagenesis libraries. The gating was made to include cells exhibiting higher target binding and display levels than the parental antibody.

4.4.2.2 Enriched antibodies exhibited superior colloidal stability while retaining target binding

Based on the enrichment analysis, four V_L and seven V_H variants were selected for expression, each showing over two-fold enrichment in a single FACS round, with the highest exhibiting over 10-fold enrichment. All the selected variants contained a single amino acid mutation compared to the parental antibody, and these mutations were found both in the CDR regions and in the framework, as shown in **Figure 22A**. Most of the enriched variants in the V_H library contained mutations either in the CDRs or in the framework residues adjacent to them. The absence of mutations in

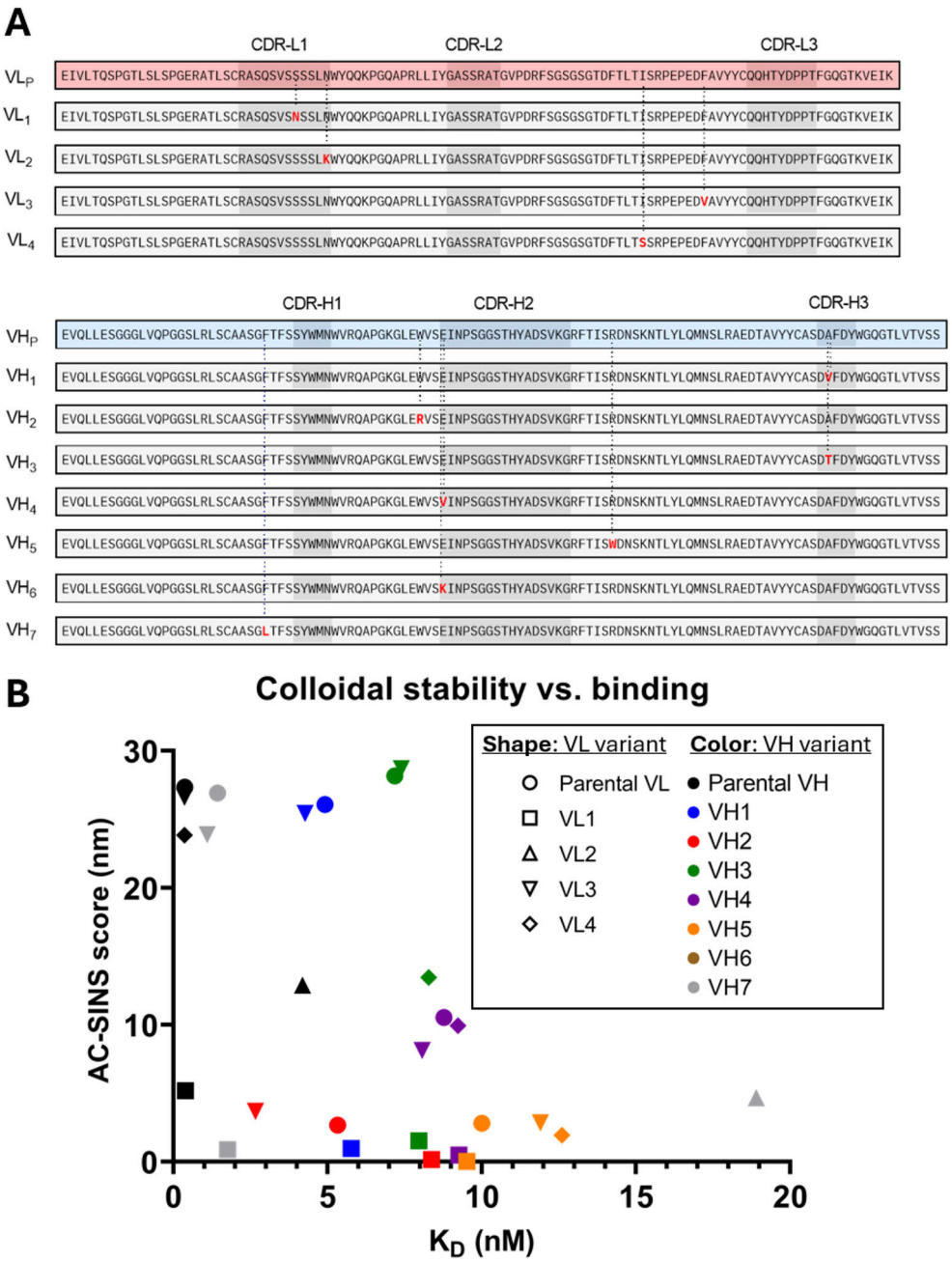

Figure 22. Sequences and the most relevant biophysical characterization results of the most enriched anti-gelsolin antibody variants. **A)** Sequences of the most enriched V_L and V_H variants. VL_P and VH_P represent the parental antibody sequences, and the red residues indicate the mutations. **B**) Results of the measured antibody colloidal stability (AC-SINS) and affinity towards the 8kDa gelsolin fragment (K_D). The shape of the symbol depicts the V_L variant, and the color of the symbol depicts the V_H variant. Only variants with K_D < 20 nM are presented in the figure.

the core framework regions in the most enriched V_H samples imply that such mutations could have potentially destabilized the antibody leading to lower display levels. Conversely, as was speculated from the FACS analysis of the V_L library, the mutations in the enriched V_L variants were more evenly distributed across the entire variable domain.

Table 3 lists the effects of individual V_H and V_L variants, when paired with the corresponding parental variable domain, on the measured biophysical properties of the antibody, as well as two of the best combinatorial variants. Additionally, **Figure 22B** illustrates the effects on colloidal stability for combinatorial variants that retained target binding.

Table 3. Characterization results of the selected anti-gelsolin V_H and V_L variants with the parental antibody. The most promising combinatorial variants VL1 + VH7 and VL3 + VH2 are also included.

V_L variant	V_H variant	AC-SINS score (nm)	Fab T_m	K_D (nM)
VLP	VHP	27.3	72.9	0.37
VL1	VHP	5.2	71.5	0.39
VL2	VHP	12.9	71.4	4.19
VL3	VHP	26.6	76.9	0.36
VL4	VHP	23.8	63.9	0.36
VLP	VH1	26.1	72.0	4.92
VLP	VH2	2.7	66.1	5.33
VLP	VH3	28.2	72.8	7.18
VLP	VH4	10.5	73.6	8.77
VLP	VH5	2.8	70.4	10.0
VLP	VH6	0.2	78.1	-
VLP	VH7	26.9	72.8	1.43
VL1	VH7	0.9	71.4	1.76
VL3	VH2	3.7	68.7	2.66

Three out of the four expressed V_L variants exhibited no change in affinity, in combination with the parental V_H, further supporting the lesser contribution of the V_L to target binding. The VL2 variant, which exhibited a 10-fold reduction in affinity, contained a mutation at the edge of CDR-L1. This mutation may have

altered the orientation of the CDR-L1 loop, potentially impacting the conformation of other CDR loops.

Conversely, all the V_H variants, in combination with the parental V_L, exhibited a significant reduction in affinity. The VH7 variant, which contained a mutation in the FR1, adjacent to CDR-H1, reduced the affinity by 4-fold, while the other variants, containing mutations in, or adjacent to CDR-H2 and CDR-H3, exhibited more than 10-fold reduction in affinity. This implies that the CDR-H2 and H3 could be primarily responsible for the target binding.

The conformational stability was largely unaffected by mutations within the CDRs, as evidenced by the absence of significant changes in the Fab T_m of these variants when paired with the parental variable domain. In contrast, framework mutations and those at the edge of CDR-H2 exhibited both stabilizing and destabilizing effects. For instance, the VL4 variant, which harbored a mutation in the FR3, showed a 9°C decrease in Fab T_m, whereas the VH6 variant, with a mutation at the edge of CDR-H2, displayed a 5.2°C increase in Fab T_m. The mutation in the VH6 variant changed the amino acid charge from negative to positive, stabilizing the structure but completely abolishing its ability to bind to the target.

The CDR-L1 mutations of the variants VL1 and VL2 significantly improved the colloidal stability of the antibody, as demonstrated by a reduction in AC-SINS score, while the framework mutations of the variants VL3 and VL4 had no effect. The V_H variants VH2, VH4, VH5, and VH6, which all contained mutations at the edge of the CDR-H2, exhibited a significant decrease in AC-SINS score, while the other V_H variants displayed no change in AC-SINS score. This implies that both CDR-L1 and H2 play a significant role in the antibody's problematic self-interaction propensity. The observed mutations could have rigidified the CDR loops, as an antibody's problematic self-interaction properties are commonly attributed to flexible CDR-CDR interactions [333,335,336].

The combinatorial effects of V_H and V_L mutations can be additive due to their locations in separate chains, as demonstrated in this study and illustrated in **Figure 22B**. For example, the VL1 variant (square) in combination with any V_H variant significantly reduced the AC-SINS score without markedly altering the affinity. Conversely, the VL2 variant (upright triangle) in combination with any V_H variant decreased AC-SINS but also adversely affected affinity. The three top-performing antibodies identified in this study were the VL1 variant combined with either the parental V_H or VH7 and the VL3 + VH2 variant, all maintaining affinities below 5 nM and AC-SINS scores under 10.

Despite these successes, the overall success rate was relatively low, if using the above criteria for defining a successful antibody candidate. The enrichment analysis identified 4 enriched V_L variants and 7 enriched V_H variants, leading to the characterization of 40 antibody variants. Among these, three variants failed to

express, eleven showed no observed binding, six exhibited significantly reduced conformational stability and 8 showed no improvement in colloidal stability.

It could be argued that the mammalian display "filter" was inefficient in this study. However, only a single round of FACS selection was done with a relatively permissive gating and antigen staining strategy. Likely, variants with significantly reduced affinity for the antigen would not have been enriched in a subsequent round of FACS with more stringent selection criteria.

Overall, the maturation campaign in this study was successful in identifying several antibody variants with significantly improved colloidal stability and retained nanomolar affinity for the 8 kDa gelsolin fragment. The success is particularly noteworthy given the limited sizes of the libraries, which were constructed using a random mutagenesis strategy without structural information on the antibody or the antibody-antigen complex. The mammalian display platform proved highly effective in identifying rare mutations that enhanced colloidal stability without compromising affinity. Furthermore, the use of a random mutagenesis strategy and characterization of multiple variants provided valuable insights into the structural properties of the antibody and its potential paratope, which could be beneficial for future engineering efforts. Notably, mammalian display also identified beneficial mutations located in the framework region – areas typically overlooked in targeted CDR maturation campaigns. This supports the use of epPCR in combination with mammalian display as a promising approach for antibody maturation.

The random mutagenesis strategy identified amino acid positions that tolerate mutations without negatively affecting stability or binding. Since epPCR predominantly introduces single base pair changes, many of the observed amino acid substitutions are conservative, meaning the original amino acid is replaced by one with similar biochemical properties. It would be worthwhile to further investigate whether more optimal substitutions could be discovered through site-saturation mutagenesis at these identified positions.

4.5 Targeted somatic hypermutation using mammalian display (III)

As the probability of identifying antibodies with desired properties from a displayed library is proportional to the size of the library, mammalian display has a disadvantage compared to other display technologies, such as phage display or ribosome display. However, the complexity of mammalian cells, coupled with the exogenous expression of activation-induced cytidine deaminase (AID), allows for *in situ* antibody maturation by mimicking *in vivo* somatic hypermutation.

Several studies have been published where exogenous AID has been overexpressed in antibody-displaying mammalian cells to introduce random

mutations along the antibody gene [236,237,245,294–298]. Given the low probability of yielding mutations with a positive effect, an approach to target mutations specifically to the variable regions was experimented. This involved the introduction of G-quadruplex structures into the variable regions and the linker of an scFv-Fc antibody gene.

4.5.1 Designing antibody construct with G-quadruplex structures (III)

G-quadruplex (G4) structures can form in single-stranded DNA and RNA within guanine-rich sequences, such as those found in telomeric nucleic acids at the ends of linear chromosomes. Guanine's ability to Hoogsteen hydrogen bond with itself facilitates the formation of ring-like structures known as G-quartets, where four guanines each form hydrogen bonds with their two neighbors. These quartets can stack to create G4 structures [337].

G4 structures have been linked to several regulatory roles in cellular processes. During DNA replication, G4s can stall replication forks and affect the replication origin activity. During transcription, G4 structures may either recruit transcription factors or inhibit the progression of RNA polymerase II. Similarly, in translation, G4 structures in mRNA can repress translation by hindering ribosome progression or the recruitment of translation initiation factors [338]. Importantly, naturally occurring G4 structures in cellular DNA have shown a possible role in recruiting AID to specific regions, such as the Ig V region [339,340]. It has also been shown that certain sequence motifs, referred to as hotspots, can act as activators for AID by attracting the enzyme and thereby inducing mutations [289]. The mutations have been shown to spread around the targeted cytidine base pairs due to the error-prone DNA repair mechanisms [341].

With this in mind, an scFv-Fc construct was designed using germline antibody sequences with naturally occurring G4 structures. The glycine-serine linker between the V_L and V_H was codon optimized to contain as many G4 structures as possible, using an online tool called G4Hunter [342]. To assess the effects of the G4 structures on the localization of AID-induced mutations, an scFv construct encoding the same amino acid sequence, but codon optimized to not include any G4 structures was designed. Both of these scFv-Fc constructs were cloned into the Bxb1-TV vector and stably transfected into CHO-LP cells.

As the antibody consisted of germline genes, it had no antigen specificity. The purpose of this experiment was to examine whether the inclusion of G4 structures in the antibody gene and the linker could increase the recruitment of AID resulting in targeting of AID-induced mutations to the variable regions. The scFv-Fc format was chosen to decrease unwanted mutations in the constant regions.

4.5.2 G4 structures attracted AID-induced mutations (III)

The two CHO-LP cell lines stably expressing the scFv-Fc constructs were transfected with an episomal vector encoding mouse AID and a geneticin resistance marker to induce mutagenesis. One day post-transfection, the cells were single-cell sorted into a selection medium (**Figure 23**) and cultured for two weeks to allow mutations to accumulate. Since AID-induced mutations in the GFP gene have previously been shown to reduce GFP signal intensity due to gene inactivation [343], two sorting gates were made to monitor the localization in both constructs.

The first gate included cells displaying the scFv-Fc antibody at levels comparable to control cells without AID transfection (**Figure 23A**). The second gate included cells with reduced antibody display, potentially due to mutations in the antibody genes or other factors such as cell cycle stage or cell health. Both the scFv-Fc-G4 construct (**Figure 23B**) and scFv-Fc without G4 (**Figure 23C**) were sorted similarly to compare mutation distribution between the two constructs. Additionally, cells displaying the scFv-Fc without AID transfection (**Figure 23A**) were sorted similarly to account for unrelated mutations.

After the cells had recovered from FACS sorting, between one and four surviving clones from the two gates were pooled for each sample, expanded, and re-transfected with the episomal AID vector. The cells were then cultured for an additional three days, to maximize the likelihood of detecting AID-induced mutations, before extracting the genomic DNA for sequencing.

The V_L and V_H regions of the scFv-Fc constructs, both with and without G4 structures, and with or without AID transfection, were sequenced using NGS. The mutation rate at each amino acid position was determined by counting the number of changes at each position and normalizing it to the total number of reads in the sample. The non-AID transfected sample was used to account for unrelated mutations caused by spontaneous mutations during the cell cultivation, as well as errors introduced during PCR and sequencing. **Figure 23D-E** shows the mutation rate distribution across the V_L and V_H genes, respectively, with and without G4 structures.

The scFv-Fc construct containing the G4 structures accumulated significantly more mutations than the construct without G4 structures, with the majority of mutations occurring near the strong G4 structure-containing linker. The cumulative mutation rate across the entire V_L region was 9.2% for the G4-containing construct, compared to 1.7% for the constructs without the G4 structures. Similarly, the cumulative mutation rate across the V_H region was 16.7% for the construct with G4

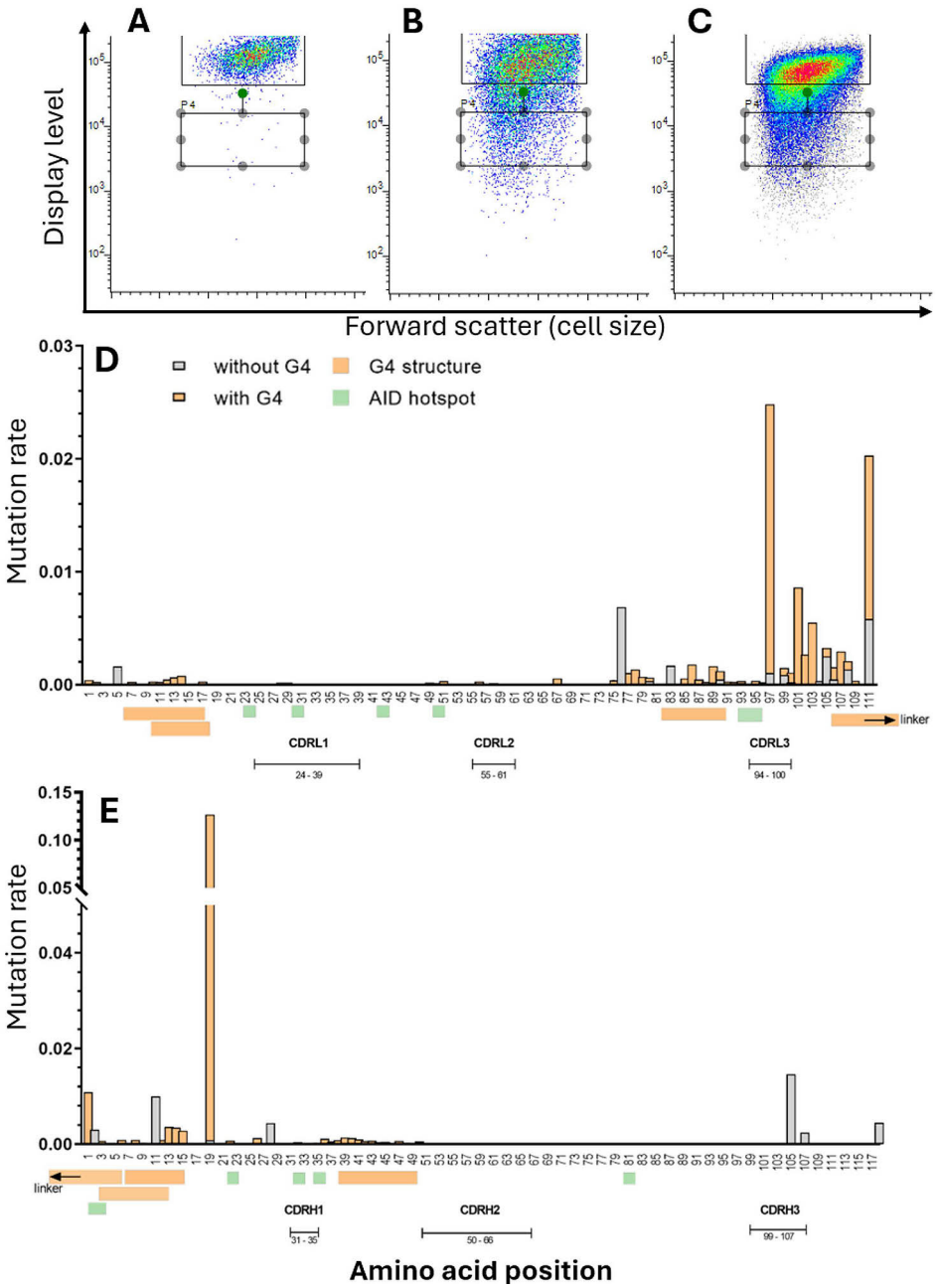

Figure 23. Sorting and mutation rate analysis of AID-transfected cells expressing a germline scFv-Fc antibody. Cells expressing the scFv-Fc without AID transfection (**A**) were sorted and used to account for unrelated mutations. Cells expressing the scFv-Fc construct with G4 structures (**B**) and without G4 structures (**C**) were transfected with exogenous AID and single-cell sorted. The cells with retained and decreased display levels were sorted to increase the probability of detecting AID-induced mutations. The mutation rate for each amino acid position was determined for V_L (**D**) and V_H (**E**). Figure edited from [344].

structures, compared to 4.0% for the construct without. This indicates that the presence of G4 structures increased the overall mutation rate by 5.4-fold in the V_L and 4.2-fold in the V_H, effectively concentrating the mutations in their proximity.

AID deaminates the targeted C-G base pairs, creating U-G mismatches that are subsequently processed by various error-prone repair pathways. These U-G mismatches can be converted into any other base pair, or they may introduce additional mutations downstream of the deaminated cytidine [345]. Interestingly, most of the observed mutations in this experiment were not cytidine transversions. For example, the most prevalent mutation in the V_L region was a T-G transversion, leading to the L97R mutation, which occurred in 2.8% of the scFv-Fc-G4 construct (**Figure 24**). This mutation was located between two G4 structures and next to three AID hot spot repeats (TGCA and AGCT [289]). AID likely deaminated the cytidine next to these hot spots, triggering an error-prone DNA repair mechanism that resulted in the T-G transversion.

Overall, this experiment provided valuable insights into how AID-induced mutations can be targeted to antibody genes through the inclusion of G4 structures via codon optimization. However, this study did not assess the functionality of the mutations, such as their impact on antigen binding or biophysical properties, which will need to be investigated separately using different antibody genes. Additionally, this experiment was limited to scFv constructs in the V_L-V_H orientation. Most mutations accumulated in the CDR-L3, FR-L4, and FR-H1 regions, which were adjacent to the strong G4 structure-containing linker. Given that CDR-H3 typically plays a more critical role in antigen binding than CDR-L3, it would be interesting to test whether mutations could be directed to the CDR-H3 region orienting the scFv in the V_H-V_L configuration. Furthermore, adding AID hotspots to the CDRs while removing them from the framework regions could further help concentrate the mutations in the CDRs.

Figure 24. DNA sequence at the most prevalent mutation in the V_L region. AID is attracted to the single-stranded DNA during DNA replication or transcription by the G4 structures (orange). The cytosine (red) is positioned adjacent to three consecutive AID hotspots (purple and green), which likely prompted AID to deaminate it to uracil. During the error-prone DNA repair process, the U-G mismatch may have been repaired, leading to the conversion of the thymine (blue) to guanine. This change resulted in the leucine (L) being mutated to arginine (R). Figure from [344].

5 Conclusions

A correlation between the poor biophysical properties of clinical therapeutic antibodies and their clinical failure has been established. This underscores the importance of screening and selecting antibodies with superior biophysical properties during the early stages of antibody discovery and engineering to reduce the risk of expensive late-stage clinical failures. Promising evidence between the biophysical properties of antibodies and their display level achieved on mammalian cells has also been shown. This prompted us to develop a novel mammalian display platform for high-throughput screening and selection of antibodies with favorable biophysical properties.

The Bxb1 integrase-based stable integration strategy was selected for the mammalian display platform due to its high fidelity and efficiency. The stable integration efficiency was further enhanced by optimizing the nuclear localization signal peptide, which was fused to the integrase to improve nuclear transport. Additionally, the co-expression of Ran GTPase-activating protein (RanGAP), which facilitates the recycling of nuclear transport proteins to active form in the cytosol, further improved nuclear transport. These improvements in stable integration efficiency enable the display of larger antibody libraries within the mammalian display platform.

Given the limited evidence supporting mammalian display's ability to distinguish antibodies with differing biophysical properties, additional data was provided in this thesis. This was achieved by displaying 37 clinical-stage antibodies with diverse biophysical properties and determining the correlation between their display levels and published biophysical properties. Statistically significant correlations were observed between the display levels and attributes such as conformational and colloidal stability, hydrophobicity, and polyspecificity.

The utility of the developed platform was further demonstrated by enhancing the biophysical properties of two antibodies using both rational and random mutagenesis strategies. Improved antibody variants were selected through FACS, with enrichment analysis confirmed by NGS. The success of the maturation campaigns was validated by soluble expression of the selected antibodies followed by comprehensive biophysical characterization.

Lastly, a method for inducing *in situ* random mutations targeted to antibody variable domains was developed. This was achieved through heterologous expression of AID and codon optimization to incorporate G-quadruplex (G4) structures into the antibody genes. Incorporating G4 structures into the variable domain genes and the scFv-Fc linker significantly increased the mutation rate and enabled mutation targeting to the sequences adjacent to the G4 structures.

This thesis presents the development of a novel mammalian display platform, supported by extensive data demonstrating its ability to select antibodies with favorable biophysical properties. The promising results presented here are expected to encourage the antibody engineering field to adopt mammalian display as a screening platform in the early phases of discovery, particularly for therapeutic applications.

6 Materials and Methods

This chapter provides a summary of the most relevant materials and methods used in the study. Detailed descriptions are presented in the relevant original publications, which are indicated by parentheses, if applicable.

6.1 Cell culture and transfections (I-III)

Adherent Flp-In CHO cell line (Invitrogen) was cultured in Ham's F-12 Nutrient Mix (Gibco) supplemented with 2 mM GlutaMAX (Gibco) and 10% fetal bovine serum (Sigma-Aldrich) at +37°C, 5% CO2 according to the manufacturer's recommendations. The serum-free suspension-adapted landing pad cell line was cultured in FectoCHO CD Medium (Polyplus), supplemented with 2 mM GlutaMAX at +37°C, 5% CO2 at 120 rpm orbital shaker with 19 mm throw. ExpiCHO cells (Gibco) were cultured in ExpiCHO Expression Medium (Gibco) at +37°C, 8% CO2. The transfections of the adherent cell line were done using Lipofectamine 3000 (Invitrogen), according to the manufacturer's instructions. The transfections of the suspension-adapted cell line were done using FectoPro (Polyplus), according to the manufacturer's instructions.

6.2 Vector construction (I-III)

The Bxb1 landing pad (LP) vector was designed to facilitate the integration of an antibody display cassette into the host cell genome via Bxb1 integrase for recombinase-mediated cassette exchange (RMCE). Within the LP construct, the CMV promoter drove the expression of a mouse IgG2a Fc surface marker, followed by a platelet-derived growth factor receptor ß (PDGFRβ) transmembrane (TM) domain, which anchors it to the cell membrane. Blasticidin S deaminase (BSD) encoding gene was positioned downstream of the surface marker, separated by a furin cleavage site and a P2A peptide, enabling the antibiotic selection of successful transfectants. The expression cassette was flanked by Bxb1 AttP and AttPm recombination sites to facilitate the RMCE of the expression cassette. The landing pad vector was synthesized by GeneArt (Thermo Fisher) with flanking restriction

sites for NheI and SphI, allowing for restriction cloning into the pcDNA5/FRT vector (Invitrogen) to create the pcDNA5/FRT-LP vector.

To facilitate Bxb1 integrase-driven RMCE, a promoterless Bxb1 targeting vector, pBxb1-TV-GFP, was constructed, with AttB and AttBm recombination sites flanking the expression cassette. This vector, which was used for initial testing and platform optimization, was bicistronic and comprised of DNA encoding a human insulin signal peptide, EGFP with a human CD8 stalk and CD8 TM domain fusion for membrane anchoring. The gene encoding puromycin N-acetyltransferase (PuroR) was placed downstream of the TM domain, separated by a furin cleavage site and a P2A peptide, enabling drug selection of stable transfectants. Bovine growth hormone (bGH) polyA was placed downstream of the PuroR gene.

For the expression of different antibodies, the EGFP encoding gene in the pBxb1-TV-GFP vector was replaced with an antibody expression cassette. This cassette included DNA encoding the antibody light chain, a furin cleavage site, a T2A peptide, an IGHV3 signal peptide, and the antibody heavy chain. This replacement was achieved by NotI/HindIII (NEB) digestion and ligation.

The original Bxb1 integrase expression vector, pBxb1-EV, consisted of DNA encoding the CMV promoter, SV40 NLS, HA tag, Bxb1 integrase, and bGH-polyA. Variants of nuclear localization signals (NLS), including Myc proto-oncogene NLS, transcription factor EGL-13 NLS, and nucleoplasmin NLS from *Xenopus laevis*, were synthesized by GeneArt (Thermo Fisher) and inserted into both the N-terminus and C-terminus of Bxb1 integrase. These insertions were achieved using BamHI-AvaI and PshAI-SphI restriction sites in the pBxb1-EV vector, respectively. Additionally, DNA encoding two copies of the nucleoplasmin NLS and a nuclear transport protein (such as importin α, importin β, RanGTP, RCC1, or RanGAP), separated by a furin cleavage site and T2A peptide, were synthesized by GeneArt. Subsequently, they were cloned into the C-terminus of Bxb1 using PshAI-SphI restriction sites in the pBxb1-EV vector.

The V_H of the scFv-Fc constructs was composed of the IGHV3-23*01, IGHD-20*01, and IGHJ4*01 alleles. The V_L of the scFv-Fc constructs was composed of the IGKV2-28*01 and IGKJ1*01 alleles. The amino acid sequence of the linker was GGGGSGAGGSGGGGTGGGGS. The Fc of the scFv-Fc construct was composed of the IGHG1*03 allele. The construct was synthesized by GeneArt and cloned to the pBxb1-TV vector by NEBuilder® HiFi DNA Assembly Master Mix (NEB). The mouse AID was codon optimized for CHO, synthesized by Twist Biosciences, and cloned into the pCEP4 vector (Thermo Scientific) by XhoI/KpnI (NEB) restriction digestion and ligation.

6.3 Generation of suspension-adapted landing pad cell line (I)

To establish a suitable CHO cell line for mammalian display, the genomic integration of the Bxb1 landing pad was performed. Flp-In CHO cells were co-transfected with pcDNA5/FRT-LP and pOG44 (Invitrogen) using Lipofectamine 2000 (Invitrogen) at a ratio of 1:9, following the manufacturer's instructions. Two days post-transfection, 600 μg/mL Hygromycin B (Gibco) was introduced. Upon reaching confluency, the cells were dissociated using Cellstripper (Corning), resuspended in PBS, supplemented with 2% fetal bovine serum, and then stained with PE-Anti-mouse IgG2a Fc antibody (Jackson ImmunoResearch) according to the manufacturer's instructions. Single-cell sorting into 96-well plates was performed to clone the cells using BD FACSMelody (BD Biosciences), with the sorting gate adjusted to isolate cells exhibiting the highest PE signal. The 96-well plates contained 67 μL of fresh media and 33 μL of conditioned media. After seven days, 12 clones were expanded into 6-well plates, and a master plate of these clones was frozen. The plated clones were subsequently co-transfected with a 1:1 ratio of pBxb1-EV and pBxb1-TV-GFP. Puromycin selection (10 μg/mL) was initiated two days post-transfection, and after 14 days, the cells were stained with PE-Anti-mouse IgG2a Fc antibody and analyzed for mEGFP and mouse IgG2a Fc expression using BD Accuri C6 Plus (BD Biosciences). One clone exhibiting a high mEGFP signal and no PE signal was identified as the landing pad cell line (CHO-LP). The flow cytometry data was analyzed using FlowJo software (BD Biosciences).

The serum-free suspension adaptation of CHO-LP cells involved detaching the cells with Trypsin-EDTA 0.05% (Gibco) and seeding them at a density of 0.5 × 10^6 cells/mL into ProCHO4 protein-free CHO medium (Lonza), supplemented with 2 mM GlutaMAX and 0.2% anti-clumping agent (Gibco), at +37°C with 5% CO2 and shaken at 120 rpm. The cells were passaged to 0.5 × 10^6 viable cells/mL every 3–4 days until viability exceeded 90% for three consecutive passages. Subsequently, the cells were adapted to FectoCHO CD Medium (Polyplus) to enhance transfectability.

6.4 Cell staining, sorting, and flow cytometry analysis (I-III)

Cell staining was performed in EasySep buffer (Stemcell Technologies) at a concentration of 50×10^6 cells/mL, keeping the samples on ice for 30 minutes for each staining step, with washes in between, as per the manufacturer's guidelines. For staining involving the target protein, the first step utilized either 10 nM mono-biotinylated PCSK9 (AcroBiosystems) or 37 nM mono-biotinylated 8 kDa gelsolin fragment (CASLO, Denmark), followed by a second staining step with PE anti-

human Ig light chain κ antibody and SAvPhire (monomeric streptavidin, Sigma-Aldrich) or AlexaFluor 647(AF647)-conjugated mouse anti-biotin antibody. The SAvPhire was conjugated using the APC Conjugation Kit—Lightning-Link (Abcam), following the manufacturer's instructions. The stained cells were resuspended in EasySep buffer to a concentration of 5×10^6 cells/mL and sorted using the BD FACSMelody Cell Sorter at a rate of 500–2000 cells per second. The sorting was conducted into 5 mL tubes containing 1 mL of medium, with cells sorted based on the display level indicated by the PE signal and antigen binding detected by the APC/AF647 signal.

The stable integration efficiency was measured 6-8 days after transfection from cells which were kept without antibiotic selection. The cells were either stained with the PE anti-human Ig light chain κ antibody or only washed with EasySep buffer in the case of EGFP measurement. The measurements were done using BD Accuri C6 Plus and analyzed using Flow Jo.

6.5 Construction of antibody libraries (I)

The bococizumab mutant library was generated by randomly mutating the codons for L94 and W95 in the V_L and P53 and F54 in the V_H using NNK oligonucleotide-directed mutagenesis. A 694 bp PCR fragment containing these mutated regions in V_L and V_H, along with the intervening sequence (including the remainder of the light chain, furin cleavage site, T2A, IGHV3 signal peptide, and the beginning of V_H), was amplified from the pBxb1-TV-Bococizumab template using the following primers: forward, 5′-GCCAGCAAAGATATTCTNNKNNKCGGACATTCGGGCAAGGA-3′; and reverse, 5′-TTGGTCCGTCCGCCMNNMNNGGAGATTTCGCCCATCCACTC-3′. The remainder of the vector was amplified with primers: forward, 5′-GGCGGACGGACCAACTACA-3′; and reverse, 5′-AGAATATCTTTGCTGGCAATAGTATGTTGC-3′, providing 17 bp and 14 bp overlaps upstream and downstream of the mutagenized PCR product, respectively. The mutagenized PCR fragment was then ligated into the amplified vector backbone using NEBuilder® HiFi DNA Assembly Master Mix (NEB), and the resulting construct was electroporated into NEB® 5-alpha Electrocompetent E. coli (NEB). The transformation mixture was plated on ampicillin agar plates, from where the colonies were scraped into 50 mL LB-ampicillin the next day. Transfection-quality plasmid DNA was prepared with Plasmid Plus Midi Kit (Qiagen) from the liquid culture after 3 h incubation at +37°C, 250 rpm.

The anti-gelsolin mutation library was constructed by inserting random mutations using error-prone PCR. For each library either the V_L or V_H sequence was randomly mutagenized using GeneMorph II Random Mutagenesis Kit (Agilent Technologies, USA) according to the manufacturer's instructions using a protocol

for high mutation rate amplification with 0.1 ng of template DNA. The V_L or V_H fragments were cloned into the vector backbone using NEBuilder® HiFi DNA Assembly Cloning kit, according to the manufacturer's instructions and electroporated into NEB® 10-beta Electrocompetent *E. coli* cells (NEB). The transformation mixture was plated, and plasmid DNA prepared as before.

6.6 Next generation sequencing and enrichment analysis (I, III)

Genomic DNA was extracted from frozen cell pellets using the Monarch® Genomic DNA Purification Kit (NEB). To facilitate the pairing of the mutated regions in V_L and V_H within the bococizumab library, an amplicon encompassing only the mutated regions, and the intervening sequence was generated as a single 778 bp fragment. This amplicon was amplified using oligonucleotides designed to hybridize immediately upstream of the mutagenized region in V_L and immediately downstream of the mutagenized region in V_H. The oligonucleotides included universal adapter sequences at their 5′ ends, enabling the incorporation of index adapters via PCR using the Nextera Index kit (Illumina).

The PCR reactions were prepared with 50 µL volumes, each containing 1,000 ng of template DNA, using the NEBNext Ultra II Q5 Master Mix (NEB). The resulting amplicons were sent to Eurofins Genomics, where index adapters were added, and the library was prepared and sequenced on the Illumina MiSeq platform using the MiSeq Reagent Kit v3 (600 cycles, paired-end). The sequence data were annotated, and the variants were clustered with 100% identity in the mutated regions using PipeBio online platform. The normalized count for each cluster in each sample was determined by dividing the number of reads in the cluster by the total number of reads in that sample. To assess enrichment after each round of sorting, the normalized count of a cluster was divided by the normalized count of that same cluster in the pre-selection sample.

The sample preparation for the anti-gelsolin antibody was done similarly, with the following modifications: The complete V_H and V_L domains were sequenced separately, and the index adapters were incorporated using Nextera XT DNA Library Prep -kit (Illumina). The V_H and V_L sequences were annotated, and the variants were clustered with 100% identity in the whole V_H or V_L domain, respectively. The enrichment factor was calculated similarly, but only variants with more than 1000 reads in the pre-selection sample with more than two-fold enrichment were included.

The next-generation sequencing for the AID transfected cells was done similarly to the bococizumab library, except the whole V_H or V_L was sequenced, and the annotation was done using a custom scaffold, which annotated residues which

differed from the reference sequence. The number of amino acid changes for each position in the sequences was calculated for each sample using Microsoft Excel.

6.7 Antibody expression and purification (I)

The selected antibody variant genes were synthesized and cloned into pTwist CMV vector by Twist Biosciences. The transient expressions were done using ExpiCHO cells and the ExpiFectamine kit (Thermo Scientific), following the manufacturer's high yield protocol. The expressions were done in 10 mL scale using TubeSpin Bioreactors (TPP). The antibodies were harvested 11 days after transfection and purified using a sequential affinity and size-exclusion chromatography procedure using Äkta Pure (Cytiva). The cell culture supernatant was initially loaded onto a HiTrap MabSelect PrismA column (Cytiva) for purification. Elution was carried out into a 2 mL loop using 0.1 M sodium citrate at pH 3.0. The eluted sample was then further purified by loading it onto a Superdex 200 Increase 10/300 GL column (Cytiva) with PBS as the running buffer.

6.8 Measurement of antibody biophysical properties (I)

6.8.1 Affinity-capture self-interaction nanoparticle spectroscopy (AC-SINS) (I)

The Affinity-capture self-interaction nanoparticle spectroscopy (AC-SINS) assay was performed following the protocol outlined by Geng et al [346]. Briefly, 20 nm gold nanoparticles (Ted Pella) were first washed and concentrated by centrifugation at 21,130 x g for 6 minutes. After removing 95% of the supernatant, the nanoparticles were resuspended to 1.5 times their original volume in Milli-Q water. These washed nanoparticles were then conjugated overnight at room temperature with 160 μg/mL of goat anti-human Fc capture antibody (Jackson ImmunoResearch Labs). Before conjugation, the antibody was buffer-exchanged twice into 20 mM potassium acetate pH 4.3 using 40 kDa MWCO Zeba spin desalting columns. Unbound anti-Fc antibodies were removed by centrifugation, followed by resuspension in 2 mM potassium acetate pH 4.3 to 50% of the original volume. Next, the SEC-purified sample antibodies were diluted to 10 μg/mL in PBS containing 100 μg/mL of a non-specific goat antibody (Jackson ImmunoResearch Labs) to reduce non-specific binding. To each well of a clear-bottomed 384-well plate (Fisher Scientific), 8 μL of the prepared capture conjugates were added, followed by 72 μL of the diluted sample antibody. The mixture was thoroughly mixed by pipetting and incubated for 2 hours. The absorbance spectra were then measured using an EnVision plate reader (Perkin

Elmer) from 500 to 600 nm in 1 nm increments. A macro was employed to fit a second-order polynomial function to the data to identify the wavelength corresponding to the maximum absorbance value (plasmon wavelength). The plasmon wavelength of a PBS blank was subtracted from the antibody sample values to calculate the AC-SINS score. All measurements were performed in triplicate.

6.8.2 Polydispersity index and melting temperature (I)

Dynamic Light Scattering (DLS) and nano Differential Scanning Fluorimetry (nanoDSF) measurements were conducted using the Nanotemper Prometheus Panta instrument. Antibody samples (~10 µL at concentrations between 0.5–1 mg/mL) were loaded into standard-grade nanoDSF capillaries and positioned on the capillary holder. DLS data was initially collected at 25°C to determine the polydispersity index (PDI) of the samples. Following DLS measurements, the samples were subjected to a controlled temperature increase at a rate of 1°C/min, starting from 20°C and ramping up to 95°C. Melting temperature (T_m) values were derived by monitoring the intrinsic fluorescence of tryptophan and tyrosine residues at emission wavelengths of 330 nm and 350 nm. The unfolding curve was generated by plotting the fluorescence intensity ratio (F350 nm/F330 nm) against temperature. The thermal stability of the sample was characterized by the thermal unfolding transition midpoint, T_m (°C), which represents the temperature at which 50% of the protein population is unfolded. The T_m corresponds to the inflection point of the unfolding curve and was determined by calculating the derivative of the curve.

6.8.3 Polyreactivity ELISA (I)

The polyreactivity ELISA was conducted according to established protocols [116,347,348]. In brief, 50 µL of each of the six different antigens—dsDNA (10 µg/mL, Sigma), ssDNA (10 µg/mL, Sigma), LPS (10 µg/mL, Sigma), KLH (10 µg/mL, Sigma), cardiolipin (10 µg/mL, Sigma), and insulin (5 µg/mL, Sigma)—were coated onto 96-well ELISA plates (VWR) and incubated overnight at room temperature (RT). The plates were then washed three times with Milli-Q water and blocked with 200 µL of ELISA buffer (PBS with 1 mM EDTA and 0.05% Tween-20) for 1–2 hours at RT. Following blocking, the plates were washed three times, and 50 µL of the antibody samples, diluted to concentrations of 1,000, 250, 62.5, and 15.6 ng/mL in PBS, were added to the wells and incubated for 2 hours at RT. The plates were then washed three times. Subsequently, 50 µL of HRP-conjugated goat anti-human IgG antibody (Jackson ImmunoResearch Labs) diluted 1:1000 in ELISA buffer was added to each well and incubated for 1 hour, followed by three additional washes. The plates were then briefly blocked with ELISA buffer for 5 minutes, washed three

times, and 100 µL of TMB substrate (Thermo Scientific) was added according to the manufacturer's instructions. After 15 minutes of incubation at RT, 100 µL of 2M HCl was added to each well to stop the reaction, and absorbance at 450 nm was measured using an EnVision plate reader. To account for the background signal, the absorbance of a blank PBS sample was subtracted from the antibody sample readings. The polyreactivity score was calculated by averaging the PBS-subtracted absorbance values for all four antibody concentrations across the six different antigens.

6.8.4 Analytical hydrophobic interaction chromatography (I)

Antibody samples were diluted to a concentration of 0.5–1 mg/mL using mobile phase A solution (1.5 M ammonium sulfate and 20 mM Tris, pH 7.0) to achieve a final ammonium sulfate concentration of 0.5 M before analysis. Two to four micrograms of the diluted antibody were loaded onto a TSKgel Butyl-NPR column (2.5 µm, 4.6 mm × 3.5 cm, Tosoh Bioscience). The analysis was conducted with a linear gradient between mobile phase A and mobile phase B (20 mM Tris, pH 7.0) over 10 minutes, with the gradient starting at 5% mobile phase B and ending at 95% mobile phase B. The flow rate was set at 0.8 mL/min. Peak retention times were monitored by measuring UV absorbance at 220 nm using an Agilent 1260 Infinity II Bio-inert LC System.

6.8.5 Affinity measurement of Bococizumab variants and anti-gelsolin mAbs using surface plasmon resonance

Kinetic analysis of the antibody variants was conducted using surface plasmon resonance (SPR) with a Biacore 8K+ instrument (Cytiva). Anti-human IgG (Fc) antibody was immobilized on a CM5 sensor chip (Cytiva) using amine coupling, achieving an immobilization level of approximately 6000 RU with the Human Antibody Capture Kit (Cytiva). The sample antibodies were then captured at a concentration of 62.5 ng/mL for 60 seconds at a flow rate of 10 µL/min, resulting in capture levels between 10 and 25 RU in the Bococizumab-PCSK9 experiment and between 60 and 120 in the anti-gelsolin experiment. In the Bococizumab experiment, a 4-fold dilution series of PCSK9 (Acro Biosystems), ranging from 50 nM to 12 pM, was passed over the captured antibody surface for 240 seconds at a flow rate of 50 µL/min, followed by a dissociation phase of 1800 seconds. In the anti-gelsolin experiment, a 4-fold dilution series of a synthetic 8 kDa gelsolin fragment peptide (Caslo, Denmark), ranging from 800 nM to 50 pM, was passed over the captured antibody surface for 300 seconds at a flow rate of 40 µL/min, followed by a dissociation phase of 600 seconds. Surface regeneration in both experiments was

achieved using 3 M $MgCl_2$ between measurement cycles. The association and dissociation constants were determined using Biacore Insight Evaluation software, applying the Langmuir 1:1 global fitting model. All measurements were performed in duplicate.

6.9 Statistical analysis (II)

Statistical analyses were done using GraphPad Prism 9 (GraphPad, San Diego, USA) and Microsoft Excel. Student's T-test with assumed equal variances was used to test for statistically significant differences between the Bxb1 NLS variants. The threshold for statistical significance (alpha level) was 0.05.

Acknowledgments

The experimental work in this study was carried out at the Protein and Antibody Engineering unit at Orion Pharma R&D in Turku, Finland, during the years 2020–2024. My doctoral training was done in the industrial PhD (iPhD) track of Drug Research Doctoral Program (DRDP) at the University of Turku. The financial support from Business Finland, Orion Pharma, DRDP, and InFlames is gratefully acknowledged. Special thanks go to Professor Antti Haapalinna and Dr. Tim Holmström for providing me the opportunity to develop my research skills in an industrial setting and for recognizing my potential.

I want to express my deepest gratitude to my supervisors, Professor Urpo Lamminmäki, Dr. Stuart Prince, and Dr. Rune Salbo. I am particularly thankful to Professor Lamminmäki for keeping my project on track, assisting me with university administration, and for our invaluable scientific discussions. I am grateful to Dr. Prince for introducing me to molecular biology, providing excellent feedback on my ideas, and helping me troubleshoot my experiments that didn't work on the first try. My thanks also go to Dr. Salbo for offering much-needed support at work, as well as after work in the palju. Together, you have helped me become an expert in antibody engineering by allowing me the freedom to pursue my research while offering invaluable insight and guidance.

I would like to thank Professor Peter Kristensen and Professor Johan Rockberg for taking the time from your busy schedules to review my thesis and for providing valuable feedback. A special thank you goes to Dr. Achim Doerner for accepting the role of opponent in my dissertation.

Working in the Protein and Antibody Engineering Unit at Orion Pharma has been a privilege. The team has fostered a safe and stimulating environment where I could grow as a scientist. First and foremost, I would like to thank my Orion supervisors during this journey. Thanks to Dr. Tim Holmström for hiring me as a student in the newly established Biologics unit in 2018, believing in my potential, and enabling my doctoral training within the industrial PhD track. Thanks also to Dr. Rune Salbo for taking on the supervisory role after reorganization and handling it admirably, with empathy and dedication, ensuring that we could focus on our most important job, the science. My gratitude goes to Dr. Bryce Nelson for guiding our technological

progress forward and leading by example; you have encouraged me to take on more responsibility and to trust in my expertise. I also wish to acknowledge Orion Pharma for the financial support provided for my reagent costs and conference participation, enabling me to pursue ambiguous research goals without financial constraints and to engage with international experts in my field.

My deepest gratitude goes to Ari Kanttinen for teaching me the fundamentals of mammalian cell culture, a cornerstone of my thesis work. Special thanks also to Dr. Antti Kulmala for supporting my experiment planning, teaching me extensively about molecular biology and library construction, introducing me to the world of NLS and signal peptides, and brainstorming new brilliant ideas with me. You have been a mentor and a person who I could always turn to when in doubt. I also thank Laura Leimu for being a pioneer in the iPhD track and for her continuous sympathy and support during our PhD journeys. My appreciation extends to Saara Östman and Elisa Lankinen, who chose to do their Master's thesis under my supervision and produced exceptional results, contributing to a patent application, remarkable findings in my thesis, and a manuscript in preparation. Thank you, Dr. Terhi Oja, Laura Leimu, Satu Kaskinoro, Mirkka Papinkivi, Mona Niiranen, and Anja Vilkman for your expertise in antibody expression, purification, and thorough characterization. Thanks also to everyone on the Turla 4th floor for the great scientific discussions, mental support, and laughs during coffee breaks.

I would like to acknowledge the organizers of the DRDP annual meetings, FinPharmaNet meetings, InFlames events, and Christmas parties. Networking with other PhD students and researchers has been invaluable, providing opportunities to learn from their experiences. Thanks to my fellow iPhD students from Orion for the camaraderie throughout this journey. In particular, I want to recognize Laura Leimu, Dr. Antti Äärelä, Dr. Kiira Kalke, Emmi Kuokkanen, Anna Brunell, Saara Östman, Miika Vuorimaa, and Paula Lehtinen for your great company during the meetings and events. I also want to thank the amazing people from DRDP and InFlames doctoral programs, whom I've had the privilege to get to know during these events. Thanks also to the PhD students and staff at the Department of Biotechnology for their support and empathy. Specifically, I want to thank Sami Oksanen, Anastasiia Kushnarova-Vakal, and Oskar Haavisto for their enjoyable company during department summer days and Christmas parties.

My gratitude also extends to Dr. Fawzi Khoder-Agha for joining The Chads and keeping our team spirit always high. Thank you for the enriching scientific discussions, the great lunch company, and for the memes and lulz. Special thanks to Dr. Antti Kulmala for being excellent company during conferences, R&D training days, and Christmas parties and for the unforgettable nights out in Turku, Helsinki, Barcelona, and Lisbon. My thanks go to my brother-in-law Roope for dragging me to the gym every Saturday morning, countless hours on Discord, for your invaluable

support when I've been at my weakest and for having the best time of my life at countless heavy metal festivals and concerts, just to name a few. To my great friends Ville and Niko, thank you for your ongoing support and understanding of my frustrations, the insightful humor and for the memorable hiking trips to Koli and Paras with me and my brother Mikko; I'm looking forward to the future hiking trips with you. I also acknowledge the Padel Boys – Juuso, Tuomas, Joni and Santeri – for sharing the joy of padel with me over the past three years. Our games and post-match analyses have provided a welcome distraction from work and a valuable way to de-stress. To all my childhood friends, thank you for the reunions and your support throughout the years.

Finally, I want to express my deepest gratitude to my parents for their unwavering love and support. Thank you for encouraging me to reach my potential and for always being there when I need it.

Turku, November 2024

List of References

1. Hirano, M., Das, S., Guo, P. & Cooper, M. D. The Evolution of Adaptive Immunity in Vertebrates. in *Advances in Immunology* vol. 109 125–157 (Adv Immunol, 2011).
2. Hoffmann, J. & Akira, S. Innate immunity. *Current Opinion in Immunology* vol. 25 1–3 (2013).
3. Iwasaki, A. & Medzhitov, R. Control of adaptive immunity by the innate immune system. *Nature Immunology* vol. 16 343–353 (2015).
4. Nemazee, D. Mechanisms of central tolerance for B cells. *Nature Reviews Immunology* vol. 17 281–294 (2017).
5. Yates, A. J. Theories and quantification of thymic selection. *Frontiers in Immunology* vol. 5 68254 (2014).
6. Teng, M. W. L., Kershaw, M. H. & Smyth, M. J. Cancer Immunoediting: From Surveillance to Escape. in *Cancer Immunotherapy: Immune Suppression and Tumor Growth: Second Edition* 85–99 (Academic Press, 2013). doi:10.1016/B978-0-12-394296-8.00007-5.
7. Murphy, K. & Weaver, C. *Janeway's immunobiology*. (Garland science, 2016).
8. Pierson, T. C., Fremont, D. H., Kuhn, R. J. & Diamond, M. S. Structural Insights into the Mechanisms of Antibody-Mediated Neutralization of Flavivirus Infection: Implications for Vaccine Development. *Cell Host and Microbe* vol. 4 229–238 (2008).
9. Edelman, G. M. Antibody structure and molecular immunology. *Science (80-.).* **180**, 830–840 (1973).
10. Schroeder, H. W. & Cavacini, L. Structure and Function of Immunoglobulins. *J. Allergy Clin. Immunol.* **125**, S41 (2010).
11. Briney, B. S., Willis, J. R., Hicar, M. D., Thomas, J. W. & Crowe, J. E. Frequency and genetic characterization of V(DD)J recombinants in the human peripheral blood antibody repertoire. *Immunology* **137**, 56–64 (2012).
12. Janeway, C. A. J., Travers, P. & Walport, M. The generation of diversity in immunoglobulins. *Immunobiol. Immune Syst. Heal. Dis. 5th Ed.* 1–11 (2001).
13. Motea, E. A. & Berdis, A. J. Terminal deoxynucleotidyl transferase: The story of a misguided DNA polymerase. *Biochimica et Biophysica Acta - Proteins and Proteomics* vol. 1804 1151–1166 (2010).
14. Desiderio, S. V. *et al.* Insertion of N regions into heavy-chain genes is correlated with expression of terminal deoxytransferase in B cells. *Nature* **311**, 752–755 (1984).
15. Jung, D., Giallourakis, C., Mostoslavsky, R. & Alt, F. W. Mechanism and control of V(D)J recombination at the immunoglobulin heavy chain locus. *Annual Review of Immunology* vol. 24 541–570 (2006).
16. Elhanati, Y. *et al.* Inferring processes underlying B-cell repertoire diversity. *Philos. Trans. R. Soc. B Biol. Sci.* **370**, (2015).
17. Rees, A. R. Understanding the human antibody repertoire. *mAbs* vol. 12 (2020).
18. Cheng, H. L. *et al.* Integrity of the AID serine-38 phosphorylation site is critical for class switch recombination and somatic hypermutation in mice. *Proc. Natl. Acad. Sci. U. S. A.* **106**, 2717–2722 (2009).

19. Stavnezer, J. & Schrader, C. E. IgH Chain Class Switch Recombination: Mechanism and Regulation. *J. Immunol.* **193**, 5370–5378 (2014).
20. Chi, X., Li, Y. & Qiu, X. V(D)J recombination, somatic hypermutation and class switch recombination of immunoglobulins: mechanism and regulation. *Immunology* vol. 160 233–247 (2020).
21. Mishra, A. K. & Mariuzza, R. A. Insights into the structural basis of antibody affinity maturation from next-generation sequencing. *Frontiers in Immunology* vol. 9 117 (2018).
22. Vajda, S., Porter, K. A. & Kozakov, D. Progress toward improved understanding of antibody maturation. *Current Opinion in Structural Biology* vol. 67 226–231 (2021).
23. Shehata, L. *et al.* Affinity Maturation Enhances Antibody Specificity but Compromises Conformational Stability. *Cell Rep.* **28**, 3300-3308.e4 (2019).
24. Davenport, T. M. *et al.* Somatic Hypermutation-Induced Changes in the Structure and Dynamics of HIV-1 Broadly Neutralizing Antibodies. *Structure* **24**, 1346–1357 (2016).
25. Köhler, G. & Milstein, C. Continuous cultures of fused cells secreting antibody of predefined specificity. *Nature* **256**, 495–497 (1975).
26. Shulman, M., Wilde, C. D. & Köhler, G. A better cell line for making hybridomas secreting specific antibodies. *Nature* vol. 276 269–270 (1978).
27. Ecker, D. M., Jones, S. D. & Levine, H. L. The therapeutic monoclonal antibody market. *mAbs* vol. 7 9–14 (2015).
28. Carrara, S. C. *et al.* From cell line development to the formulated drug product: The art of manufacturing therapeutic monoclonal antibodies. *International Journal of Pharmaceutics* vol. 594 120164 (2021).
29. Mullard, A. FDA approves 100th monoclonal antibody product. *Nature reviews. Drug discovery* vol. 20 491–495 (2021).
30. Crescioli, S. *et al.* Antibodies to watch in 2024. *MAbs* **16**, (2024).
31. Kinch, M. S., Kraft, Z. & Schwartz, T. Monoclonal antibodies: Trends in therapeutic success and commercial focus. *Drug Discov. Today* **28**, 103415 (2023).
32. Antibody Therapy Market Size, Growth Analysis 2023-2032. https://www.gminsights.com/industry-analysis/antibody-therapy-market.
33. Grilo, A. L. & Mantalaris, A. The Increasingly Human and Profitable Monoclonal Antibody Market. *Trends Biotechnol.* **37**, 9–16 (2019).
34. Redman, J. M., Hill, E. M., AlDeghaither, D. & Weiner, L. M. Mechanisms of action of therapeutic antibodies for cancer. *Molecular Immunology* vol. 67 28–45 (2015).
35. Kuan, C. T., Wikstrand, C. J. & Bigner, D. D. EGF mutant receptor vIII as a molecular target in cancer therapy. in *Endocrine-Related Cancer* vol. 8 83–96 (2001).
36. Okamoto, I. *et al.* Expression of constitutively activated EGFRvIII in non-small cell lung cancer. *Cancer Sci.* **94**, 50–56 (2003).
37. Fan, Q. W. *et al.* EGFR Phosphorylates Tumor-Derived EGFRvIII Driving STAT3/5 and Progression in Glioblastoma. *Cancer Cell* **24**, 438–449 (2013).
38. Shuptrine, C. W., Surana, R. & Weiner, L. M. Monoclonal antibodies for the treatment of cancer. *Seminars in Cancer Biology* vol. 22 3–13 (2012).
39. Chen, J. S., Lan, K. & Hung, M. C. Strategies to target HER2/neu overexpression for cancer therapy. *Drug Resist. Updat.* **6**, 129–136 (2003).
40. Mitri, Z., Constantine, T. & O'Regan, R. The HER2 Receptor in Breast Cancer: Pathophysiology, Clinical Use, and New Advances in Therapy. *Chemother. Res. Pract.* **2012**, 1–7 (2012).
41. Franklin, M. C. *et al.* Insights into ErbB signaling from the structure of the ErbB2-pertuzumab complex. *Cancer Cell* **5**, 317–328 (2004).
42. Dawood, S. & Sirohi, B. Pertuzumab: A new anti-HER2 drug in the management of women with breast cancer. *Futur. Oncol.* **11**, 923–931 (2015).
43. Behrens, L. M., van Egmond, M. & van den Berg, T. K. Neutrophils as immune effector cells in antibody therapy in cancer. *Immunological Reviews* vol. 314 280–301 (2023).

44. Sulica, A., Morel, P., Metes, D. & Herberman, R. B. Ig-binding receptors on human NK cells as effector and regulatory surface molecules. *International Reviews of Immunology* vol. 20 371–414 (2001).
45. Gül, N. *et al.* Macrophages eliminate circulating tumor cells after monoclonal antibody therapy. *J. Clin. Invest.* **124**, 812–823 (2014).
46. Reid, K. B. M. Complement component C1q: Historical perspective of a functionally versatile, and structurally unusual, serum protein. *Front. Immunol.* **9**, 355171 (2018).
47. Kolev, M., Towner, L. & Donev, R. Complement in cancer and cancer immunotherapy. *Archivum Immunologiae et Therapiae Experimentalis* vol. 59 407–419 (2011).
48. Petricevic, B. *et al.* Trastuzumab mediates antibody-dependent cell-mediated cytotoxicity and phagocytosis to the same extent in both adjuvant and metastatic HER2/neu breast cancer patients. *J. Transl. Med.* **11**, 307 (2013).
49. Shiravand, Y. *et al.* Immune Checkpoint Inhibitors in Cancer Therapy. *Current Oncology* vol. 29 3044–3060 (2022).
50. Sadeghi Rad, H. *et al.* Understanding the tumor microenvironment for effective immunotherapy. *Medicinal Research Reviews* vol. 41 1474–1498 (2021).
51. Havel, J. J., Chowell, D. & Chan, T. A. The evolving landscape of biomarkers for checkpoint inhibitor immunotherapy. *Nature Reviews Cancer* vol. 19 133–150 (2019).
52. de Mello, R. A., Veloso, A. F., Esrom Catarina, P., Nadine, S. & Antoniou, G. Potential role of immunotherapy in advanced non-small-cell lung cancer. *Onco. Targets. Ther.* **Volume 10**, 21–30 (2016).
53. Beldi-Ferchiou, A. *et al.* PD-1 mediates functional exhaustion of activated NK cells in patients with Kaposi sarcoma. *Oncotarget* **7**, 72961–72977 (2016).
54. Jenkins, R. W., Barbie, D. A. & Flaherty, K. T. Mechanisms of resistance to immune checkpoint inhibitors. *Br. J. Cancer* **118**, 9–16 (2018).
55. Carter, P. J. & Lazar, G. A. Next generation antibody drugs: Pursuit of the 'high-hanging fruit'. *Nature Reviews Drug Discovery* vol. 17 197–223 (2018).
56. Labrijn, A. F., Janmaat, M. L., Reichert, J. M. & Parren, P. W. H. I. Bispecific antibodies: a mechanistic review of the pipeline. *Nature Reviews Drug Discovery* vol. 18 585–608 (2019).
57. Nisonoff, A., Wissler, F. C. & Lipman, L. N. Properties of the major component of a peptic digest of rabbit antibody. *Science (80-.).* **132**, 1770–1771 (1960).
58. Nisonoff, A. & Rivers, M. M. Recombination of a mixture of univalent antibody fragments of different specificity. *Archives of Biochemistry and Biophysics* vol. 93 460–462 (1961).
59. Staerz, U. D., Kanagawa, O. & Bevan, M. J. Hybrid antibodies can target sites for attack by T cells. *Nature* **314**, 628–631 (1985).
60. Heiss, M. M. *et al.* The trifunctional antibody catumaxomab for the treatment of malignant ascites due to epithelial cancer: Results of a prospective randomized phase II/III trial. *Int. J. Cancer* **127**, 2209–2221 (2010).
61. Newman, M. J. & Benani, D. J. A review of blinatumomab, a novel immunotherapy. *J. Oncol. Pharm. Pract.* **22**, 639–645 (2016).
62. Brinkmann, U. & Kontermann, R. E. The making of bispecific antibodies. *mAbs* vol. 9 182–212 (2017).
63. Mandikian, D. *et al.* Relative target affinities of T-cell–dependent bispecific antibodies determine biodistribution in a solid tumor mouse model. *Mol. Cancer Ther.* **17**, 776–785 (2018).
64. Bortoletto, N., Scotet, E., Yoichi, M., D'Oro, U. & Lanzavecchia, A. Optimizing anti-CD3 affinity for effective T cell targeting against tumor cells. *European Journal of Immunology* vol. 32 3102–3107 (2002).
65. Leong, S. R. *et al.* An anti-CD3/anti-CLL-1 bispecific antibody for the treatment of acute myeloid leukemia. *Blood* **129**, 609–618 (2017).
66. Yun, H. D. *et al.* Trispecific killer engager CD16xIL15xCD33 potently induces NK cell activation and cytotoxicity against neoplastic mast cells. *Blood Adv.* **2**, 1580–1584 (2018).

67. Pegu, A. *et al.* Activation and lysis of human CD4 cells latently infected with HIV-1. *Nat. Commun.* **6**, 1–9 (2015).
68. Li, Z. *et al.* Pretargeting and Bioorthogonal Click Chemistry-Mediated Endogenous Stem Cell Homing for Heart Repair. *ACS Nano* **12**, 12193–12200 (2018).
69. Geuijen, C. A. W. *et al.* Unbiased Combinatorial Screening Identifies a Bispecific IgG1 that Potently Inhibits HER3 Signaling via HER2-Guided Ligand Blockade. *Cancer Cell* **33**, 922-936.e10 (2018).
70. Weisser, N. E. *et al.* An anti-HER2 biparatopic antibody that induces unique HER2 clustering and complement-dependent cytotoxicity. *Nat. Commun.* **14**, (2023).
71. Kolumam, G. *et al.* Sustained Brown Fat Stimulation and Insulin Sensitization by a Humanized Bispecific Antibody Agonist for Fibroblast Growth Factor Receptor 1/βKlotho Complex. *EBioMedicine* **2**, 730–743 (2015).
72. Sampei, Z. *et al.* Identification and Multidimensional Optimization of an Asymmetric Bispecific IgG Antibody Mimicking the Function of Factor VIII Cofactor Activity. *PLoS One* **8**, e57479 (2013).
73. Yu, Y. J. *et al.* Boosting brain uptake of a therapeutic antibody by reducing its affinity for a transcytosis target. *Sci. Transl. Med.* **3**, (2011).
74. Johnsen, K. B., Burkhart, A., Thomsen, L. B., Andresen, T. L. & Moos, T. Targeting the transferrin receptor for brain drug delivery. *Progress in Neurobiology* vol. 181 101665 (2019).
75. Pornnoppadol, G. *et al.* Bispecific antibody shuttles targeting CD98hc mediate efficient and long-lived brain delivery of IgGs. *Cell Chem. Biol.* (2023) doi:10.1016/j.chembiol.2023.09.008.
76. Beck, A. *et al.* The next generation of antibody-drug conjugates comes of age. *Discovery medicine* vol. 10 329–339 (2010).
77. Beck, A., Goetsch, L., Dumontet, C. & Corvaïa, N. Strategies and challenges for the next generation of antibody-drug conjugates. *Nature Reviews Drug Discovery* vol. 16 315–337 (2017).
78. Gogia, P., Ashraf, H., Bhasin, S. & Xu, Y. Antibody–Drug Conjugates: A Review of Approved Drugs and Their Clinical Level of Evidence. *Cancers* vol. 15 (2023).
79. Shastry, M. *et al.* Rise of Antibody-Drug Conjugates: The Present and Future. *Am. Soc. Clin. Oncol. Educ. B.* **43**, e390094 (2023).
80. Damelin, M., Zhong, W., Myers, J. & Sapra, P. Evolving Strategies for Target Selection for Antibody-Drug Conjugates. *Pharm. Res.* **32**, 3494–3507 (2015).
81. Rudnick, S. I. *et al.* Influence of affinity and antigen internalization on the uptake and penetration of anti-HER2 Antibodies in Solid Tumors. *Cancer Res.* **71**, 2250–2259 (2011).
82. Cheng, J. *et al.* Molecular Mechanism of HER2 Rapid Internalization and Redirected Trafficking Induced by Anti-HER2 Biparatopic Antibody. *Antibodies* **9**, 1–21 (2020).
83. Damelin, M. *et al.* Anti-EFNA4 calicheamicin conjugates effectively target triple-negative breast and ovarian tumor-initiating cells to result in sustained tumor regressions. *Clin. Cancer Res.* **21**, 4165–4173 (2015).
84. Wagner-Rousset, E. *et al.* Antibody-drug conjugate model fast characterization by LC-MS following IdeS proteolytic digestion. *MAbs* **6**, 173–184 (2014).
85. Kovtun, Y. V. *et al.* Antibody-drug conjugates designed to eradicate tumors with homogeneous and heterogeneous expression of the target antigen. *Cancer Res.* **66**, 3214–3221 (2006).
86. Kovtun, Y. V. & Goldmacher, V. S. Cell killing by antibody-drug conjugates. *Cancer Lett.* **255**, 232–240 (2007).
87. Panowski, S., Bhakta, S., Raab, H., Polakis, P. & Junutula, J. R. Site-specific antibody drug conjugates for cancer therapy. *MAbs* **6**, 34–45 (2014).
88. Shen, B. Q. *et al.* Conjugation site modulates the in vivo stability and therapeutic activity of antibody-drug conjugates. *Nat. Biotechnol.* **30**, 184–189 (2012).
89. Tian, F. *et al.* A general approach to site-specific antibody drug conjugates. *Proc. Natl. Acad. Sci. U. S. A.* **111**, 1766–1771 (2014).

90. Albers, A. E. *et al.* Exploring the effects of linker composition on site-specifically modified antibody–drug conjugates. *Eur. J. Med. Chem.* **88**, 3–9 (2014).
91. Ekholm, F. S. *et al.* Introducing Glycolinkers for the Functionalization of Cytotoxic Drugs and Applications in Antibody–Drug Conjugation Chemistry. *ChemMedChem* **11**, 2501–2505 (2016).
92. Saunders, K. O. Conceptual approaches to modulating antibody effector functions and circulation half-life. *Frontiers in Immunology* vol. 10 449325 (2019).
93. Liu, Z. *et al.* Asymmetrical Fc engineering greatly enhances Antibodydependent Cellular Cytotoxicity (ADCC) effector function and stability of the modified Antibodies. *J. Biol. Chem.* **289**, 3571–3590 (2014).
94. Li, T. *et al.* Modulating IgG effector function by Fc glycan engineering. *Proc. Natl. Acad. Sci. U. S. A.* **114**, 3485–3490 (2017).
95. Mimura, Y. *et al.* Glycosylation engineering of therapeutic IgG antibodies: challenges for the safety, functionality and efficacy. *Protein and Cell* vol. 9 47–62 (2018).
96. de Taeye, S. W., Rispens, T. & Vidarsson, G. The ligands for human igG and their effector functions. *Antibodies* vol. 8 30 (2019).
97. Stavenhagen, J. B. *et al.* Fc optimization of therapeutic antibodies enhances their ability to kill tumor cells in vitro and controls tumor expansion in vivo via low-affinity activating Fcγ receptors. *Cancer Res.* **67**, 8882–8890 (2007).
98. Moore, G. L., Chen, H., Karki, S. & Lazar, G. A. Engineered Fc variant antibodies with enhanced ability to recruit complement and mediate effector functions. *MAbs* **2**, 181–189 (2010).
99. Falconer, D. J., Subedi, G. P., Marcella, A. M. & Barb, A. W. Antibody Fucosylation Lowers the FcγRIIIa/CD16a Affinity by Limiting the Conformations Sampled by the N162-Glycan. *ACS Chem. Biol.* **13**, 2179–2189 (2018).
100. Herter, S. *et al.* Glycoengineering of Therapeutic Antibodies Enhances Monocyte/Macrophage-Mediated Phagocytosis and Cytotoxicity. *J. Immunol.* **192**, 2252–2260 (2014).
101. Zhou, S., Liu, M., Ren, F., Meng, X. & Yu, J. The landscape of bispecific T cell engager in cancer treatment. *Biomarker Research* vol. 9 1–23 (2021).
102. Brezski, R. J. & Georgiou, G. Immunoglobulin isotype knowledge and application to Fc engineering. *Current Opinion in Immunology* vol. 40 62–69 (2016).
103. Tao, M. H. & Morrison, S. L. Studies of aglycosylated chimeric mouse-human IgG. Role of carbohydrate in the structure and effector functions mediated by the human IgG constant region. *J. Immunol.* **143**, 2595–2601 (1989).
104. Mimura, Y. *et al.* The influence of glycosylation on the thermal stability and effector function expression of human IgG1-Fc: Properties of a series of truncated glycoforms. *Mol. Immunol.* **37**, 697–706 (2000).
105. Li, M. *et al.* Next generation of anti-PD-L1 Atezolizumab with enhanced anti-tumor efficacy in vivo. *Sci. Rep.* **11**, 1–11 (2021).
106. Xu, D. *et al.* In vitro characterization of five humanized OKT3 effector function variant antibodies. *Cell. Immunol.* **200**, 16–26 (2000).
107. Woodle, E. S. *et al.* Phase I trial of a humanized, Fc receptor nonbinding OKT3 antibody, huOKT3γ1(Ala-Ala) in the treatment of acute renal allograft rejection. *Transplantation* **68**, 608–616 (1999).
108. Oganesyan, V., Gao, C., Shirinian, L., Wu, H. & Dall'Acqua, W. F. Structural characterization of a human Fc fragment engineered for lack of effector functions. *Acta Crystallogr. Sect. D Biol. Crystallogr.* **64**, 700–704 (2008).
109. Hollmén, M. *et al.* Nonclinical Characterization of Bexmarilimab, a Clever-1-Targeting Antibody for Supporting Immune Defense Against Cancers. *Mol. Cancer Ther.* **21**, 1207–1218 (2022).
110. Ghetie, V. & Ward, E. S. Multiple roles for the major histocompatibility complex class I-related receptor FcRn. *Annual Review of Immunology* vol. 18 739–766 (2000).

111. Lee, C. H. *et al.* An engineered human Fc domain that behaves like a pH-toggle switch for ultra-long circulation persistence. *Nat. Commun.* **10**, 1–11 (2019).
112. Igawa, T., Haraya, K. & Hattori, K. Sweeping antibody as a novel therapeutic antibody modality capable of eliminating soluble antigens from circulation. *Immunological Reviews* vol. 270 132–151 (2016).
113. Ridgway, J. B. B., Presta, L. G. & Carter, P. 'Knobs-into-holes' engineering of antibody C(H)3 domains for heavy chain heterodimerization. *Protein Eng.* **9**, 617–621 (1996).
114. Labrijn, A. F. *et al.* Efficient generation of stable bispecific IgG1 by controlled Fab-arm exchange. *Proc. Natl. Acad. Sci. U. S. A.* **110**, 5145–5150 (2013).
115. Labrijn, A. F. *et al.* Controlled Fab-arm exchange for the generation of stable bispecific IgG1. *Nat. Protoc.* **9**, 2450–2463 (2014).
116. Jain, T. *et al.* Biophysical properties of the clinical-stage antibody landscape. *Proc. Natl. Acad. Sci. U. S. A.* **114**, 944–949 (2017).
117. Starr, C. G. & Tessier, P. M. Selecting and engineering monoclonal antibodies with drug-like specificity. *Curr. Opin. Biotechnol.* **60**, 119–127 (2019).
118. Bailly, M. *et al.* Predicting Antibody Developability Profiles Through Early Stage Discovery Screening. *MAbs* **12**, (2020).
119. Xu, Y. *et al.* Structure, heterogeneity and developability assessment of therapeutic antibodies. *mAbs* vol. 11 239–264 (2019).
120. Chennamsetty, N., Voynov, V., Kayser, V., Helk, B. & Trout, B. L. Design of therapeutic proteins with enhanced stability. *Proc. Natl. Acad. Sci. U. S. A.* **106**, 11937–11942 (2009).
121. Lauer, T. M. *et al.* Developability index: A rapid in silico tool for the screening of antibody aggregation propensity. *J. Pharm. Sci.* **101**, 102–115 (2012).
122. Raybould, M. I. J. *et al.* Five computational developability guidelines for therapeutic antibody profiling. *Proc. Natl. Acad. Sci. U. S. A.* **116**, 4025–4030 (2019).
123. Sankar, K., Krystek, S. R., Carl, S. M., Day, T. & Maier, J. K. X. AggScore: Prediction of aggregation-prone regions in proteins based on the distribution of surface patches. *Proteins Struct. Funct. Bioinforma.* **86**, 1147–1156 (2018).
124. Courtois, F., Agrawal, N. J., Lauer, T. M. & Trout, B. L. Rational design of therapeutic mAbs against aggregation through protein engineering and incorporation of glycosylation motifs applied to bevacizumab. *MAbs* **8**, 99–112 (2016).
125. Dyson, M. R. *et al.* Beyond affinity: selection of antibody variants with optimal biophysical properties and reduced immunogenicity from mammalian display libraries. *MAbs* **12**, (2020).
126. Huhtinen, O., Salbo, R., Lamminmäki, U. & Prince, S. Selection of biophysically favorable antibody variants using a modified Flp-In CHO mammalian display platform. *Front. Bioeng. Biotechnol.* **11**, 1170081 (2023).
127. Makowski, E. K. *et al.* Reduction of therapeutic antibody self-association using yeast-display selections and machine learning. *MAbs* **14**, (2022).
128. Meza, N. P. *et al.* Predicting Colloidal Stability of High-Concentration Monoclonal Antibody Formulations in Common Pharmaceutical Buffers Using Improved Polyethylene Glycol Induced Protein Precipitation Assay. *Mol. Pharm.* **20**, 5842–5855 (2023).
129. Kingsbury, J. S. *et al.* A single molecular descriptor to predict solution behavior of therapeutic antibodies. *Sci. Adv.* **6**, (2020).
130. Sule, S. V., Dickinson, C. D., Lu, J., Chow, C. K. & Tessier, P. M. Rapid analysis of antibody self-association in complex mixtures using immunogold conjugates. *Mol. Pharm.* **10**, 1322–1331 (2013).
131. Liu, Y. *et al.* High-throughput screening for developability during early-stage antibody discovery using self-interaction nanoparticle spectroscopy. *MAbs* **6**, 483–492 (2014).
132. Geng, S. B., Wittekind, M., Vigil, A. & Tessier, P. M. Measurements of Monoclonal Antibody Self-Association Are Correlated with Complex Biophysical Properties. *Mol. Pharm.* **13**, 1636–1645 (2016).

133. Avery, L. B. *et al.* Establishing in vitro in vivo correlations to screen monoclonal antibodies for physicochemical properties related to favorable human pharmacokinetics. *MAbs* **10**, 244–255 (2018).
134. Hedberg, S. H. M., Rapley, J., Haigh, J. M. & Williams, D. R. Cross-interaction chromatography as a rapid screening technique to identify the stability of new antibody therapeutics. *Eur. J. Pharm. Biopharm.* **133**, 131–137 (2018).
135. Jacobs, S. A., Wu, S. J., Feng, Y., Bethea, D. & O'Neil, K. T. Cross-interaction chromatography: A rapid method to identify highly soluble monoclonal antibody candidates. *Pharm. Res.* **27**, 65–71 (2010).
136. Lowe, D. *et al.* Aggregation, stability, and formulation of human antibody therapeutics. in *Advances in Protein Chemistry and Structural Biology* vol. 84 41–61 (Academic Press, 2011).
137. Wang, W., Singh, S., Zeng, D. L., King, K. & Nema, S. Antibody structure, instability, and formulation. *Journal of Pharmaceutical Sciences* vol. 96 1–26 (2007).
138. Oyama, H. *et al.* Relation of Colloidal and Conformational Stabilities to Aggregate Formation in a Monoclonal Antibody. *J. Pharm. Sci.* **109**, 308–315 (2020).
139. Cunningham, O., Scott, M., Zhou, Z. S. & Finlay, W. J. J. Polyreactivity and polyspecificity in therapeutic antibody development: risk factors for failure in preclinical and clinical development campaigns. mAbs vol. 13 (Taylor and Francis Ltd., 2021).
140. Bumbaca, D. *et al.* Highly specific off-target binding identified and eliminated during the humanization of an antibody against FGF receptor 4. *MAbs* **3**, 376–386 (2011).
141. Loberg, L. I. *et al.* Off-target binding of an anti-amyloid beta monoclonal antibody to platelet factor 4 causes acute and chronic toxicity in cynomolgus monkeys. *MAbs* **13**, (2021).
142. MacLachlan, T. K. *et al.* Classic and evolving approaches to evaluating cross reactivity of mAb and mAb-like molecules – A survey of industry 2008–2019. *Regul. Toxicol. Pharmacol.* **121**, 104872 (2021).
143. Notkins, A. L. Polyreactivity of antibody molecules. *Trends Immunol.* **25**, 174–179 (2004).
144. Laustsen, A. H., Greiff, V., Karatt-Vellatt, A., Muyldermans, S. & Jenkins, T. P. Animal Immunization, in Vitro Display Technologies, and Machine Learning for Antibody Discovery. *Trends in Biotechnology* vol. 39 1263–1273 (2021).
145. Parthiban, K. *et al.* A comprehensive search of functional sequence space using large mammalian display libraries created by gene editing. *MAbs* **11**, 884–898 (2019).
146. Pucca, M. B. *et al.* History of envenoming therapy and current perspectives. *Frontiers in Immunology* vol. 10 467484 (2019).
147. Gray, A. *et al.* Animal-free alternatives and the antibody iceberg. *Nature Biotechnology* vol. 38 1234–1239 (2020).
148. Halder, M., Barroso, J. & Whelan, M. EURL ECVAM Recommendation on Non-Animal-Derived Antibodies. (2020).
149. Pedrioli, A. & Oxenius, A. Single B cell technologies for monoclonal antibody discovery. *Trends in Immunology* vol. 42 1143–1158 (2021).
150. Mitra, S. & Tomar, P. C. Hybridoma technology; advancements, clinical significance, and future aspects. *J. Genet. Eng. Biotechnol.* **19**, 1–12 (2021).
151. Tang, D. C., Devit, M. & Johnston, S. A. Genetic immunization is a simple method for eliciting an immune response. *Nature* **356**, 152–154 (1992).
152. Chames, P., Van Regenmortel, M., Weiss, E. & Baty, D. Therapeutic antibodies: Successes, limitations and hopes for the future. *British Journal of Pharmacology* vol. 157 220–233 (2009).
153. Jones, P. T., Dear, P. H., Foote, J., Neuberger, M. S. & Winter, G. Replacing the complementarity-determining regions in a human antibody with those from a mouse. *Nature* **321**, 522–525 (1986).
154. Watier, H. & Reichert, J. M. Evolution of Antibody Therapeutics. in *Wiley Online LibraryH Watier, JM ReichertProtein Therapeutics, 2017•Wiley Online Library* 25–49 (2017). doi:10.1002/9783527699124.ch2.

155. Mountain, A. & Adair, J. R. Engineering antibodies for therapy. *Biotechnol. Genet. Eng. Rev.* **10**, 1–142 (1992).
156. Tsurushita, N., Hinton, P. R. & Kumar, S. Design of humanized antibodies: From anti-Tac to Zenapax. *Methods* **36**, 69–83 (2005).
157. Queen, C. *et al.* A humanized antibody that binds to the interleukin 2 receptor. *Proc. Natl. Acad. Sci. U. S. A.* **86**, 10029–10033 (1989).
158. Lu, R. M. *et al.* Development of therapeutic antibodies for the treatment of diseases. *Journal of Biomedical Science* vol. 27 1–30 (2020).
159. Reddy, S. T. *et al.* Monoclonal antibodies isolated without screening by analyzing the variable-gene repertoire of plasma cells. *Nat. Biotechnol.* **28**, 965–969 (2010).
160. Lonberg, N. *et al.* Antigen-specific human antibodies from mice comprising four distinct genetic modifications. *Nature* **368**, 856–859 (1994).
161. Green, L. L. *et al.* Antigen–specific human monoclonal antibodies from mice engineered with human Ig heavy and light chain YACs. *Nat. Genet.* **7**, 13–21 (1994).
162. Mendez, M. J. *et al.* Functional transplant of megabase human immunoglobulin loci recapitulates human antibody response in mice. *Nat. Genet.* **15**, 146–156 (1997).
163. Choi, T. K. *et al.* Transgenic mice containing a human heavy chain immunoglobulin gene fragment cloned in a yeast artificial chromosome. *Nat. Genet.* **4**, 117–123 (1993).
164. Davies, N. P. *et al.* Creation of Mice Expressing Human Antibody Light Chains by Introduction of a Yeast Artificial Chromosome Containing the Core Region of the Human Immunoglobulin K Locus. *Bio/Technology* **11**, 911–914 (1993).
165. Jakobovits, A., Amado, R. G., Yang, X., Roskos, L. & Schwab, G. From XenoMouse technology to panitumumab, the first fully human antibody product from transgenic mice. *Nature Biotechnology* vol. 25 1134–1143 (2007).
166. Murphy, A. J. *et al.* Mice with megabase humanization of their immunoglobulin genes generate antibodies as efficiently as normal mice. *Proc. Natl. Acad. Sci. U. S. A.* **111**, 5153–5158 (2014).
167. Zlot, C. H. *et al.* Generation of monoclonal antibodies specific for mouse apolipoprotein B- 100 in apolipoprotein B-48-only mice. *J. Lipid Res.* **40**, 76–84 (1999).
168. Gibson, T. B., Ranganathan, A. & Grothey, A. Randomized phase III trial results of Panitumumab, a fully human anti-epidermal growth factor receptor monoclonal antibody, in metastatic colorectal cancer. *Clinical Colorectal Cancer* vol. 6 29–31 (2006).
169. Moroni, M. *et al.* Gene copy number for epidermal growth factor receptor (EGFR) and clinical response to antiEGFR treatment in colorectal cancer: A cohort study. *Lancet Oncol.* **6**, 279–286 (2005).
170. IJspeert, H. *et al.* Strategies for B-cell receptor repertoire analysis in primary immunodeficiencies: From severe combined immunodeficiency to common variable immunodeficiency. *Front. Immunol.* **6**, (2015).
171. Corti, D. & Lanzavecchia, A. Efficient Methods To Isolate Human Monoclonal Antibodies from Memory B Cells and Plasma Cells. *Microbiol. Spectr.* **2**, (2014).
172. Fitzgerald, V. & Leonard, P. Single cell screening approaches for antibody discovery. *Methods* vol. 116 34–42 (2017).
173. Tiller, T. *et al.* Efficient generation of monoclonal antibodies from single human B cells by single cell RT-PCR and expression vector cloning. *J. Immunol. Methods* **329**, 112–124 (2008).
174. Lundkvist, A., Horling, J., Athlin, L., Rosen, A. & Niklasson, B. Neutralizing human monoclonal antibodies against Puumala virus, causative agent of nephropathia epidemica: A novel method using antigen-coated magnetic beads for specific B cell isolation. *J. Gen. Virol.* **74**, 1303–1310 (1993).
175. Love, J. C., Ronan, J. L., Grotenbreg, G. M., Van Der Veen, A. G. & Ploegh, H. L. A microengraving method for rapid selection of single cells producing antigen-specific antibodies. *Nat. Biotechnol.* **24**, 703–707 (2006).

176. Mazutis, L. *et al.* Single-cell analysis and sorting using droplet-based microfluidics. *Nat. Protoc.* **8**, 870–891 (2013).
177. Diercks, A. H. *et al.* A microfluidic device for multiplexed protein detection in nano-liter volumes. *Anal. Biochem.* **386**, 30–35 (2009).
178. Fitzgerald, V. *et al.* Exploiting highly ordered subnanoliter volume microcapillaries as microtools for the analysis of antibody producing cells. *Anal. Chem.* **87**, 997–1003 (2015).
179. Rijal, P. *et al.* Therapeutic Monoclonal Antibodies for Ebola Virus Infection Derived from Vaccinated Humans. *Cell Rep.* **27**, 172-186.e7 (2019).
180. Bornholdt, Z. A. *et al.* Isolation of potent neutralizing antibodies from a survivor of the 2014 Ebola virus outbreak. *Science (80-.).* **351**, 1078–1083 (2016).
181. Corti, D. *et al.* Protective monotherapy against lethal Ebola virus infection by a potently neutralizing antibody. *Science (80-.).* **351**, 1339–1342 (2016).
182. Awi, N. J. & Teow, S.-Y. Antibody-Mediated Therapy against HIV/AIDS: Where Are We Standing Now? *J. Pathog.* **2018**, 1–9 (2018).
183. Nogales, A. *et al.* A highly potent and broadly neutralizing H1 influenza-specific human monoclonal antibody. *Sci. Rep.* **8**, 1–15 (2018).
184. Fu, Y. *et al.* A broadly neutralizing anti-influenza antibody reveals ongoing capacity of haemagglutinin-specific memory B cells to evolve. *Nat. Commun.* **7**, 1–13 (2016).
185. Nakamura, G. *et al.* An in vivo human-plasmablast enrichment technique allows rapid identification of therapeutic influenza A antibodies. *Cell Host Microbe* **14**, 93–103 (2013).
186. Chai, N. *et al.* A broadly protective therapeutic antibody against influenza B virus with two mechanisms of action. *Nat. Commun.* **8**, 1–18 (2017).
187. Goodwin, E. *et al.* Infants Infected with Respiratory Syncytial Virus Generate Potent Neutralizing Antibodies that Lack Somatic Hypermutation. *Immunity* **48**, 339-349.e5 (2018).
188. Gilman, M. S. A. *et al.* Rapid profiling of RSV antibody repertoires from the memory B cells of naturally infected adult donors. *Sci. Immunol.* **1**, (2016).
189. Westendorf, K. *et al.* LY-CoV1404 (bebtelovimab) potently neutralizes SARS-CoV-2 variants. *Cell Rep.* **39**, 110812 (2022).
190. Keam, S. J. Tixagevimab + Cilgavimab: First Approval. *Drugs* **82**, 1001–1010 (2022).
191. Cathcart, A. L. *et al.* The dual function monoclonal antibodies VIR-7831 and VIR-7832 demonstrate potent in vitro and in vivo activity against SARS-CoV-2. *bioRxiv* 2021.03.09.434607 (2021) doi:10.1101/2021.03.09.434607.
192. Valldorf, B. *et al.* Antibody display technologies: selecting the cream of the crop. *Biological Chemistry* vol. 403 455–477 (2022).
193. Wang, B. *et al.* Discovery of high affinity anti-ricin antibodies by B cell receptor sequencing and by yeast display of combinatorial VH:VL libraries from immunized animals. *MAbs* **8**, 1035–1044 (2016).
194. Grzeschik, J. *et al.* Yeast Surface Display in Combination with Fluorescence-activated Cell Sorting Enables the Rapid Isolation of Antibody Fragments Derived from Immunized Chickens. *Biotechnol. J.* **14**, 1800466 (2019).
195. Schröter, C. *et al.* Selection of Antibodies with Tailored Properties by Application of High-Throughput Multiparameter Fluorescence-Activated Cell Sorting of Yeast-Displayed Immune Libraries. *Mol. Biotechnol.* **60**, 727–735 (2018).
196. Cai, X. & Garen, A. Anti-melanoma antibodies from melanoma patients immunized with genetically modified autologous tumor cells: Selection of specific antibodies from single-chain Fv fusion phage libraries. *Proc. Natl. Acad. Sci. U. S. A.* **92**, 6537–6541 (1995).
197. Trott, M. *et al.* Functional characterization of two scFv-Fc antibodies from an HIV controller selected on soluble HIV-1 Env complexes: A neutralizing V3- and a trimer-specific gp41 antibody. *PLoS One* **9**, e97478 (2014).
198. Almagro, J. C., Pedraza-Escalona, M., Arrieta, H. I. & Pérez-Tapia, S. M. Phage display libraries for antibody therapeutic discovery and development. *Antibodies* vol. 8 44 (2019).

199. De Haard, H. J. *et al.* A large non-immunized human Fab fragment phage library that permits rapid isolation and kinetic analysis of high affinity antibodies. *J. Biol. Chem.* **274**, 18218–18230 (1999).
200. Vaughan, T. J. *et al.* Human Antibodies With Sub-Nanomolar Affinities Isolated From A Large Non-Immunized Phage Display Library. *Nat. Biotechnol.* **14**, 309–314 (1996).
201. Knappik, A. *et al.* Fully synthetic human combinatorial antibody libraries (HuCAL) based on modular consensus frameworks and CDRs randomized with trinucleotides. *J. Mol. Biol.* **296**, 57–86 (2000).
202. Prassler, J. *et al.* HuCAL PLATINUM, a synthetic fab library optimized for sequence diversity and superior performance in mammalian expression systems. *J. Mol. Biol.* **413**, 261–278 (2011).
203. Frenzel, A. *et al.* Designing Human Antibodies by Phage Display. *Transfusion Medicine and Hemotherapy* vol. 44 312–318 (2017).
204. Chan, C. E. Z., Lim, A. P. C., MacAry, P. A. & Hanson, B. J. The role of phage display in therapeutic antibody discovery. *International immunology* vol. 26 649–657 (2014).
205. Smith, G. P. Filamentous fusion phage: Novel expression vectors that display cloned antigens on the virion surface. *Science (80-.).* **228**, 1315–1317 (1985).
206. McCafferty, J., Griffiths, A. D., Winter, G. & Chiswell, D. J. Phage antibodies: filamentous phage displaying antibody variable domains. *Nat. 1990 3486301* **348**, 552–554 (1990).
207. Press release: The Nobel Prize in Chemistry 2018 - NobelPrize.org. https://www.nobelprize.org/prizes/chemistry/2018/press-release/.
208. Kempeni, J. Preliminary results of early clinical trials with the fully human anti-TNFα monoclonal antibody D2E7. *Ann. Rheum. Dis.* **58**, I70–I72 (1999).
209. Alfaleh, M. A. *et al.* Phage Display Derived Monoclonal Antibodies: From Bench to Bedside. *Frontiers in Immunology* vol. 11 567223 (2020).
210. Ledsgaard, L., Kilstrup, M., Karatt-Vellatt, A., McCafferty, J. & Laustsen, A. H. Basics of antibody phage display technology. *Toxins* vol. 10 236 (2018).
211. Weber, M. *et al.* A highly functional synthetic phage display library containing over 40 billion human antibody clones. *PLoS One* **9**, e100000 (2014).
212. Wrublewski, D. T. Analysis for Science Librarians of the 2018 Nobel Prize in Chemistry: Directed Evolution of Enzymes and Phage Display of Peptides and Antibodies. *Sci. Technol. Libr.* **38**, 51–69 (2019).
213. Zhu, X. *et al.* Identification of internalizing human single-chain antibodies targeting brain tumor sphere cells. *Mol. Cancer Ther.* **9**, 2131–2141 (2010).
214. Nielsen, U. B. & Marks, J. D. Internalizing antibodies and targeted cancer therapy: Direct selection from phage display libraries. *Pharmaceutical Science and Technology Today* vol. 3 282–291 (2000).
215. Chalouni, C. & Doll, S. Fate of Antibody-Drug Conjugates in Cancer Cells. *Journal of Experimental and Clinical Cancer Research* vol. 37 1–12 (2018).
216. Bonvin, P. *et al.* De novo isolation of antibodies with pH-dependent binding properties. *MAbs* **7**, 294–302 (2015).
217. Brockmann, E. C., Cooper, M., Strömsten, N., Vehniäinen, M. & Saviranta, P. Selecting for antibody scFv fragments with improved stability using phage display with denaturation under reducing conditions. *J. Immunol. Methods* **296**, 159–170 (2005).
218. Anand, T. *et al.* Phage Display Technique as a Tool for Diagnosis and Antibody Selection for Coronaviruses. *Current Microbiology* vol. 78 1124–1134 (2021).
219. Frenzel, A., Schirrmann, T. & Hust, M. Phage display-derived human antibodies in clinical development and therapy. *mAbs* vol. 8 1177–1194 (2016).
220. Plückthun, A. Ribosome display: A perspective. *Methods in Molecular Biology* vol. 805 13–28 (2012).
221. Lipovsek, D. & Plückthun, A. In-vitro protein evolution by ribosome display and mRNA display. *Journal of Immunological Methods* vol. 290 51–67 (2004).

222. Kunamneni, A., Ogaugwu, C., Bradfute, S. & Durvasula, R. Ribosome display technology: Applications in disease diagnosis and control. *Antibodies* vol. 9 1–17 (2020).
223. Hanes, J., Jermutus, L., Weber-Bornhauser, S., Bosshard, H. R. & Plückthun, A. Ribosome display efficiently selects and evolves high-affinity antibodies in vitro from immune libraries. *Proc. Natl. Acad. Sci. U. S. A.* **95**, 14130–14135 (1998).
224. Boder, E. T. & Wittrup, K. D. Yeast surface display for screening combinatorial polypeptide libraries. *Nat. Biotechnol.* **15**, 553–557 (1997).
225. Boder, E. T., Raeeszadeh-Sarmazdeh, M. & Price, J. V. Engineering antibodies by yeast display. *Archives of Biochemistry and Biophysics* vol. 526 99–106 (2012).
226. Wang, Z., Mathias, A., Stavrou, S. & Neville, D. M. A new yeast display vector permitting free scFv amino termini can augment ligand binding affinities. *Protein Eng. Des. Sel.* **18**, 337–343 (2005).
227. Benatuil, L., Perez, J. M., Belk, J. & Hsieh, C. M. An improved yeast transformation method for the generation of very large human antibody libraries. *Protein Eng. Des. Sel.* **23**, 155–159 (2010).
228. Tillotson, B. J., Lajoie, J. M. & Shusta, E. V. Yeast display-based antibody affinity maturation using detergent-solubilized cell lysates. *Methods Mol. Biol.* **1319**, 65–78 (2015).
229. Elter, A. *et al.* Humanization of Chicken-Derived scFv Using Yeast Surface Display and NGS Data Mining. *Biotechnol. J.* **16**, 2000231 (2021).
230. Schröter, C. *et al.* A generic approach to engineer antibody pH-switches using combinatorial histidine scanning libraries and yeast display. *MAbs* **7**, 138–151 (2015).
231. Ferrara, F. *et al.* Using Phage and Yeast Display to Select Hundreds of Monoclonal Antibodies: Application to Antigen 85, a Tuberculosis Biomarker. *PLoS One* **7**, e49535 (2012).
232. Akamatsu, Y., Pakabunto, K., Xu, Z., Zhang, Y. & Tsurushita, N. Whole IgG surface display on mammalian cells: Application to isolation of neutralizing chicken monoclonal anti-IL-12 antibodies. *J. Immunol. Methods* **327**, 40–52 (2007).
233. Zhou, C., Jacobsen, F. W., Cai, L., Chen, Q. & Shen, D. Development of a novel mammalian cell surface antibody display platform. *MAbs* **2**, 508–518 (2010).
234. Apaja, P. M. & Lukacs, G. L. Protein homeostasis at the plasma membrane. *Physiology* vol. 29 265–277 (2014).
235. Sun, Z. & Brodsky, J. L. Protein quality control in the secretory pathway. *J. Cell Biol.* **218**, 3171–3187 (2019).
236. Bowers, P. M. *et al.* Coupling mammalian cell surface display with somatic hypermutation for the discovery and maturation of human antibodies. *Proc. Natl. Acad. Sci. U. S. A.* **108**, 20455–20460 (2011).
237. Bowers, P. M. *et al.* Mammalian cell display for the discovery and optimization of antibody therapeutics. *Methods* **65**, 44–56 (2014).
238. Higuchi, K. *et al.* Cell display library for gene cloning of variable regions of human antibodies to hepatitis B surface antigen. *J. Immunol. Methods* **202**, 193–204 (1997).
239. Ho, M. & Pastan, I. Mammalian cell display for antibody engineering. *Methods Mol. Biol.* **525**, 337 (2009).
240. Beerli, R. R. *et al.* Isolation of human monoclonal antibodies by mammalian cell display. *Proc. Natl. Acad. Sci. U. S. A.* **105**, 14336–41 (2008).
241. Zhang, H., Wilson, I. A. & Lerner, R. A. Selection of antibodies that regulate phenotype from intracellular combinatorial antibody libraries. *Proc. Natl. Acad. Sci. U. S. A.* **109**, 15728–15733 (2012).
242. Waldmeier, L. *et al.* Transpo-mAb display: Transposition-mediated B cell display and functional screening of full-length IgG antibody libraries. *MAbs* **8**, 726–740 (2016).
243. O'Gorman, S., Fox, D. T. & Wahl, G. M. Recombinase-mediated gene activation and site-specific integration in mammalian cells. *Science (80-.).* **251**, 1351–1355 (1991).

244. Zhang, L. *et al.* Recombinase-mediated cassette exchange (RMCE) for monoclonal antibody expression in the commercially relevant CHOK1SV cell line. *Biotechnol. Prog.* **31**, 1645–1656 (2015).
245. Chen, C., Li, N., Zhao, Y. & Hang, H. Coupling recombinase-mediated cassette exchange with somatic hypermutation for antibody affinity maturation in CHO cells. *Biotechnol. Bioeng.* **113**, 39–51 (2016).
246. Chen, C., Wang, Z., Kang, M., Lee, K. B. & Ge, X. High-fidelity large-diversity monoclonal mammalian cell libraries by cell cycle arrested recombinase-mediated cassette exchange. *Nucleic Acids Res.* **2023**, 1–13 (2023).
247. Mason, D. M. *et al.* High-throughput antibody engineering in mammalian cells by CRISPR/Cas9-mediated homology-directed mutagenesis. *Nucleic Acids Res.* **46**, 7436–7449 (2018).
248. Parola, C. *et al.* Antibody discovery and engineering by enhanced CRISPR-Cas9 integration of variable gene cassette libraries in mammalian cells. *MAbs* **11**, 1367–1380 (2019).
249. Duportet, X. *et al.* A platform for rapid prototyping of synthetic gene networks in mammalian cells. *Nucleic Acids Res.* **42**, 13440–13451 (2014).
250. Inniss, M. C. *et al.* A novel Bxb1 integrase RMCE system for high fidelity site-specific integration of mAb expression cassette in CHO Cells. *Biotechnol. Bioeng.* **114**, 1837–1846 (2017).
251. Matreyek, K. A., Stephany, J. J. & Fowler, D. M. A platform for functional assessment of large variant libraries in mammalian cells. *Nucleic Acids Res.* **45**, e102–e102 (2017).
252. Matreyek, K. A., Stephany, J. J., Chiasson, M. A., Hasle, N. & Fowler, D. M. An improved platform for functional assessment of large protein libraries in mammalian cells. *Nucleic Acids Res.* **48**, 1–12 (2019).
253. Gaidukov, L. *et al.* A multi-landing pad DNA integration platform for mammalian cell engineering. *Nucleic Acids Res.* **46**, 4072–4086 (2018).
254. Doudna, J. A. & Charpentier, E. The new frontier of genome engineering with CRISPR-Cas9. *Science* vol. 346 (2014).
255. Xu, Z. *et al.* Accuracy and efficiency define Bxb1 integrase as the best of fifteen candidate serine recombinases for the integration of DNA into the human genome. *BMC Biotechnol.* **13**, 87 (2013).
256. Kim, A. I. *et al.* Mycobacteriophage Bxb1 integrates into the Mycobacterium smegmatis groEL1 gene. *Mol. Microbiol.* **50**, 463–473 (2003).
257. Ghosh, P., Bibb, L. A. & Hatfull, G. F. Two-step site selection for serine-integrase-mediated excision: DNA-directed integrase conformation and central dinucleotide proofreading. *Proc. Natl. Acad. Sci. U. S. A.* **105**, 3238–3243 (2008).
258. Ghosh, P., Pannunzio, N. R., Hatfull, G. F. & Gottesman, M. Synapsis in phage Bxb1 integration: Selection mechanism for the correct pair of recombination sites. *J. Mol. Biol.* **349**, 331–348 (2005).
259. Brown, W. R. A., Lee, N. C. O., Xu, Z. & Smith, M. C. M. Serine recombinases as tools for genome engineering. *Methods* vol. 53 372–379 (2011).
260. Ghanbari, S. *et al.* Targeted integration in CHO cells using CRIS-PITCh/Bxb1 recombinase–mediated cassette exchange hybrid system. *Appl. Microbiol. Biotechnol.* **107**, 769–783 (2023).
261. Roelle, S. M., Kamath, N. D. & Matreyek, K. A. Mammalian Genomic Manipulation with Orthogonal Bxb1 DNA Recombinase Sites for the Functional Characterization of Protein Variants. *ACS Synth. Biol.* **12**, 3352–3365 (2023).
262. Turan, S., Zehe, C., Kuehle, J., Qiao, J. & Bode, J. Recombinase-mediated cassette exchange (RMCE) - A rapidly-expanding toolbox for targeted genomic modifications. *Gene* **515**, 1–27 (2013).
263. Ghosh, P., Kim, A. I. & Hatfull, G. F. The orientation of mycobacteriophage Bxb1 integration is solely dependent on the central dinucleotide of attP and attB. *Mol. Cell* **12**, 1101–1111 (2003).

264. Zhang, D. *et al.* A novel antibody humanization method based on epitopes scanning and molecular dynamics simulation. *PLoS One* **8**, e80636 (2013).
265. Kaleli, N. E., Karadag, M. & Kalyoncu, S. Phage display derived therapeutic antibodies have enriched aliphatic content: Insights for developability issues. *Proteins Struct. Funct. Bioinforma.* **87**, 607–618 (2019).
266. Gram, H. *et al.* In vitro selection and affinity maturation of antibodies from a naive combinatorial immunoglobulin library. *Proc. Natl. Acad. Sci. U. S. A.* **89**, 3576–3580 (1992).
267. Simons, J. F. *et al.* Affinity maturation of antibodies by combinatorial codon mutagenesis versus error-prone PCR. *MAbs* **12**, (2020).
268. Julian, M. C. *et al.* Co-evolution of affinity and stability of grafted amyloid-motif domain antibodies. *Protein Eng. Des. Sel.* **28**, 339–350 (2015).
269. Marks, J. D. *et al.* By-passing immunization: Building high affinity human antibodies by chain shuffling. *Bio/Technology* **10**, 779–783 (1992).
270. Teixeira, A. A. R. *et al.* Simultaneous affinity maturation and developability enhancement using natural liability-free CDRs. *MAbs* **14**, (2022).
271. Krykbaev, R. A., Liu, W. R., Jeffrey, P. D. & Margolies, M. N. Phage Display-selected Sequences of the Heavy-chain CDR3 Loop of the Anti-digoxin Antibody 26-10 Define a High Affinity Binding Site for Position 16-substituted Analogs of Digoxin. *J. Biol. Chem.* **276**, 8149–8158 (2001).
272. Douthwaite, J. A. *et al.* Affinity maturation of a novel antagonistic human monoclonal antibody with a long VH CDR3 targeting the Class a GPCR formyl-peptide receptor 1. *MAbs* **7**, 152–166 (2015).
273. Yang, W. P. *et al.* CDR walking mutagenesis for the affinity maturation of a potent human anti-HIV-1 antibody into the picomolar range. *J. Mol. Biol.* **254**, 392–403 (1995).
274. Qu, L., Qiao, X., Qi, F., Nishida, N. & Hoshino, T. Analysis of Binding Modes of Antigen-Antibody Complexes by Molecular Mechanics Calculation. *J. Chem. Inf. Model.* **61**, 2396–2406 (2021).
275. Hameduh, T., Haddad, Y., Adam, V. & Heger, Z. Homology modeling in the time of collective and artificial intelligence. *Computational and Structural Biotechnology Journal* vol. 18 3494–3506 (2020).
276. Sun, Y., Jiao, Y., Shi, C. & Zhang, Y. Deep learning-based molecular dynamics simulation for structure-based drug design against SARS-CoV-2. *Comput. Struct. Biotechnol. J.* **20**, 5014–5027 (2022).
277. Guest, J. D. *et al.* An expanded benchmark for antibody-antigen docking and affinity prediction reveals insights into antibody recognition determinants. *Structure* **29**, 606-621.e5 (2021).
278. Yoshida, K. *et al.* Exploring designability of electrostatic complementarity at an antigen-antibody interface directed by mutagenesis, biophysical analysis, and molecular dynamics simulations. *Sci. Rep.* **9**, 1–11 (2019).
279. Li, J. *et al.* Affinity maturation of antibody fragments: A review encompassing the development from random approaches to computational rational optimization. *International Journal of Biological Macromolecules* vol. 247 125733 (2023).
280. Cannon, D. A. *et al.* Experimentally guided computational antibody affinity maturation with de novo docking, modelling and rational design. *PLoS Comput. Biol.* **15**, e1006980 (2019).
281. Nelson, B. *et al.* Structure-Guided Combinatorial Engineering Facilitates Affinity and Specificity Optimization of Anti-CD81 Antibodies. *J. Mol. Biol.* **430**, 2139–2152 (2018).
282. Barderas, R., Desmet, J., Timmerman, P., Meloen, R. & Casal, J. I. Affinity maturation of antibodies assisted by in silico modeling. *Proc. Natl. Acad. Sci. U. S. A.* **105**, 9029–9034 (2008).
283. Jumper, J. *et al.* Highly accurate protein structure prediction with AlphaFold. *Nature* **596**, 583–589 (2021).
284. Adolf-Bryfogle, J., Xu, Q., North, B., Lehmann, A. & Dunbrack, R. L. PyigClassify: A database of antibody CDR structural classifications. *Nucleic Acids Res.* **43**, D432–D438 (2015).

285. Ruffolo, J. A., Guerra, C., Mahajan, S. P., Sulam, J. & Gray, J. J. Geometric potentials from deep learning improve prediction of CDR H3 loop structures. *Bioinformatics* **36**, I268–I275 (2020).
286. Ruffolo, J. A., Sulam, J. & Gray, J. J. Antibody structure prediction using interpretable deep learning. *Patterns* **3**, 100406 (2022).
287. Abanades, B., Georges, G., Bujotzek, A. & Deane, C. M. ABlooper: Fast accurate antibody CDR loop structure prediction with accuracy estimation. *Bioinformatics* **38**, 1877–1880 (2022).
288. Ruffolo, J. A., Chu, L. S., Mahajan, S. P. & Gray, J. J. Fast, accurate antibody structure prediction from deep learning on massive set of natural antibodies. *Nat. Commun.* **14**, 1–13 (2023).
289. Tang, C., Bagnara, D., Chiorazzi, N., Scharff, M. D. & MacCarthy, T. AID Overlapping and Polη Hotspots Are Key Features of Evolutionary Variation Within the Human Antibody Heavy Chain (IGHV) Genes. *Front. Immunol.* **11**, (2020).
290. Wang, C. L., Harper, R. A. & Wabl, M. Genome-wide somatic hypermutation. *Proc. Natl. Acad. Sci. U. S. A.* **101**, 7352–7356 (2004).
291. Qiao, Q. *et al.* AID Recognizes Structured DNA for Class Switch Recombination. *Mol. Cell* **67**, 361-373.e4 (2017).
292. Klasen, M., Spillmann, F. J. X., Lorens, J. B. & Wabl, M. Retroviral vectors to monitor somatic hypermutation. *J. Immunol. Methods* **300**, 47–62 (2005).
293. Yoshikawa, K. *et al.* AID enzyme-induced hypermutation in an actively transcribed gene in fibroblasts. *Science (80-.).* **296**, 2033–2036 (2002).
294. Chen, S. *et al.* Affinity maturation of anti-TNF-alpha scFv with somatic hypermutation in non-B cells. *Protein Cell* **3**, 460–469 (2012).
295. McConnell, A. D. *et al.* High Affinity Humanized Antibodies without Making Hybridomas; Immunization Paired with Mammalian Cell Display and In Vitro Somatic Hypermutation. *PLoS One* **7**, 49458 (2012).
296. Su, Y. C. *et al.* Mimicking the germinal center reaction in hybridoma cells to isolate temperature-selective anti-PEG antibodies. *MAbs* **6**, 1069–1083 (2014).
297. Chen, C. *et al.* Enhancers Improve the AID-Induced Hypermutation in Episomal Vector for Antibody Affinity Maturation in Mammalian Cell Display. *Antibodies* **7**, 42 (2018).
298. Luo, R. *et al.* High efficiency CHO cell display-based antibody maturation. *Sci. Rep.* **10**, 8102 (2020).
299. Yang, L. *et al.* Engineering and optimising deaminase fusions for genome editing. *Nat. Commun.* **7**, 1–12 (2016).
300. Komor, A. C., Kim, Y. B., Packer, M. S., Zuris, J. A. & Liu, D. R. Programmable editing of a target base in genomic DNA without double-stranded DNA cleavage. *Nature* **533**, 420–424 (2016).
301. Hess, G. T. *et al.* Directed evolution using dCas9-targeted somatic hypermutation in mammalian cells. *Nat. Methods* **13**, 1036–1042 (2016).
302. Ma, Y. *et al.* Targeted AID-mediated mutagenesis (TAM) enables efficient genomic diversification in mammalian cells. *Nat. Methods* **13**, 1029–1035 (2016).
303. Kuscu, C. & Adli, M. CRISPR-Cas9-AID base editor is a powerful gain-of-function screening tool. *Nature Methods* vol. 13 983–984 (2016).
304. Liu, L. D. *et al.* Intrinsic Nucleotide Preference of Diversifying Base Editors Guides Antibody Ex Vivo Affinity Maturation. *Cell Rep.* **25**, 884-892.e3 (2018).
305. Devilder, M. C. *et al.* Ex vivo evolution of human antibodies by CRISPR-X: From a naive B cell repertoire to affinity matured antibodies. *BMC Biotechnol.* **19**, (2019).
306. Olorunniji, F. J., Rosser, S. J. & Stark, W. M. Site-specific recombinases: molecular machines for the Genetic Revolution. *Biochem. J.* **473**, 673–684 (2016).
307. Dhara, V. G. *et al.* Recombinant Antibody Production in CHO and NS0 Cells: Differences and Similarities. *BioDrugs* **32**, 571–584 (2018).
308. de Felipe, P. *et al.* E unum pluribus: multiple proteins from a self-processing polyprotein. *Trends Biotechnol.* **24**, 68–75 (2006).

309. Fang, J. *et al.* An antibody delivery system for regulated expression of therapeutic levels of monoclonal antibodies In Vivo. *Mol. Ther.* **15**, 1153–1159 (2007).
310. Chng, J. *et al.* Cleavage efficient 2A peptides for high level monoclonal antibody expression in CHO cells. *MAbs* **7**, 403–412 (2015).
311. Fang, Y., Jang, H. S., Watson, G. W., Wellappili, D. P. & Tyler, B. M. Distinctive nuclear localization signals in the oomycete Phytophthora sojae. *Front. Microbiol.* **8**, (2017).
312. Lange, A. *et al.* Classical nuclear localization signals: Definition, function, and interaction with importin α. *J. Biol. Chem.* **282**, 5101–5105 (2007).
313. Marfori, M. *et al.* Molecular basis for specificity of nuclear import and prediction of nuclear localization. *Biochim. Biophys. Acta - Mol. Cell Res.* **1813**, 1562–1577 (2011).
314. Kosugi, S. *et al.* Design of Peptide Inhibitors for the Importin α/β Nuclear Import Pathway by Activity-Based Profiling. *Chem. Biol.* **15**, 940–949 (2008).
315. Goldfarb, D. S., Corbett, A. H., Mason, D. A., Harreman, M. T. & Adam, S. A. Importin α: A multipurpose nuclear-transport receptor. *Trends Cell Biol.* **14**, 505–514 (2004).
316. Huhtinen, O., Prince, S., Lamminmäki, U., Salbo, R. & Kulmala, A. Increased stable integration efficiency in CHO cells through enhanced nuclear localization of Bxb1 serine integrase. *BMC Biotechnol.* **24**, 44 (2024).
317. Xu, Z. & Brown, W. R. A. Comparison and optimization of ten phage encoded serine integrases for genome engineering in Saccharomyces cerevisiae. *BMC Biotechnol.* **16**, 1–10 (2016).
318. Jusiak, B. *et al.* Comparison of Integrases Identifies Bxb1-GA Mutant as the Most Efficient Site-Specific Integrase System in Mammalian Cells. *ACS Synth. Biol.* **8**, 16–24 (2019).
319. Garcia-Bustos, J., Heitman, J. & Hall, M. N. Nuclear protein localization. *BBA - Reviews on Biomembranes* vol. 1071 83–101 (1991).
320. Goldfarb, D. S., Gariépy, J., Schoolnik, G. & Kornberg, R. D. Synthetic peptides as nuclear localization signals. *Nature* **322**, 641–644 (1986).
321. Kapelner, R. A., Fisher, R. S., Elbaum-Garfinkle, S. & Obermeyer, A. C. Protein charge parameters that influence stability and cellular internalization of polyelectrolyte complex micelles. *Chem. Sci.* **13**, 14346–14356 (2022).
322. Chen, K. *et al.* A gene delivery system containing nuclear localization signal: Increased nucleus import and transfection efficiency with the assistance of RanGAP1. *Acta Biomater.* **48**, 215–226 (2017).
323. Dobson, C. L. *et al.* Engineering the surface properties of a human monoclonal antibody prevents self-association and rapid clearance in vivo. *Sci. Rep.* **6**, (2016).
324. Liang, H. *et al.* Proprotein Convertase Substilisin/Kexin Type 9 Antagonism Reduces Low-Density Lipoprotein Cholesterol in Statin-Treated Hypercholesterolemic Nonhuman Primates. *J. Pharmacol. Exp. Ther.* **340**, 228–236 (2012).
325. Ridker, P. M. *et al.* Lipid-Reduction Variability and Antidrug-Antibody Formation with Bococizumab. *N. Engl. J. Med.* **376**, 1517–1526 (2017).
326. Sun, A. & Benet, L. Z. Late-Stage Failures of Monoclonal Antibody Drugs: A Retrospective Case Study Analysis. Pharmacology vol. 105 145–163 (Karger Publishers, 2020).
327. Rosenberg, A. S. Effects of protein aggregates: An Immunologic perspective. *AAPS Journal* vol. 8 E501–E507 (2006).
328. Dudgeon, K. *et al.* General strategy for the generation of human antibody variable domains with increased aggregation resistance. *Proc. Natl. Acad. Sci. U. S. A.* **109**, 10879–10884 (2012).
329. Leimu, L. *et al.* Development of an in vitro aggregation assay for long synthetic polypeptide, amyloidogenic gelsolin fragment AGelD187N 173–242. *PLoS One* **18**, e0290179 (2023).
330. Holm, P. Part 1: The role of amyloid fibrils in protein aggregation diseases and molecular therapy. Part 2: Isolation of single-chain Fraction variable antibodies that bind to the toxic 8 kDa-fragment of gelsolin using phage display. (2019).
331. Haavisto, O. Selection, screening and testing of recombinant Fabs against mutated amyloidogenic gelsolin peptide : the causative agent of hereditary gelsolin amyloidosis. (2021).

332. Leimu, L. *et al.* Epitope-specific antibody fragments block aggregation of AGelD187N, an aberrant peptide in gelsolin amyloidosis. *J. Biol. Chem.* **300**, 107507 (2024).
333. Mieczkowski, C. *et al.* Characterization and modeling of reversible antibody self-association provide insights into behavior, prediction, and correction. *Antibodies* **10**, 8 (2021).
334. Starr, C. G. *et al.* Ultradilute Measurements of Self-Association for the Identification of Antibodies with Favorable High-Concentration Solution Properties. *Mol. Pharm.* **18**, 2744–2753 (2021).
335. Domnowski, M. *et al.* Generation of mAb Variants with Less Attractive Self-Interaction but Preserved Target Binding by Well-Directed Mutation. *Mol. Pharm.* **18**, 236–245 (2021).
336. Hebditch, M., Roche, A., Curtis, R. A. & Warwicker, J. Models for Antibody Behavior in Hydrophobic Interaction Chromatography and in Self-Association. *J. Pharm. Sci.* **108**, 1434–1441 (2019).
337. Nakanishi, C. & Seimiya, H. G-quadruplex in cancer biology and drug discovery. *Biochem. Biophys. Res. Commun.* **531**, 45–50 (2020).
338. Lerner, L. K. & Sale, J. E. Replication of G quadruplex DNA. *Genes* vol. 10 95 (2019).
339. Tang, C. & MacCarthy, T. Characterization of DNA G-Quadruplex Structures in Human Immunoglobulin Heavy Variable (IGHV) Genes. *Front. Immunol.* **12**, 671944 (2021).
340. Honkonen, E. & Alinikula, J. Role of G-quadruplexes in targeting of somatic hypermutation. (2021).
341. Liu, M. & Schatz, D. G. Balancing AID and DNA repair during somatic hypermutation. *Trends in Immunology* vol. 30 173–181 (2009).
342. Bedrat, A., Lacroix, L. & Mergny, J. L. Re-evaluation of G-quadruplex propensity with G4Hunter. *Nucleic Acids Res.* **44**, 1746–1759 (2016).
343. Buerstedde, J. M., Alinikula, J., Arakawa, H., McDonald, J. J. & Schatz, D. G. Targeting Of Somatic Hypermutation By immunoglobulin Enhancer And Enhancer-Like Sequences. *PLoS Biol.* **12**, (2014).
344. Östman, S. Utilization of activation-induced cytidine deaminase (AID) in mammalian cell display for therapeutic antibody discovery. (2022).
345. Maul, R. W. & Gearhart, P. J. AID and somatic hypermutation. in *Advances in Immunology* vol. 105 159–191 (NIH Public Access, 2010).
346. Geng, S. B. *et al.* Facile Preparation of Stable Antibody-Gold Conjugates and Application to Affinity-Capture Self-Interaction Nanoparticle Spectroscopy. *Bioconjug. Chem.* **27**, 2287–2300 (2016).
347. Wardemann, H. *et al.* Predominant autoantibody production by early human B cell precursors. *Science (80-.).* **301**, 1374–1377 (2003).
348. Mouquet, H. *et al.* Polyreactivity increases the apparent affinity of anti-HIV antibodies by heteroligation. *Nature* **467**, 591–595 (2010).

TURUN
YLIOPISTO
UNIVERSITY
OF TURKU

Painosalama, Turku, Finland 2024

ISBN 978-951-29-9949-1 (PRINT)
ISBN 978-951-29-9950-7 (PDF)
ISSN 2736-9390 (Print)
ISSN 2736-9684 (Online)